Springer Theses
Recognizing Outstanding Ph.D. Research

Shib Sankar Ganguli

Integrated Reservoir Studies for CO_2-Enhanced Oil Recovery and Sequestration

Application to an Indian Mature Oil Field

Springer

Springer Theses

Recognizing Outstanding Ph.D. Research

Aims and Scope

The series "Springer Theses" brings together a selection of the very best Ph.D. theses from around the world and across the physical sciences. Nominated and endorsed by two recognized specialists, each published volume has been selected for its scientific excellence and the high impact of its contents for the pertinent field of research. For greater accessibility to non-specialists, the published versions include an extended introduction, as well as a foreword by the student's supervisor explaining the special relevance of the work for the field. As a whole, the series will provide a valuable resource both for newcomers to the research fields described, and for other scientists seeking detailed background information on special questions. Finally, it provides an accredited documentation of the valuable contributions made by today's younger generation of scientists.

Theses are accepted into the series by invited nomination only and must fulfill all of the following criteria

- They must be written in good English.
- The topic should fall within the confines of Chemistry, Physics, Earth Sciences, Engineering and related interdisciplinary fields such as Materials, Nanoscience, Chemical Engineering, Complex Systems and Biophysics.
- The work reported in the thesis must represent a significant scientific advance.
- If the thesis includes previously published material, permission to reproduce this must be gained from the respective copyright holder.
- They must have been examined and passed during the 12 months prior to nomination.
- Each thesis should include a foreword by the supervisor outlining the significance of its content.
- The theses should have a clearly defined structure including an introduction accessible to scientists not expert in that particular field.

More information about this series at http://www.springer.com/series/8790

Shib Sankar Ganguli

Integrated Reservoir Studies for CO_2-Enhanced Oil Recovery and Sequestration

Application to an Indian Mature Oil Field

Doctoral Thesis accepted by
Academy of Scientific and Innovative Research

Springer

Author
Dr. Shib Sankar Ganguli
Academy of Scientific and Innovative Research (AcSIR)/CSIR-National Geophysical Research Institute
Hyderabad, Telangana State
India

Supervisor
Prof. V.P. Dimri
CSIR-National Geophysical Research Institute
Hyderabad, Telangana State
India

ISSN 2190-5053 ISSN 2190-5061 (electronic)
Springer Theses
ISBN 978-3-319-55842-4 ISBN 978-3-319-55843-1 (eBook)
DOI 10.1007/978-3-319-55843-1

Library of Congress Control Number: 2017934318

Printed on acid-free paper

This Springer imprint is published by Springer Nature
The registered company is Springer International Publishing AG
The registered company address is: Gewerbestrasse 11, 6330 Cham, Switzerland

Dedicated to my beloved parents

Thank you for instilling in me the virtues of perseverance and commitment and encouraging me to strive for excellence.

Supervisor's Foreword

It gives me immense pleasure to write the foreword of this excellent Ph.D. work. It is very widely accepted that CO_2 sequestration through enhanced oil recovery (EOR) can aid to climate change mitigation by reducing about 20% of CO_2 emission in the atmosphere. CO_2-EOR and sequestration is a cutting edge and imminent research in India, and there is an urgent need for the assessment of Indian hydrocarbon reservoirs for feasible CO_2-EOR and storage. This involves integrated reservoir studies such as reservoir flow modeling and simulation, rock physics, and seismic to recommend better cost-effective and technologically efficient CO_2-EOR and storage model, in particular for an Indian mature oil field.

Shib Sankar Ganguli was seriously involved in this joint Indo-Norwegian project funded by Norwegian Embassy in India and conducted his Ph.D. work in National Geophysical Research Institute, since 2011. One of the most challenging queries of this study was how to identify an Indian mature hydrocarbon field which would be feasible for CO_2-EOR followed by permanent storage, prior to its abandonment, with limited data provided by the operator. Moreover, as per the review by the operator, the studied field is not suitable for miscible CO_2 injection. In this view, I must admit that Shib has worked hard and come up with an outstanding scientific solution by developing a new injection scheme for miscible CO_2 displacement and better CO_2 EOR and storage model for Cambay Basin, India.

This work contributes significantly to the feasibility study of CO_2-EOR and sequestration in an Indian mature oil field for the first time in India with cross-disciplinary approach that combines the results from reservoir modeling and flow simulation, rock physics modeling, geomechanics, and time-lapse (4D) seismic monitoring study. The key findings of this work indicate that the field under study has great potential for EOR followed by CO_2 storage just after its economic abandonment. Just as certainly, I strongly believe this work is not only limited to

Indian mature oil fields, but also can be implemented anywhere in the world if justified properly with integrated approach. Moreover, this study provides a valuable resource and can be treated as a base work which can aid to better understanding of CO_2-EOR and storage in future. My heartiest congratulations go to Shib for this excellent piece of work.

Hyderabad, India
December 2016

Prof. V.P. Dimri

Parts of this thesis have been published in the following journal articles:

Ganguli, S. S., Vedanti, N., Akervoll, I., & Dimri, V. P. (2016a). Assessing the Feasibility of CO_2-Enhanced Oil Recovery and Storage in Mature Oil Field: A Case Study from Cambay Basin. *Jour. of Geol. Soc. of India*, *88*(3), 273–280.
Ganguli, S. S., Vedanti, N., & Dimri, V. P. (2016b). 4D reservoir characterization using well log data for feasible CO_2-enhanced oil recovery at Ankleshwar, Cambay Basin-a rock physics diagnostic and modelling approach. *Jour. of Applied Geophy.*, *135*, 111–121.

Acknowledgements

My journey to get a Ph.D. degree from Academy of Scientific and Innovative Research (AcSIR) at CSIR-National Geophysical Research Institute (NGRI) has been the most delightful, eloquent, and enriching experience for me. During this journey, I am obliged to the people, without whom significant contributions and support this dissertation would have not been possible.

First and foremost, I would like to acknowledge the kind support and encouragement of Prof. V.P. Dimri. I have been fortunate to have him as my Ph.D. mentor. He is an outstanding teacher, mentor, scientist, and most importantly a great human being with immense knowledge, insights, experience, patience, and time. He has not only shaped my thesis, but also shaped me from a naïve student to a researcher, and for that I am indebted to him. Thank you for caring not only about my research, but about my personal matters, my frustrating enquiries, nurturing my future, etc. I am truthfully obliged to him for believing on me, providing freedom all the time and energy on me more than past 4 years.

The next person whom I would like to thank is Dr. Nimisha Vedanti, my Ph.D. Co-supervisor. She has been a great source of support for my research, both in educational and financial aspects. She has been the project in-charge of research group dealing with Indo-Norwegian collaboration project on CO_2-EOR study at CSIR-NGRI, which is unique and exciting group to do research, and I am thankful to her for giving me the opportunity to work with this group. Whenever, my research work seemed like tough work, she has provided great encouragement to complete the assignments.

I would like to express my gratitude to Prof. Mrinal K. Sen, Dr. S.K. Ghosh, and Dr. Kalachand Sain, members of my Doctorial Advisory Committee (DAC) of AcSIR, CSIR-NGRI for their priceless guidance and support during my Ph.D. journey. I have been fortunate to have their technical comments/suggestions to improve my research.

I wish to thank Dr. R.K. Tiwari, Coordinator, AcSIR for providing constant support and motivation. It was really fruitful to have his motivational words for continuing career in research.

I am fortunate to avail two financial supports to complete my Ph.D., a part of which was borne by The Royal Norwegian Embassy at New Delhi, and CSIR-Senior Research Fellowship. My sincere thanks to ONGC Pvt. Ltd. for sharing data with me to complete the thesis.

In 2013, I did internship with SINTEF Petroleum Research at Trondheim, Norway, and it was awesome to interact with Dr. Idar Akervoll, Dr. Per E Bergmo, Dr. R. Holt, Dr. Lindeberg, Dr. Dag, and others. The advice I received from them was a turning point and I returned with great many ideas which helped me to shape this thesis.

To Dr. Om P. Pandey, thank you for spending your valuable time with me discussing my research problems and providing direction to solve those.

I extend my sincere gratitude to Dr. R.P. Srivastava for inspiring and making me realize for the first time that Ph.D. degree would be a better option for sustainable career. He was truly a great support during my early career at NGRI. My sincere thanks are also due to Dr. Kirti Srivastava, Dr. A.R. Bansal, Dr. A. Chamoli, and all other former and present research members of theoretical and computational research group for giving me such a great opportunity to discuss my work with them.

I would like to extend my special gratefulness to Dr. Prakash Kumar for showing me the importance of everlasting curiosity in science and providing technical suggestions whenever I discuss with him. Thanks to Dr. Biswajit Mandal and Dr. M. Ojha for giving me continuous encouragement and guidance, starting from the day one to the last day of my Ph.D.

My special thanks to my lovely friends Sunil, Upananda, Anoop, and Arjun for their love and support during this wonderful journey. Thanks to Uma, Ajay, Ahmed, Deepak, Parveen, Nagarjuna, and Swamy for every kind of support during my research at NGRI. My special regards to Mrs. Vani for taking care of all administrative works at AcSIR.

Last but not the least, I deeply indebted to my parents, sisters, and fiancée, Pallavi, for their extraordinary love, patience, and encouragement. Huge thanks to Pallavi for walking beside me through every difficult situations of my journey to Ph.D. I would have not finished this dissertation without her constant support. I dedicate this dissertation to my parents and my best compassionate Pallavi.

Contents

Chapter 1
Introduction

1.1 Background and Motivation

1.1.1 CO_2-Enhanced Oil Recovery and Sequestration-An Overview

With the dawn of floating oil prices, growing energy demand, declining oil field productivity and hard to discover new giant field, the oil operators are now increasing its focus on the improvement of oil recovery from mature hydrocarbon fields. This coupled with the realization that continuous spewing of excessive anthropogenic carbon dioxide (CO_2) from fossil fuel combustion or other industrial sources to the atmosphere has led the world to witness extreme climatic conditions. Till 2013, the world spewed $\sim$35.3 billion metric tons (Gt) of CO_2 due to human intervention, which have continued to grow by 2.5% per year on average over the past decade (Mann et al. 1998; Chiaramonte 2008; Friedlingstein et al. 2014; Scott et al. 2015). Figure 1.1 demonstrates CO_2 emission pathways until 2100 and the extent of net negative emissions by carbon capture and storage, which is considered to be an important climate change mitigation (Fuss et al. 2014). India too did not lag behind and experienced a dramatic growth of about 5.7% per year in fossil-fuel CO_2 emissions during 2000–2009 to about 6.4% per year from 2010–2013 onwards, and thus became the world's third largest fossil-fuel CO_2-emitting country (Dimri 2014; Friedlingstein et al. 2014).

One of the attractive and emerging technologies for climate change mitigation due to CO_2 emission is CO_2-enhanced oil recovery (EOR) apart from its geological sequestration, also sometimes known as *Carbon Capture and Storage* (CCS). With the help of technical and economical assessments, experts suggest that CCS could contribute up to 20% of CO_2 emission reductions, which is equivalent to the cutbacks anticipated from efficiency improvements and large-scale deployment of renewable energy resources (Benson and Cole 2008). This technology involves capturing of CO_2 from emission sources such as petroleum extractive plants (or

S.S. Ganguli, *Integrated Reservoir Studies for CO_2-Enhanced Oil Recovery and Sequestration*, Springer Theses,
DOI 10.1007/978-3-319-55843-1_1

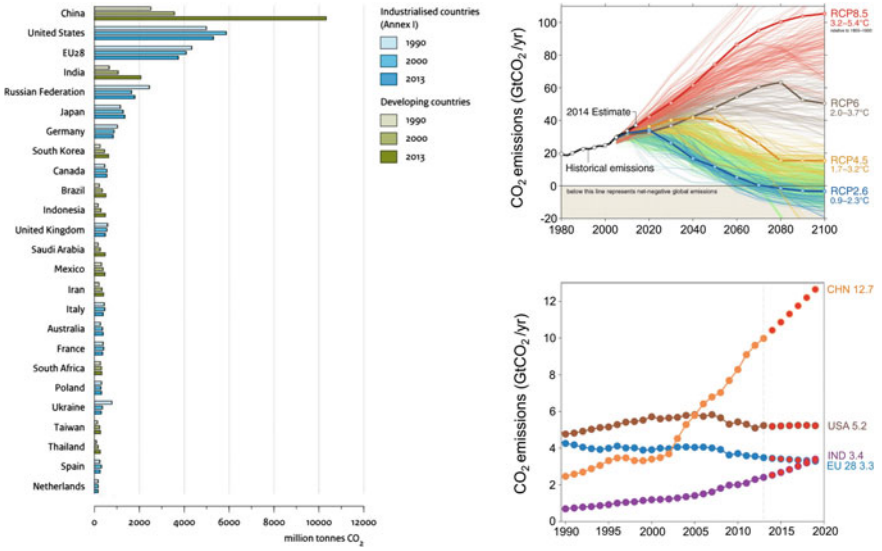

Fig. 1.1 Representation of CO_2 emissions: country wise from fossil-fuel use and cement production (*left*), historical CO_2 emission from fossil-fuel combustion and industry (*black curve*, *top right*) including four representative concentration pathways (RCPs) used to project climate change in the IPCC Working Group 1 contribution to IPCC fifth assessment report (AR5); CO_2 emission from top four emitters (*bottom right*). For more, readers are referred to Fuss et al. (2014), Friedlingstein et al. (2014)

fossil fired plants), transporting CO_2 via pipeline to the injection site, compressing CO_2 to achieve the injection pressure, and then injecting it into the reservoir. In general, injected CO_2 will behave as a supercritical fluid (Tc = 31.1 °C and Pc = 7.38 MPa) at most reservoir conditions.

Hard to discover new giant hydrocarbon fields for meeting the ever growing energy demand has led the operators to focus on improving oil recovery from mature hydrocarbon fields. Moreover, a significant amount of oil (more than half of the original oil in place in the reservoir) is usually left in the reservoir after secondary oil recovery such as water flooding, either as bypassed oil zones or as capillary trapped phenomena. In this context, CO_2-EOR has proven as a state-of-the-art technique for rejuvenating oil production in mature oil fields.

In general, oil and gas production is classified into three recovery processes: primary, secondary, and tertiary. Primary recovery, which uses the innate energy of the reservoir, reservoir fluids and the adjoining aquifer to produce hydrocarbons, which can be broadly divided mainly into gas cap drive, solution gas drive, water drive and combination drive. Secondary recovery process involves injection of a substance (generally water) to re-pressurize the reservoir (Lake 1989). The tertiary recovery, also called enhanced oil recovery (EOR) is the process, which is implemented in oil and gas fields to increase the recovery of crude oil that can be extracted from the field. EOR, sometimes also known as improved oil recovery can be

accomplished by various techniques such as thermal, chemical (surfactant, polymer, etc.) and gas (miscible/immiscible) injection.

Amongst the various EORs, CO_2-EOR is found to be widely used process since it provides a unique opportunity to gain a considerable financial return for storing anthropogenic CO_2 once oil production diminishes prior to its abandonment. During this process, injected CO_2 interacts physically and chemically with the reservoir rock and the contained oil, creating favourable conditions to mobilize the stranded oil and forming a concentrated oil bank that is swept towards a production well (Fig. 1.2). These conditions include (i) reduction in the interfacial tension between the displaced (oil) and displacing fluid (CO_2), (ii) expansion of volume of oil (oil swelling) and subsequent reduction in its viscosity as CO_2 dissolves in the oil, and (iii) maintenance of favourable mobility ratio and conformance to improve the volume sweep efficiency (Tzimas et al. 2005). Sometimes, CO_2 floods involve injection of water-alternating-gas (WAG) flooding.

A successful CO_2-EOR project could add 5–15% of additional oil recovery after primary and secondary recovery efforts, which is typically in the range of ~30–35% of oil originally in place (OOIP) (NETL report 2010). Recent studies have endorsed that CO_2-EOR could push total ultimate oil recovery in some reservoirs to more than 60% of OOIP (NETL report 2010).

In the recent years, oil and gas production industries are practicing a policy which has implications for sequestration in large as a global concern for climate change mitigation apart from CO_2-EOR. Despite the fact that CO_2 sequestration shares some technical characteristics and procedures with CO_2-EOR, it is different in terms of its objectives. In EOR projects, the aim is to maximize the profit by minimizing the total amount of CO_2 injected per barrel of oil produced in the field.

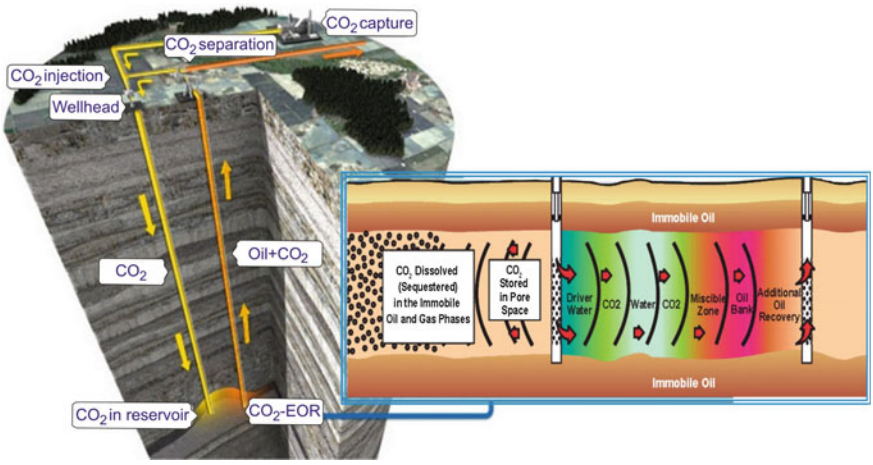

Fig. 1.2 Schematic representation of CO_2-EOR and sequestration subsequently in a field. Cross-section of formation of oil bank during water-alternating-gas injection is also depicted (modified after Global CCS Institute)

While in sequestration, the objective is to store a large amount of CO_2 in underground formations.

1.1.2 Global Status of CO_2-Enhanced Oil Recovery and Sequestration

The idea of geological sequestration first came in 1972 when first successful industrial field-scale CO_2-EOR project was commenced in SACROC field, USA. Since then and over the several decades, CO_2-EOR has been underway in USA, starting initially in the oil field of Permian Basin, and then expanding to numerous other regions of the country, predominantly the Gulf Coast and Rocky Mountains (Kuuskraa and Wallace 2014). Currently, there are 125 active CO_2-EOR projects in operation, which contributes ~300,000 barrels of daily oil production. Apart from USA, there are several large scale CO_2-EOR projects going on at other places such as at Weyburn oil field, Canada (Wilson et al. 2004; White 2009), Ghawar oil field in Saudi Arabia, Bati Raman heavy oil field in Turkey, and series of heavy oil fields in Trinidad. In the recent years, interest for CO_2-EOR project has also emerged in Abu Dhabi, Brazil, China, Malaysia, the North Sea, etc.

Currently there are 13 large scale CCS projects in operation targeting total CO_2 capture capacity of around 20 million tonnes (Mt) annually, with further 9 under construction (Fig. 1.3).

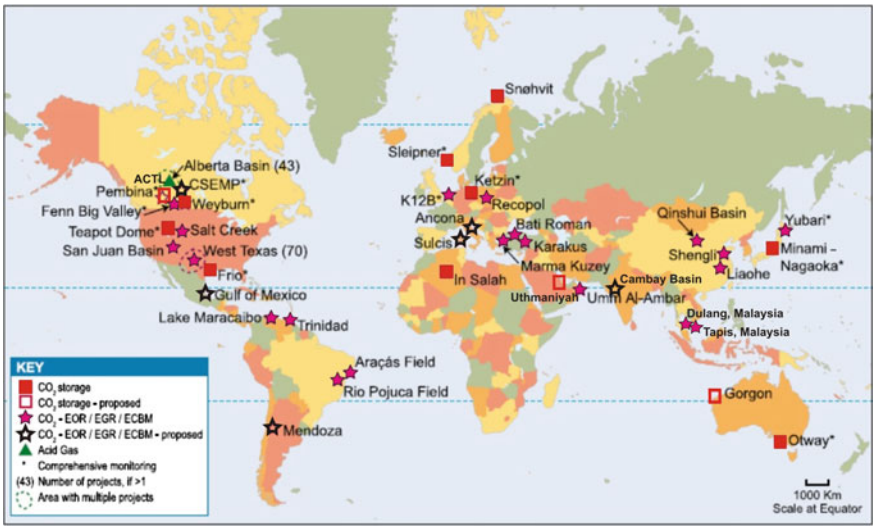

Fig. 1.3 Location of sites in the world map where CO_2-EOR and storage are planned or underway (adapted after Metz et al. 2005). The key represents various activities such as storage, EOR, EGR, etc. using CO_2

Table 1.1 Summary of some major geological sites of CO_2 EOR and sequestration (CCS) around the world with their capacities and other details (modified after Bert et al. 2005)

Project (operator)	Country	Daily CO_2 inj. rate (tons)	Total CO_2 stored	Storage project type	Storage formation	Status
Sleipner (Statoil)	Norway	3000	15 Mt	CCS	Offshore brine sandstone	Operational Aug., 1996
Weyburn (Encana)	Canada	5000	20 Mt	EOR/CCS	Onshore carbonate oil reservoir	Operational Nov., 2000
In Salah (BP)	Algeria	4000	3.8 Mt	EOR/CCS	Onshore sandstone (SS) gas reservoir	Operated 2004–2011
Snøhvit (Statoil)	Norway	2000	2 Mt	CCS	Offshore brine sandstone	Operational Oct., 2007
Cranfield (SECARB)	USA	4000	4.7 Mt	EOR/CCS	Saline sandstone reservoir	Operational April, 2009
Otway (CO2CRC)	Australia	3000	65,445 tons	CCS	Gas bearing sandstone	Operational Jan., 2008
Gorgon (Chevron)	Australia	3 Mt/Yr (proposed)	–	CCS	Island brine sandstone	Under construction

Apart from above, wide range of small scale CCS pilot projects have also been reported, such as Nagaoka project in Japan (Spetzler et al. 2008; Nakatsuka et al. 2010), Frio brine project in Texas (Hovorka and Knox 2003). These are much smaller in comparison to industrial scale projects (>1 Mt of CO_2 annually) like Sleipner in the North Sea (Chadwick et al. 2004), In Salah in Algeria (Riddiford et al. 2005; Iding and Ringrose 2010), CO2CRC Otway project in Australia (Bérard et al. 2008; Dodds et al. 2009) and Weyburn-Midale in Canada (Riding 2005). Table 1.1 summarizes the brief details with current status of CCS projects in the world.

1.1.3 CO_2 Sequestration in Mature Hydrocarbon Reservoirs

There are several favourable traps to store CO_2 in geological sinks (porous medium) such as mature oil and gas reservoirs, deep saline aquifers, oceans, deep unmineable coal seams, deep saline filled basalt formations, etc. (Pamukcu 2006; Farajzadeh 2009). The effectiveness of CO_2 sequestration in reservoirs however, depends on their storage capacity, reservoir stability, risk of leakage, and the retention time (Hawkins 2004; Rochelle et al. 2004), and thus depleted oil and gas reservoirs

(Koide et al. 1993; Holt et al. 1995; Bachu 2000; Jessen et al. 2005; Pawar et al. 2006; Godec et al. 2011; Pang et al. 2013; Hornafius and Hornafius 2015) have received greatest attention. Hydrocarbon bearing reservoirs are appealing as safe storage sites since they have proven capacity of holding buoyant reservoir fluids for millions of years, and are best understood to have required geologic cap rock (Gough and Shackley 2006; Bickle 2009; Hill et al. 2013; Dimri 2014).

In addition to their potential capacities, mature hydrocarbon reservoirs can also offset the storage expenses through CO_2-EOR, which is a recent practice in most of the oil industries. When an oil field is in depleting stage soon after the secondary recovery phase, it becomes uneconomical, and in such cases CO_2-EOR has been found to be quite fruitful in maximizing oil recovery. Moreover, due to the exploration and development activities undergone in the field, mature oil fields can provide the entire well organized CO_2 transportation and injection infrastructure, dense pre-injection data for subsequent storage and effective monitoring of CO_2, once the field is abandoned. Nevertheless, fewer regulatory barriers may be encountered, which can be handled through experience. Additionally, depleted gas fields may signify a globally substantial storage resource, but till date, there have been only a few direct measurements to support this statement (Jenkins et al. 2012).

1.2 Research Objectives and Scope

Reduction of anthropogenic CO_2 in the atmosphere and growing energy demand are two substantial concerns confronting the economic development of any nation including India. This coupled with the realization that CO_2-EOR and storage is an impending technology in India, a systematic research on CO_2-EOR and sink capacity for Indian scenario is desirable.

Present study has been carried out to ascertain the potential of an Indian mature oil field in terms of CO_2-EOR and sequestration. The main motivating queries behind this study are:

- Which Indian hydrocarbon reservoirs can contribute to the mitigation of climate change due to anthropogenic CO_2 emission in the atmosphere?
- Is it feasible to perform CO_2-enhanced oil recovery in an oil field from Cambay Basin, India and storing anthropogenic CO_2, prior to its abandonment?
- Will CO_2 injection result in significant oil recovery from a mature oil field of Cambay Basin?
- If all the above aspects are feasible, then how much is the volume of oil can be recovered and the volume of CO_2 that can be stored in this field?

Thus the major objective of this research is to identify the potential of CO_2-EOR and sequestration in an Indian mature oil field, i.e. Ankleshwar oil field at Cambay Basin, with the help of integrated inputs from various geophysical and reservoir engineering studies. In the focus of this, we attempt:

(a) To develop a suitable cost-efficient methodology to (i) enhance the oil production from Ankleshwar field using miscible CO_2 flooding, and (ii) sequestrate a significant amount of anthropogenic CO_2 for climate change mitigation if feasible.
(b) Develop an effective production strategy by investigating the relative impact of reservoir operational parameters on CO_2-EOR process, and identifying the key operational parameters that could help in ultimate oil recovery from Ankleshwar oil field.
(c) To study the CO_2-reservoir fluid interaction at the prevailing P&T conditions in Ankleshwar reservoir and its impact on seismic properties during the EOR process.
(d) Integration of various geophysical techniques such as Rock physics, Geomechanics, Time-lapse seismic (4D) to understand the CO_2-EOR and safe CO_2 storage process at Ankleshwar.

1.3 Thesis Outline

Based on the above objectives, this thesis has been composed of eight chapters. Broadly, the thesis consists of two parts, the first part deals with the assessment of ultimate oil recovery from the mature oil field under study with the help of reservoir engineering study (Chap. 3), whereas the second part focused on the integrated geophysical evaluation of this field in terms of CO_2-EOR and safe CO_2 storage (Chaps. 4 to 7). This Chapter covers the Introduction part of the thesis, in which, we reviewed the significant contributions of several authors pertaining to CO_2-EOR and sequestration in mature hydrocarbon reservoirs, and the importance and status of various CCS projects undergoing around the globe.

In Chap. 2, "Ankleshwar Oil Field-A Proposed CO_2 Injection Site", an overview of the Ankleshwar oil field in Cambay Basin including geologic setting and litho-stratigraphy of the area, reservoir structure, production history and preliminary studies conducted by the operator for CO_2-EOR and sequestration pilot project, source of CO_2 to be injected in the field, has been deliberated.

In Chap. 3, "Reservoir Modeling and Fluid Flow Simulations of Ankleshwar Oil Field, Cambay Basin", we test the feasibility of CO_2-EOR and sequestration at Ankleshwar oil field. In the view of this, the first part of this chapter focuses on the development of several 3D reservoir models mimicking the reservoir structure, and performing fluid flow simulations to recommend the best suitable model for the estimation of ultimate oil recovery efficiency from the field. Also, this study is the first to suggest a suitable injection fluid composition for miscible displacement in this field. The rest of the chapter covers the sensitivity study of various operational parameters such as grid size, Todd and Longstaff mixing parameters, etc. on the reservoir performance, and CO_2 sequestration potential of this mature oil field. Parts of this Chapter were done in collaboration with SINTEF Petroleum Research Center

at Trondheim, Norway. This work was presented in 50th Annual International Convention of Indian Geophysical Union at Hyderabad (Ganguli et al. 2014).

In Chap. 4, "Acoustic Properties of Reservoir Fluids-CO_2 System", we present models to evaluate the acoustic properties of the reservoir fluids-CO_2 system at the prevailing temperature and pressure conditions in Ankleshwar reservoir. Keeping in mind the most productive sand layers of Ankleshwar formation (i.e. S3+4), we studied the feasibility of seismic responses due to the changes in fluid pressure, composition and saturation during CO_2-EOR and sequestration at Ankleshwar.

In Chap. 5, "Rock Physics Modeling of Ankleshwar Reservoir: A CO_2-EOR Perspective", an isotropic rock physics model of Ankleshwar sands is developed for reservoir characterization. We combine the previous study on acoustic properties of reservoir fluids-CO_2 system to conduct rock physics diagnostic study, fluid replacement modeling and rock physics template analysis (static and dynamic) for Ankleshwar oil field. Further, quantitative time lapse (4D) relative changes in elastic parameters due to CO_2 injection were also analysed for reducing exploration risks and effective reservoir management. This work was published in Jour. of Applied Geophy. (Ganguli et al. 2016b).

In Chap. 6, "Implication of CO_2-EOR and Storage at Ankleshwar Oil Field- A Reservoir Geomechanics Viewpoint", the geomechanical characterization for both pre- and post-CO_2 injection scenarios have been considered for Ankleshwar reservoir. This is performed with reference to identify the most likely risk associated with CO_2 sequestration project. In this chapter, we integrate the results from the previous chapters (Chaps. 4 and 5) for the development of 1D mechanical earth model for the determination of formation strength with respect to CO_2 injection, quantitative analysis of in-situ stress distribution within the wells, time lapse stress response due to CO_2 saturation changes, etc. Part of this work was published in Jour. of Geo. Soc. of India (Ganguli et al. 2016a).

In Chap. 7, "Time Lapse Monitoring of CO_2 Response at Ankleshwar Oil Field: A Seismic Modeling Approach for Feasible CO_2-EOR and Storage", we incorporated the inputs from previous chapters and performed numerical seismic forward modeling on the reservoir model to simulate the response of seismic wave propagation for feasible CO_2-EOR and storage at Ankleshwar. The major objectives of this chapter was to identify the ability of time lapse seismic to monitor the injected CO_2, adjust the rate and pressure of the injection, to obtain better oil sweep efficiency and decide long-term fate of CO_2 within the Ankleshwar formation.

Finally, Chap. 8 presents the conclusions and future follow up research based on the present study.

References

Bachu S (2000) Sequestration of CO_2 in geological media: criteria and approaches for site selection in response to climate change. Energy Convers Manage 41:953–970

Benson SM, Cole DR (2008) CO_2 sequestration in deep sedimentary formations. Elements 4:325–331

Bérard T, Sinha BK, Van Ruth P, Dance T, John Z, Tan C, (2008) Stress estimation at the otway CO_2 storage site, Australia. In: SPE Asia pacific oil and gas conference and exhibition, Perth, Australia

Bert M, Davidson O, De Coninck HC, Loos M, Meyer L, (2005) IPCC special report on carbon dioxide capture and storage. Working Group III of the Intergovernmental panel on climate change. Cambridge University Press, Cambridge, New York, USA

Bickle MJ (2009) Geological carbon storage. Nat Geosci 2:815–818

Chadwick RA, Zweigel P, Gregersen U, Kirby GA, Holloway S, Johannessen PN (2004) Geological reservoir characterization of a CO_2 storage site: The Utsira Sand, Sleipner, Northern North Sea. Energy 29:1371–1381

Chiaramonte L (2008) Geomechanical characterization and reservoir simulation of a CO_2 sequestration project in a mature oil field, Teapot Dome, Wy. Ph.D. Thesis, Stanford University

Dimri VP (2014) Use and abuse of excess CO_2-an overview. J Ind Geophys Union 18:205–209

Dodds K, Daley T, Freifeld B, Urosevic M, Kepic A, Sharma S (2009) Developing a monitoring and verification plan with reference to the Australian Otway CO_2 pilot project. Lead Edge 28:812–818

Farajzadeh R (2009) Enhanced transport phenomena in CO_2 sequestration and CO_2 EOR. Master Thesis, Delft University of Technology, The Netherlands

Friedlingstein P, Andrew RM, Rogelj J, Peters GP, Canadell JG, Knutti R, Luderer G, Raupach MR, Schaeffer M, Van Vuuren DP, Le Quéré C (2014) Persistent growth of CO_2 emissions and implications for reaching climate targets. Nat Geosci 7:709–715

Fuss S, Canadell JG, Peters GP, Tavoni M, Andrew RM, Ciais P, Jackson RB, Jones CD, Kraxner F, Nakicenovic N, Le Quéré C, Raupach MR, Sharifi A, Smith P, Yamagata Y (2014) Betting on negative emissions. Nat Clim Change 4:850–853

Ganguli SS, Vedanti N, Akervoll I, Bergmo PE (2014) An estimation of CO_2-EOR potential from a sector model in a mature oil field, Cambay Basin, India. 50th IGU International Convention, Hyderabad, India, p 293

Ganguli SS, Vedanti N, Akervoll I, Dimri VP (2016a) Assessing the feasibility of CO_2-enhanced oil recovery and storage in mature oil field: a case study from Cambay Basin. J Geo Soc India 88:273–280

Ganguli SS, Vedanti N, Dimri VP (2016b) 4D reservoir characterization using well log data for feasible CO_2-enhanced oil recovery at Ankleshwar, Cambay Basin - a rock physics diagnostic and modeling approach. J App Geophy 135:111–121

Godec M, Kuuskraa V, Van Leeuwen T, Stephen Melzer L, Wildgust N (2011) CO_2 storage in depleted oil fields: the worldwide potential for carbon dioxide enhanced oil recovery. Energy Procedia 4:2162–2169

Gough C, Shackley S (2006) Towards a multi-criteria methodology for assessment of geological carbon storage options. Clim Change 74:141–174

Hawkins DG (2004) No exit: thinking about leakage from geologic carbon storage sites. Energy 29 (9–10):1571–1578

Hill B, Hovorka S, Melzer S (2013) Geologic carbon storage through enhanced oil recovery. Energy Procedia 37:6808–6830

Holt T, Jensen JI, Lindeberg E (1995) Underground storage of CO_2 in aquifers and oil reservoirs. Energy Convers Manage 36:535–538

Hornafius KY, Hornafius JS (2015) Carbon negative oil: a pathway for CO_2 emission reduction goals. Int J Greenhouse Gas Control 37:492–503

Hovorka SD, Knox PR (2003) Frio brine sequestration pilot in the Texas Gulf Coast. In: Proceedings of the sixth international conference on greenhouse gas control technologies, Kyoto, Japan, pp 583–587

Iding M, Ringrose P (2010) Evaluating the impact of fractures on the performance of the In Salah CO_2 storage site. Int J Greenhouse Gas Control 4:242–248

Jenkins CR, Cook PJ, Ennis-King J, Undershultz J, Boreham C, Dance T, Caritat PD, Etheridge DM, Freifeld BM, Hortle A, Kirste D, Paterson L, Pevzner R, Schacht U, Sharma S, Stalker L, Urosevic M (2012) Safe storage and effective monitoring of CO_2 in depleted gas fields. Proc Natl Acad Sci 109:E35–E41

Jessen K, Kovscek AR, Orr FM (2005) Increasing CO_2 storage in oil recovery. Energy Convers Manage 46:293–311

Koide H, Tazaki Y, Noguchi Y, Iijima M, Ito K, Shindo Y (1993) Underground storage of carbon dioxide in depleted natural gas reservoirs and in useless aquifers. Eng Geol 34:175–179

Kuuskraa V, Wallace M (2014) CO_2-EOR set for growth as new CO_2 supplies emerge. Oil Gas J 112(4):66–77

Lake LW (1989) Enhanced oil recovery. Prentice Hall, New Jersey

Mann ME, Bradley RS, Hughes MK (1998) Global-scale temperature patterns and climate forcing over the past six centuries. Nature 392:779–787

Metz B, Davidson O, De Coninck H, Loos M, Meyer L (2005) IPCC special report on carbon dioxide capture and storage. Cambridge University Press, New York, USA

Nakatsuka Y, Xue Z, Garcia H, Matsuoka T (2010) Experimental study on CO_2 monitoring and quantification of stored CO_2 in saline formations using resistivity measurements. Int J Greenhouse Gas Control 4:209–216

National Energy Technology Laboratory (NETL) (2010) Carbon dioxide enhanced oil recovery. Department of Energy, The ENERGY lab report, U.S

Pamukcu Y (2006) Simulating oil recovery during CO_2 sequestration into mature oil reservoir. Master thesis, Middle East Technical University

Pang Z, Kong Y, Li Y, Li J (2013) Water-rock interaction in CO_2 sequestration in a depleted oil reservoir pilot test. Procedia Earth Planet Sci 7:656–659

Pawar RJ, Warpinski NR, Lorenz JC, Benson RD, Grigg RB, Stubbs BA, Stauffer PH, Krumhansl JL, Cooper SP, Svec RK (2006) Overview of a CO_2 sequestration field test in the West Perl Queen reservoir, New Mexico. Environ Geosci 13:163–180

Riddiford F, Wright I, Bishop C, Espie T, Tourqui A (2005) Monitoring geological storage the In Salah Gas CO_2 storage project. In: Proceedings of the 7th international conference on greenhouse gas control technologies, Canada, pp 1353–1359

Riding JB (2005) The IEA Weyburn CO_2 monitoring and storage project—integrated results from Europe. In: Proceedings of the 7th international conference on greenhouse gas control technologies, Canada, pp 2075–2078

Rochelle CA, Czernichowski-Lauriol I, Milodowski AE (2004) The impact of chemical reactions on CO_2 storage in geological formations: a brief review. Geol Soc London Spec Publ 233 (1):87–106

Scott V, Haszeldine RS, Tett SFB, Oschlies A (2015) Fossil fuels in a trillion tonne world. Nat Clim Change 5:419–423

Spetzler J, Xue Z, Saito H, Nishizawa O (2008) Case story: time-lapse seismic crosswell monitoring of CO_2 injected in an onshore sandstone aquifer. Geophys J Int 172:214–225

Tzimas E, Georgakaki A, Garcia Cortes C, Peteves SD (2005) Enhanced oil recovery using carbon dioxide in the european energy system. Report EUR 21895 EN, Institute for Energy, The Netherlands

White D (2009) Monitoring CO_2 storage during EOR at the Weyburn-Midale Field. The Lead Edge 28:838–842

Wilson M, Monea M, Whittaker S, White D, Law D, Chalaturnyk R (2004) IEA GHG Weyburn CO_2 monitoring and storage project summary report 2000–2004, PTRC

Chapter 2
Ankleshwar Oil Field: A Proposed CO_2 Injection Site

2.1 Introduction

Ankleshwar oil field is one of the main onshore Cenozoic hydrocarbons bearing anticline of deltaic origin known in the Cambay Basin, runs into the Gulf of Cambay in an approximately ENE-WSW direction (Fig. 2.1). The utter jejune in the overall oil scenario in India received a promising impetus when Ankleshwar field was discovered in 1960, has been on production since August 15, 1961, and is at mature stage of exploitation. The Field is being operated by Oil and Natural Gas Corporation of India Pvt. Ltd. (ONGC). Initially, the field was with meagre oil production of 100 cubic meter per day (Sm^3/day), which rose with the further development and reached $\sim$5800 Sm^3/day by April, 1966. Till date, it has produced $\sim$49% of the oil in place reserves under natural aquifer drive and massive peripheral water flooding for about 50 years. Still, a significant amount of unswept pockets of oil is left in this reservoir, providing an ample scope for tertiary recovery operation. As of 2011, the field was producing at an oil rate of 391 Sm^3/day with an average water cut of 88 %, which was found to be uneconomical to operate (ONGC Pvt. Ltd., personal communication). In this perspective, a CO_2 EOR and sequestration pilot study has been projected by the operator, targeting the most productive sand layers of Ankleshwar formation.

In this chapter, we will describe the geology, reservoir structure, production history, and previous study carried out for feasible CO_2-EOR and sequestration at the proposed field.

S.S. Ganguli, *Integrated Reservoir Studies for CO_2-Enhanced Oil Recovery and Sequestration*, Springer Theses,
DOI 10.1007/978-3-319-55843-1_2

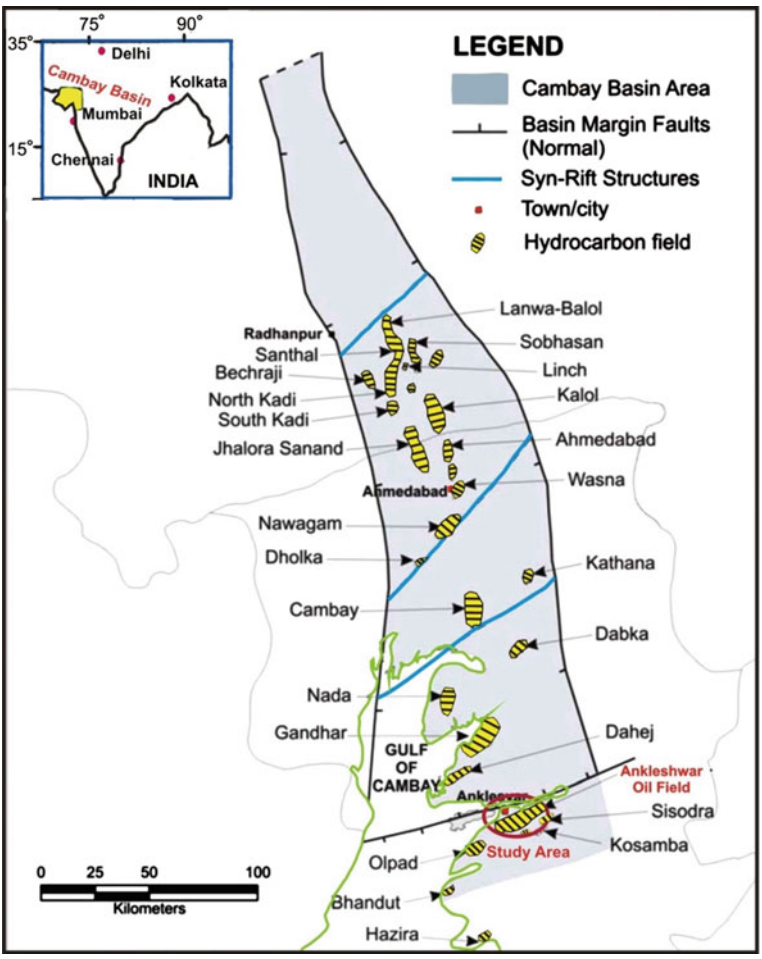

Fig. 2.1 The location map of the Ankleshwar oil field, with other major hydrocarbon bearing fields/structures in Cambay Basin, Western India. The *red ellipse* represents the field under study

2.2 Tectonics and Geologic Setting

The geotectonics and sediment deposition have played pivotal role in the evolution of Ankleshwar oil field along with other hydrocarbon bearing fields in Cambay Basin. Cambay Basin is a pericratonic rift graben situated in western India, came into existence during the late Mesozoic era with the development of major tensional faults along pre-existing basement (Biswas et al. 1993; Raju and Srinivasan 1993). It is believed that the regional tectonic is an overprint of the lithospheric thinning due to thermal expansion and the subsequent rift propagation took place along the pre-existing tectonic elements. The rift initiation took place around 65 Ma,

concomitant with the colossal Deccan volcanism, and is characterized by basin bounding extensional fault (listric/normal fault) aiding the initial basin subsidence with the upliftment of basin margin or rift shoulders (Biswas et al. 1993). Southern part of the basin is broad as compared to the northern part where the basin width is narrowed down, indicates possible diminishment of rift propagation (Fig. 2.1). The structural evolution of Cambay Basin can be categorised in three major parts: Syn-rift, Post-rift and Late post-rift thermal subsidence phase (Raju and Srinivasan 1993). Based on the transverse fault system, the entire basin can be divided into five tectonic blocks such as Sanchor-Patan, Ahmedabad-Mehsana, Tarapur, Broach and Narmada block. Ankleshwar oil field is located in the Narmada block and believed to be largely affected by the rifting event took place during late Cretaceous.

The study area, Ankleshwar oil field, is situated in the southern part of Cambay Basin, covering an area of 32 sq. km (Fig. 2.1). The geological section of this oil field encompasses thick sedimentary column of tertiary age (Eocene to Pliocene), deposited over the Deccan traps (Mukherjee 1981). The Deccan traps are composed of mostly labradorite and augite. The drilled thickness of the traps in this oil field was reported to be 320 m (ONGC report 2010). The entire area supposed to have subsided during late Paleocene, resulting in deposition of monotonous Cambay shale, which is composed of grey shales in thin alternations with silty and carbonaceous shales, considered as the main source rock. Subsequent to subsidence, several sand reservoirs developed in the progradational and retrogradational sequence of deposition during Upper to mid Eocene period. These Eocene sandstones are permeable and porous intervals with different level of cementation that affects their porosity and permeability. Further, these Eocene sedimentary rocks in this field can be broadly divided into Lower, Middle and Upper groups, depending upon the lithologic properties. The Lower Eocene deposits are the oldest sedimentary rocks drilled in this oil field, contains shales with separate clay sandstones. While, Middle group includes 262–316 m thick most productive deposits, with alternating shales and poorly cemented quartz sandstones, composed of fine to medium sized sand grains. This group is inferred to have been deposited mostly along the distributary channels and allied environments of lower deltaic complex. The Upper Eocene sediments are 82–203 m thick represented by sandstones, siltstones, and shales with numerous fauna (ONGC report 2010).

The individual oil bearing sand layers were designated in most of the case and were numbered progressively from top to bottom in each case. In total, 11 sand groups (S1–S11 bottom upwards) has been identified, constituting the pay zones, where S1–S5 represents the Middle sand group and S6–S11 represent the Upper sand group. Amongst all, S3 and S4 sand groups of fine to medium grained is the most productive, and essential target for CO_2-EOR. The main oil pools, confined to Middle and Upper sand groups, were discovered during the early exploratory drills in the formation. Thick shale interbedded with trapwacke, trap conglomerate and thin coal layers were also deposited above the trap (Srivastava et al. 2015).

2.3 Stratigraphy

The stratigraphy of Ankleshwar oil field consists of Paleocene to Pleistocene strata of marine and non-marine origin, overlying Deccan traps of Mesozoic-Cenozoic era. The post-trappean sedimentary sequence with boundaries of the time units of this basin has been classified into several rock stratigraphic units, illustrated in Fig. 2.2. The detail stratigraphic features resulted from the study of 478 core cuts are briefly described below.

Non-conformably overlying the Deccan traps is Olpad formation, a Paleocene sequence of exclusively traps derived non-marine sediments consisting of dark claystones and splintery shales (ONGC report 2010). It is barren and has varying thickness between 18–123 m. Also, it is separated from the overlying Cambay Shale group by an erosional unconformity.

The Cambay Shale group is conformable and 220–470 m thick, composed of monotonous grey shales in thin alterations with silty and carbonaceous shales, occasionally sideritic.

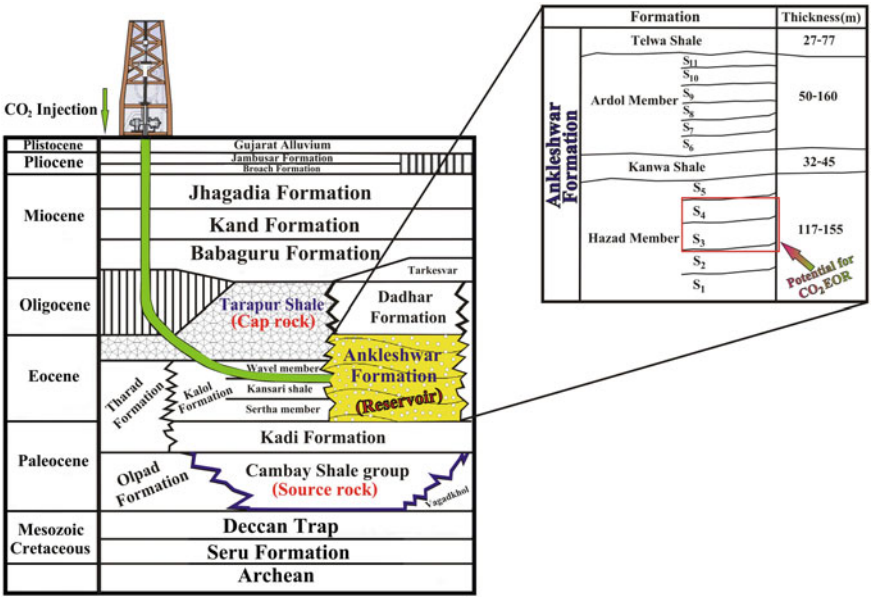

Fig. 2.2 Schematic distribution of the Litho–Stratigraphy of the study area. CO_2 injection is proposed into the Ankleshwar formation; particularly within S3+4 pay sands, the most productive layer. The trajectory of the possible injection well is shown within Ankleshwar formation

The Ankleshwar formation of Middle to Upper Eocene is the main stratigraphic unit in terms of hydrocarbon potential. It overlies the Cambay Shale group, comprises of a thick sequence (300–400 m) of prograding deltaic origin sediments. The sand isolith maps for individual horizons of this formation bring out bird-foot lobate type delta depositional model (ONGC report 2010). Marine influence for Middle and Upper sands is also validated by the presence of chloride-calcium type formation waters. This productive group can be further divided into four sub-lithological units: Ardol, Hazad, Telwa, and Kanwa, covering shales and sands. The Hazad unit, forms the major reservoir rock, is essentially sandstone deposited in a prograding deltaic facies. Kanwa shale acts as effective cap rock for this deltaic sequence, indicating a marine transgressive system due to the presence of planktonic foraminifera (Raina et al. 2010). The Upper Eocene Ardol member exhibit fairly good reservoir rock characteristics and accounts for about 15 percentages of volume of accumulated hydrocarbons. The Telwa shale member of late Eocene, devoid of coarser clastics, acts as cap rock for this sand unit.

Conformably overlying the Telwa shale member of Ankleshwar formation is Dadhar formation. It is about 90–145 m thick and encompasses interbedded sandstones, shales and a bioclastic limestone.

Non-conformably overlying Dadhar unit, the Tarkesvar formation comprises of molten red and grey claystones, grey shales and poorly sorted sandstones. This is barren and corresponds to late Oligocene to early Miocene age.

Babaguru formation of Miocene age is composed predominantly of sands with interbedded clays and occasionally shales. The succeeding Kand formation mainly includes grey claystone with local sandstone (sometimes known as kankar), and occasionally clay conglomerates (ONGC report 2010).

The Kand formation is disconformably overlain by Gujarat Alluvium comprising grey, brownish grey and bluish grey silty clays. This stratigraphic unit is of Recent to Sub-Recent age, which is about 15–40 m thick over Ankleshwar oil field.

2.4 Reservoir Structure

The reservoir structure is basically a doubly plunging asymmetric anticlinal fold of ENE-WSW trend, dissected by seven major faults. The long axis of the reservoir is $\sim$17 km and the width is $\sim$3 km. The North—Western flank has gentle dip of less than 8° whereas South-Eastern flank is steeper with maximum of 18° dip. The North-Eastern limb of the anticline is altered by a normal fault, which is also parallel to the anticlinal strike. It seems that main controlling factors for oil

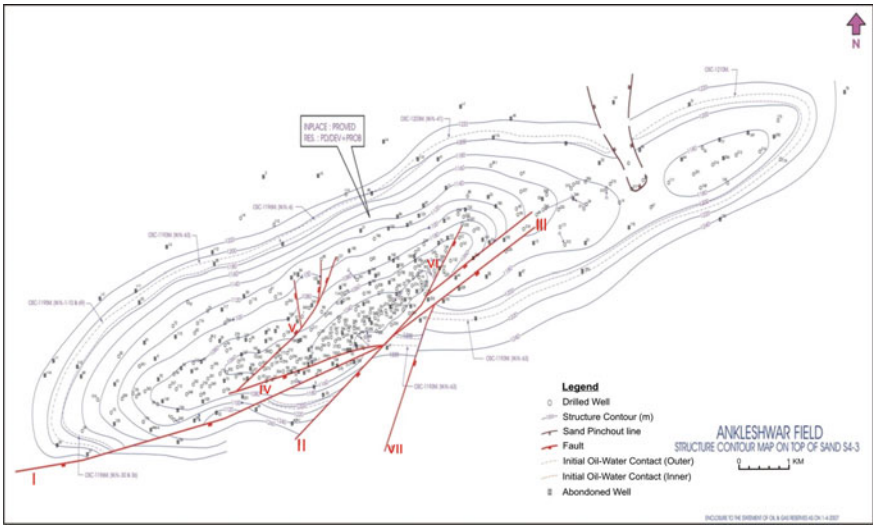

Fig. 2.3 Representation of the structure contour map on the top of sand S4 from the most productive sand layer of Ankleshwar formation. Legend represents the various structural features with well locations and oil-water contacts (ONGC, personal communication)

distribution within the reservoir are due to series of faulting and lateral variations in continuity of the layers and reservoir properties.

The operator has prepared structure contour maps on the reservoir tops of all classified horizons and layers to understand the structural features and its impact on the production scenario of the oil field. Figure 2.3 demonstrates the variable structural features of the main productive sand layer by contour map drawn on the top of sand S4, a part of Middle sand group. We can clearly see the fault system within this reservoir which indicates reverse faults, which have been verified from number of wells. Amongst all, Faults I and II are the key ones which affect almost the entire stratigraphic column. Repetition of horizons at different well locations helped to delineate various faults in this structure. Besides the seven major faults depicted in Fig. 2.3, there are several other faults of small magnitude and extent. Also, the layers are not continuous throughout the reservoir and some layers encountered pinch-outs in between, which pose production challenges.

The limb of the anticlinal reservoir and the most productive sand layers were also noticed in seismic section obtained from this field. The fault closure at levels of pay sand S3+4 and structural high at Hazad formation can be clearly noticeable in the seismic section (Fig. 2.4).

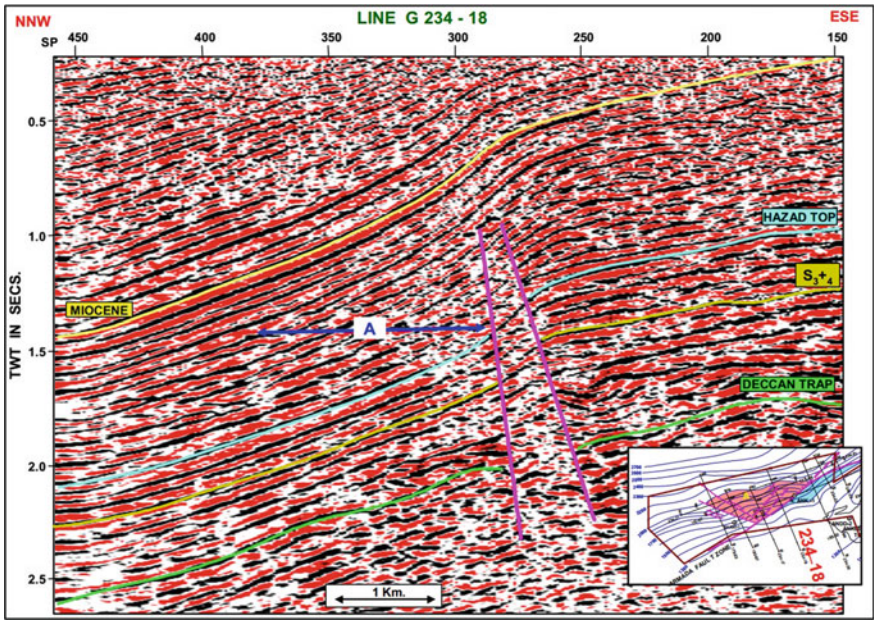

Fig. 2.4 Seismic section across the Ankleshwar oil field with various stratigraphical units (ONGC, personal communication)

2.5 Production Scenario

Ankleshwar oil field has produced cumulatively 65.35 million metric tons (MMt) as on April, 2011 against the estimated oil in place of 134.71 MMt. Average rate of production was 7500 Sm^3/day during the year 1967–68, which reached to 7700 Sm^3/day in the next year and the peak rate of about 8300 Sm^3/day was attained towards the end of 1969 (ONGC, personal communication). Later, during 1973–74, the oil production declined to $\sim$7800 Sm^3/day from 8300 Sm^3/day due to ceasure of large number of wells and inadequacy in work over facilities accessible at that time. Nevertheless, during early 1975, the oil production increased to 8300 Sm^3/day due to drilling of few infill wells. In spite of remedial measures taken from time to time, there has been a decline in oil production from this field since 1977–78, and his uniform deteriorating trend till the year 2000 is summarized in Table 2.1.

According to the operator, the reason for this kind of production behaviour is due to substantial increase in water cut (due to premature water breakthrough), increase in frequency of ceasing due to water loading, etc.

As we stated earlier, there are in total 11 producing sands of Ankleshwar formation, but pay sand S3+4 is the largest reservoir unit within the Middle productive group. In the view of this, we discuss the production performance of S3+4 sand layer. Sand S3+4, including its six sub-layers (S3−1, S3−2, S4−1, S4−2, S4−3, S4

Table 2.1 Summary of the oil production (Sm^3/day) from the oil field under study during the year 1976–2000 (ONGC report 2010)

Duration (Year)	Oil production (Sm^3/day)	Duration (year)	Oil production (Sm^3/day)	Duration (year)	Oil production (Sm^3/day)
1976–77	8326	1984–85	4364	1992–93	1529
1977–78	7898	1985–86	4256	1993–94	1259
1978–79	7829	1986–87	3636	1994–95	1232
1979–80	6591	1987–88	3226	1995–96	1202
1980–81	6227	1988–89	2659	1996–97	958
1981–82	5448	1989–90	2067	1997–98	918
1982–83	3602	1990–91	1874	1998–99	800
1983–84	4257	1991–92	1759	1999–00	794

−4) produced about 38.8% of the total production from this oil field. This unit has produced in total ∼36.3 MMt of oil with an oil rate of 159 Sm^3/day, and average water cut was 91.3% as on April, 2011 (Fig. 2.5).

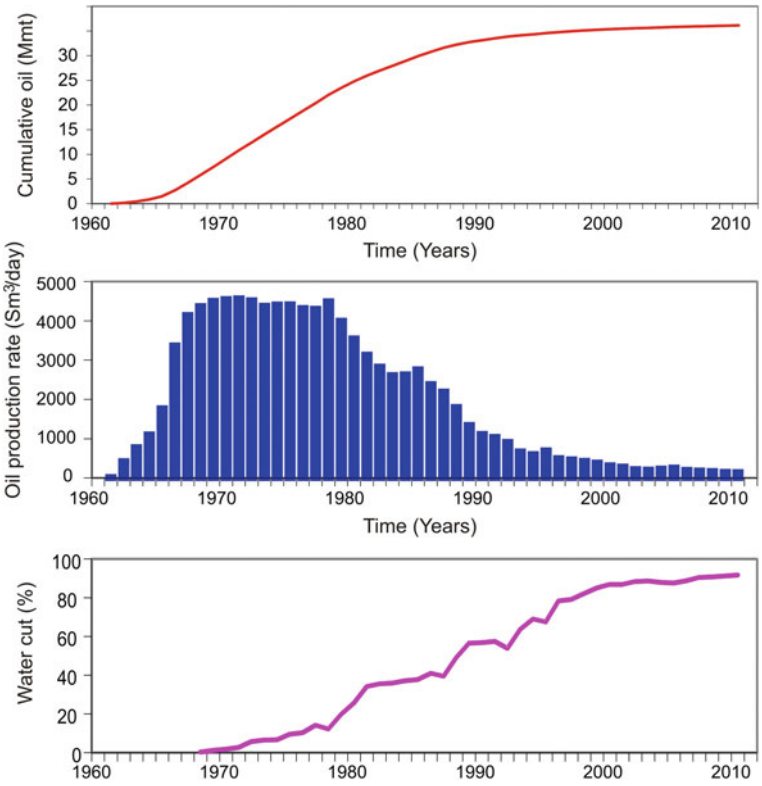

Fig. 2.5 Representation of the production performance of S3+4, the most productive sand layer of Ankleshwar formation (ONGC report 2010)

2.6 Previous Work

A CO_2-EOR and sequestration pilot project is planned by the operator in Ankleshwar oil field and S3+4 sand unit of Ankleshwar formation was chosen as the target for the appropriate depth range, regional extent, the oil production significance and excellent cap rock. It is proposed that CO_2 will be supplied from the gas processing plant at Hazira, which exhaust CO_2 of about 600,000 m^3/d, situated ~70 km away from the injection site.

Preliminary simulation and laboratory studies on representative Berea cylindrical core with oil from Ankleshwar field have been performed to evaluate the potential of CO_2 injection in mobilizing the residual oil within water flooded sand unit of S3 +4 at Institute of Reservoir Studies (IRS), Ahmedabad of ONGC. Experiments using CO_2, N_2, and HC gases at an injection rate of 1 cc/h were verified (IRS, ONGC, personal communication). The core study suggests that injection of CO_2 will lead to 11.8% of incremental oil recovery over water flood, unlike in the case of N_2 and HC gas injection at the same rate, where comparatively low incremental oil recovery is envisaged, which is about 4.8 and 4.0% of HCPV, respectively. In order to choose an optimum CO_2 injection rate, a series of experiments were conducted at different CO_2 flow rates such as 1 and 5 cc/h, respectively (IRS, ONGC, personal communication, Srivastava et al. 2015). Experiments suggest that repeated injection of CO_2 at the rate of 1 cc/h followed by one week closure ensued highest incremental oil recovery over water flood, i.e. 15.71% of HCPV.

However, the simulation study envisaged the most likely, high and low cases of oil recovery possibilities in the next 30–35 years of CO_2 injection, and suggests that at the high, most likely and low case, about 7, 4.5 and 2.3% of incremental oil recovery over the base case is feasible, respectively (Fig. 2.6).

As per the studies carried out by IRS-Ahmedabad, this project would require further 12 new injectors at the crest and 67 producers at the flank of the anticline. It is also envisaged that this project will help in sequestrating 7.5 MMt of CO_2 during the entire life span.

2.7 Conclusions

In this chapter, we presented an overview of the Ankleshwar oil field's geology, oil bearing structure, stratigraphy, as well as the production performance and preliminary results from the experiments carried out at IRS-Ahmedabad, the R&D center of ONGC. The results are fairly encouraging to conduct further study in detail to evaluate the prospect of CO_2 injection for EOR and sequestration. Accordingly, we conducted several studies including reservoir simulation and other geophysical techniques such as seismic, rock physics, geomechanics, etc. to understand the CO_2-EOR and sequestration at the proposed site, Ankleshwar oil field, which will be presented in the following chapters.

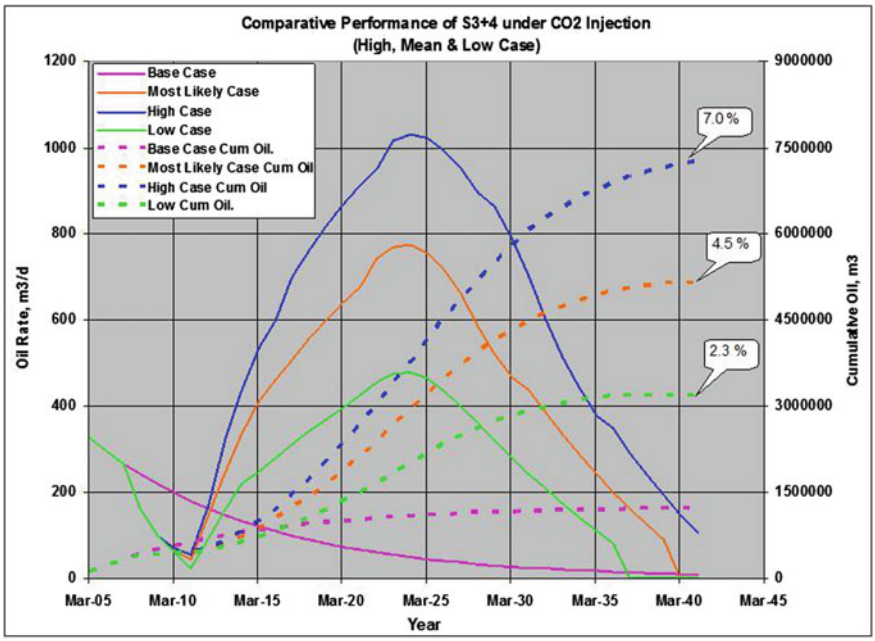

Fig. 2.6 Results from the comparative production performance of S3+4 sand unit under CO_2 injection (ONGC, personal communication). The legend signifies the various possible case scenarios such as base case, most likely, high and low case, respectively

References

Biswas SK, Bhasin AL, Jokhan Ram (1993) Classification of Indian sedimentary basins in the framework of plate tectonics. In: Biswas, SK, Dave A Garg P, Pandey J, Maithani A, Thomas NJ (eds) Proceedings of the second seminar on petroliferous basins of India, vol 1. pp 1–46

Mukherjee MK (1981) Evolution of Ankleshwar anticline, Cambay basin, India. Geologic Notes, AAPG, pp 336–345

Oil and Natural Gas Corporation of India (ONGC) (2010) Annual report of Ankleshwar asset for the year 2009–2010 by Sub-surface team. Ankleshwar asset, ONGC

Raina A, Pande HC, Saxena RK, Singh H, Singh RR (2010) Genetic characterization of shallow hydrocarbon gases by High Resolution Carbon Isotopic Studies: A case study of South Cambay Basin in India. Petrotech conference, New Delhi, India, PID: 20100353

Raju ATR, Srinivasan S (1993) Cambay basin—Petroleum habitat. In: Biswas SK, Dave A, Garg P, Pandey J, Maithani A, Thomas NJ (eds) Proceedings of the second seminar on petroliferous basins of India, vol 2. Indian Petroleum Publishers, pp 33–78

Srivastava RP, Vedanti N, Akervoll I, Bergmo P, Yerramilli RC, Yerramilli SS, Dimri VP (2015) Study of CO_2 EOR in a sector model from mature oil field, Cambay basin, India. In: Mukherjee S (ed) Petroleum geosciences: Indian contexts. Springer International Publishing, pp 87–98

Chapter 3
Reservoir Modeling and Fluid Flow Simulations of Ankleshwar Oil Field, Cambay Basin

3.1 Introduction

In recent years, mature oil and gas reservoirs are becoming increasingly attractive targets for enhanced oil recovery (EOR) by CO_2 injection due to the twin advantages such as EOR and mitigating the impact of CO_2 on climate. A cost effective EOR can extend the production life of an oil field for several years (Orr and Taber 1984; Bondor 1992; Akervoll and Bergmo 2010; Dimri et al. 2012; Muggeridge et al. 2014). However, to accomplish an accurate and complete evaluation of hydrocarbon reservoirs in terms of CO_2-EOR, development of state-of-the art reservoir modeling is necessary. Reservoir modeling is an indispensable tool in the study of field development planning and reservoir management, and is recognized as the construction of a 3D numerical depiction of the hydrocarbon reservoir, preferable in depth, mimicking the reservoir structure (e.g., as demarcated by stratigraphic horizons and faults); petrophysical properties (e.g., porosity, permeability); and fluid distribution such as water/oil saturation (Michelena and Gringarten 2009).

In this chapter, we report the development of various CO_2-EOR models based on Ankleshwar oil field to estimate the incremental oil recovery efficiency using limited data provided by the operator. The objective of this work is to determine the optimal strategy for CO_2 injection in a mature oil field with respect to increased oil recovery and utilization of CO_2 for storage if feasible. Further, we investigated the possibility of miscible displacement in the Ankleshwar oil field of Cambay Basin by analysing the impact various operational parameters on oil recovery.

3.2 3D Reservoir Model

Reservoir models play crucial role in understanding and predicting the main geological, geophysical and reservoir engineering components in the entire lifetime of an oil field. It takes geological model as an input and delivers the input for flow

S.S. Ganguli, *Integrated Reservoir Studies for CO_2-Enhanced Oil Recovery and Sequestration*, Springer Theses,
DOI 10.1007/978-3-319-55843-1_3

simulation, and that's why a good model building should focus on the end goal, whether it is in terms of estimation of original-oil-in-place (OOIP), the design of tertiary recovery methods, prediction of gas breakthrough, optimization of CO_2-EOR and storage, etc. (Caers 2005).

As mentioned earlier in Chap. 2, Ankleshwar oil field in Cambay Basin, Western India is a mature oil field that witnessed massive water flooding for about 50 years, providing an ample scope for tertiary recovery operations. In order to evaluate the scientific and technical feasibility of CO_2-EOR potential in the Ankleshwar oil field, development of geomodel is essential which can predict the reservoir behaviour with respect to massive CO_2 flooding.

One of the main aspects of building the 3D geomodel is to understand the data and quality check of the data including existing well logs (porosity, permeability, saturations, etc.), structural maps (major horizons, thickness maps, fluid contacts, etc.) and laboratory measured data (PVT data, etc.). We have used Petrel, a commercial software package by Schlumberger to construct the reservoir models.

3.2.1 Reservoir Characterization and Geomodel Building

As mentioned in Chap. 2, the stratigraphy of the Ankleshwar oil field contains marine and non-marine origin sedimentary deposits of Tertiary age (Eocene to Pliocene) and igneous formation of Mesozoic-Cenozoic age (Mukherjee 1981). The depth of pay sand intervals and source formation ranges from ~850 to ~1560 m below the surface. The development of reservoir model comprises the construction of reservoir grids keeping in mind the stratigraphy, geometry, fluid characterization, rock-fluid properties, well placement, model initialization, rate schedules, prediction of miscibility development pressure, etc.

We developed the geomodel, initially, using structural contour maps and thickness maps of top sands provided by the operator. The reservoir is a doubly plunging asymmetric anticlinal fold with a gentle plunge, except on the western end and an ENE-WSW trending axis dissected by 7 major faults (ONGC report 2010). Keeping these in mind and incorporating all the classified horizons/layers including fault lines associated with the reservoir structure, the geomodel is developed. The surfaces have been segmented at the intersection with the reservoir-bounding fault to construct the detailed model focusing on anticlinal structure. We then performed quality check to ensure the consistency by correcting the depth surfaces at all available well points.

To build the detailed geomodel, we also used well tops available from ~130 wells from the oil field. This has helped in correct positioning of the horizons. Furthermore, based on reservoir property and geology we divided the 11 producing sand layers into 10 sub-layers e.g. the maximum producing S4 is divided in 4 sub-layers named S4-1 to S4-4 (Fig. 3.1). The lower sandstone interval was incorporated as an explicit aquifer layer beneath the reservoir. We then incorporated the reservoir rock properties (porosity, permeability, etc.) obtained from core

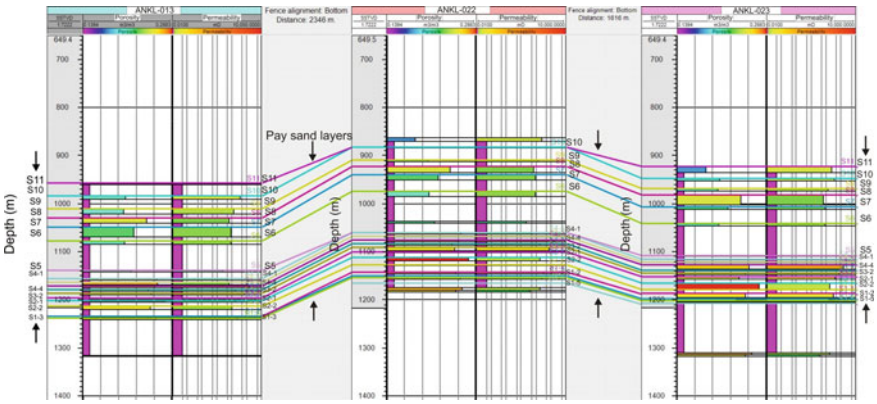

Fig. 3.1 Representation of the pay sand layers and sub-layers including the petrophysical properties such as porosity and permeability within the Ankleshwar formation using well log section. The *arrow* represents the pay sand layers of Ankleshwar reservoir. Example of pinching out of the sublayers between the wells is also very clear

measurements into the geomodel. Apart from the cores, the porosity was also determined from acoustic, density and neutron logs to ensure consistency in the distribution of the properties in each horizon or layer. Likewise, the permeability also determined using hydrodynamic investigations (pressure build up curves and indicator diagrams), since it found to be varied widely both as per the areas and thicknesses of individual layers (ONGC Pvt. Ltd., personal communication).

3.2.2 Description of Geomodels

Based on the generic sandstone oil reservoir with realistic heterogeneities, an initial complex reservoir model is built which consists of 11 major layers (S1-S11) and 10 sub-layers correspond to the Ankleshwar formation (Fig. 3.2). This model is with reference to the anticlinal structure with gentle dips and interchangeable layers of sand and shale. The resolution of the simulation grid cells in horizontal x-direction is 50.61 m, y-direction is 49.33 m and grid cell heights vary from $\sim$4 to 12 m, depending upon the thickness of the corresponding horizon. The number of grid cells in this model is 1,25,17,234 (698 $\times$ 227 $\times$ 79). The depth of the reservoir model extends from $\sim$1010 to 1342 m. There are in total, 130 wells and the average distance between the wells is $\sim$500 m. All the wells used in the simulation study are vertical with an effective wellbore radius of 10.2 in. The skin factor at the wellbore was assigned to zero value. We adopted the well placement pattern following ONGC's field well placement criteria including the injectors and producers.

The model is initialized keeping all the wells on production rate control from the beginning of the simulation. Additionally, keeping in view the permeability

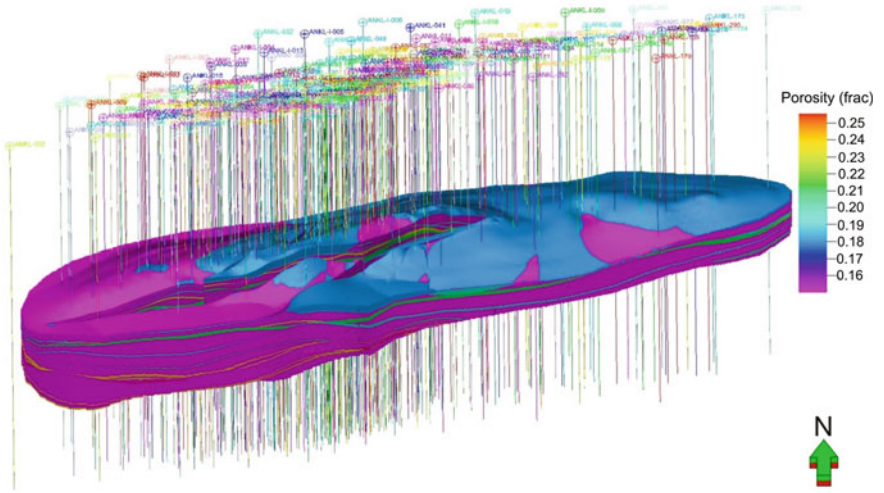

Fig. 3.2 Schematic illustration of the complex reservoir model with porosity in fraction as the property within the Ankleshwar formation. In total, ~130 wells are displayed including 18 water and 18 gas injectors. The arrow at the bottom right indicates geographical north

variation and heterogeneity of reservoir sands some of the injection wells were drilled selectively. Water injection was planned simultaneously for all the layers within Ankleshwar formation in spite of their varying permeability.

In the present work, two different injection strategies including continuous CO_2 and CO_2- Water-alternating-gas (WAG) injection and has been considered to evaluate the best injection strategy for Ankleshwar oil field. All the reservoir properties such as porosity, permeability, rock compressibility, etc. stored in the cells were provided by the operator (ONGC). The layers are not continuous throughout the reservoir and some pinch-outs were observed in between, which pose production challenges. The productive layers in the Ankleshwar formation are separated by impermeable shales that do not allow any vertical fluid flow, leading to permeability anisotropy. The shale layers were assigned 100% water saturation and zero permeability. In addition to this, faulting in the reservoir has severely controlled the fluid flow distribution, therefore, we assumed that vertical fluid flow is negligible. Figure 3.3 illustrates the permeability distribution of the Ankleshwar complex model based on real field data. A sector is cut from the reservoir model to illustrate the permeability distribution in deeper layers of the model.

In order to evaluate the model's performance for CO_2-EOR, the base model is subjected to numerical black-oil and compositional simulators, ECLIPSE 100 and 300, commercial packages by Schlumberger. Immiscible CO_2 injection is conducted in 45° API reservoir-oil simulations. Detailed properties and the working formulations of the simulators are described in the following section in this chapter. We found that dealing with such big model of 1,25,17,234 grid cells offers huge computational cost. Therefore, we decided to focus into S3 and S4 sand layers

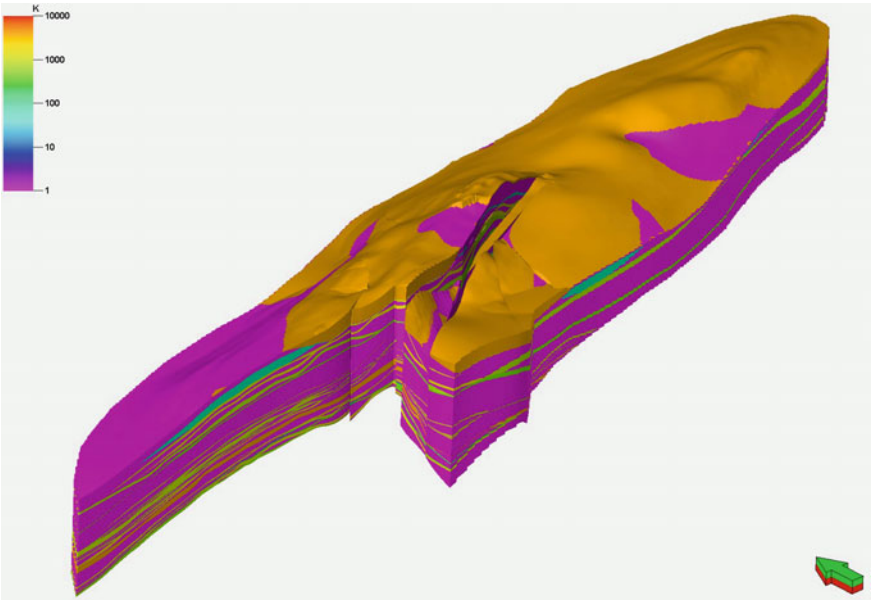

Fig. 3.3 A diagram showing the permeability distribution of the Ankleshwar complex model. A sector is cut from the reservoir model to illustrate the permeability distribution in deeper layers of the model. The *arrow* at the *bottom right* indicates the geographical north

(clubbed together and referred as S3+4), the most productive layers of the reservoir holding oil in place of 552 MMbbls.

In this view, we constructed a sector model including S3+4 horizons, penetrated by 60 injectors (water and CO_2) and 106 producers to study the effect of CO_2-WAG injection on the reservoir. Geologically the model is E-W trending doubly plunging anticline, cut by reverse fault at southern flank (Fig. 3.4). The areal extent of the model is 9400 m in length and 5780 m in width. In total 10 faults were modeled from the available fault sticks with the major ones running in northeast-southwest direction. The developed model represents two main lithologies, sand layers separated by the shale layers. The resolution of the simulation grid cells in horizontal x-direction is 50 m, y-direction is 47 m and grid cell height is 0.9 m throughout the model. The number of grid cells in this model is 5,97,320 ($218 \times 137 \times 20$). The average distance between the wells is around 500 m. The depth of the reservoir model extends from $\sim$1020 to 1330 m.

We followed the similar procedure for reservoir simulation using E-100, and we found that CO_2-WAG resulted in $\sim$5% of incremental recovery with immiscible CO_2 injection. The oil in this field is light to near volatile and pure CO_2 is not miscible with oil due to high minimum miscibility pressure (MMP). MMP is defined as the lowest pressure at which multi-contact miscibility can be achieved. Immiscible displacement takes place at reservoir pressure below MMP, and miscible displacement takes place when reservoir pressure is above MMP. Our aim is

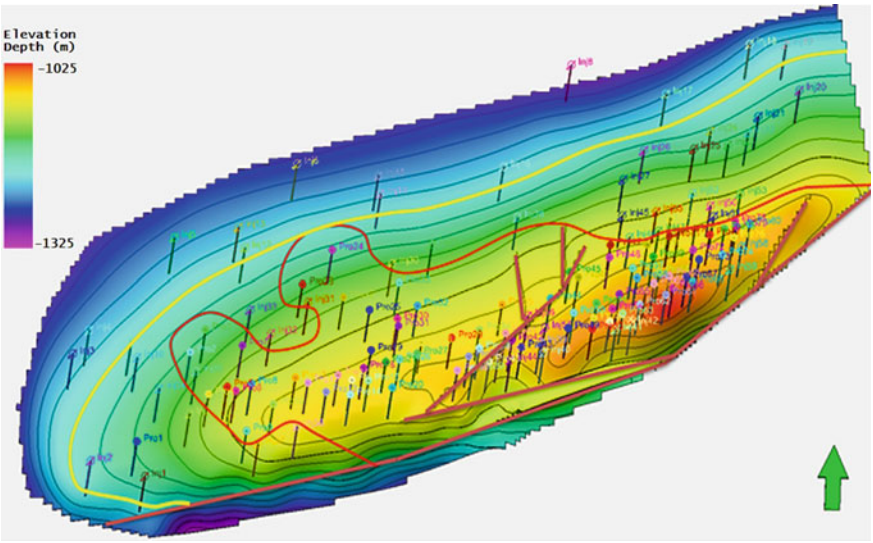

Fig. 3.4 Geometry of the sector model with the injectors (*open circles*) and producers (*closed circles*) in depth domain. The Oil-Water-Contact is set at 1200 m (*yellow contour*). The crest of the structure is towards southeast and dominated by faults (*brown lines*). The area enclosed by the *red line* is dominated by the production wells. The *green arrow* at the *bottom right* indicates the geographical north

to develop an optimized simulation model which can lead to miscible CO_2 displacement for oil recovery as miscible injection works more efficiently than the immiscible one (Clark et al. 1958; Bondor 1992). In this perspective, we developed a conceptual CO_2-EOR model keeping in mind S3+4, and a new injection scheme, a mixture of HC components and CO_2 that reduced the MMP from 134 to 93 bar, encourages for miscible CO_2 flooding. The details of this injection scheme will be discussed in the following section of this chapter.

The conceptual CO_2-EOR model consists of 4,99,100 (155 × 140 × 23) grid cells representing six sand layers of Hazad and Ardol formation and five shale layers alternatively within the sands representing Telwa and Kanwa formation (Fig. 3.5a). The resolution of the simulation grid cells in horizontal x-direction is 12.50 m, y-direction is 12.50 m and the average grid cell height is 2.37 m. The depth of the reservoir model extends from ∼1075 to 1265 m. The simulation model is penetrated by two wells, one injector (I1, water and CO_2) and one producer (P1). The production well is located in the up dip direction or at the crest of the model, while the injector is located in the down-flank. The average distance between the wells is around 920 m. Aquifer lying below the reservoir has provided a strong pressure support for oil production.

Further, to investigate the sensitivity of the grid and recommend an optimum grid solution with least computational cost, and to maintain numerical stability with a minimal loss of detail for the CO_2-EOR study, this cell model was coarsened (i.e.

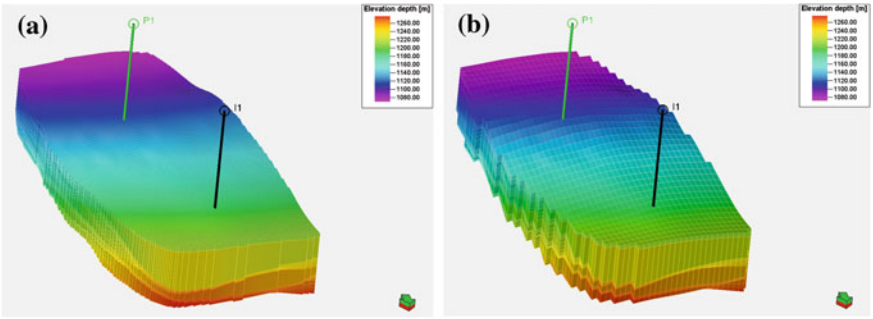

Fig. 3.5 Geometry of the 3D conceptual simulation model with one injector (I1) and one producer (P1) in depth domain: **a** very fine scale (*Left*), and **b** upscaled model (*Right*). The *arrow* at the *bottom right* indicates the geographical north

lower resolution) but maintaining the original heights. After this, the porosity and permeability distribution was upscaled based on those in the fine grid model using Petrel. This corresponds to a total of 29,716 (38 × 34 × 23) grid cells (Fig. 3.5b). Basically, Upscaling (or homogenization) is essentially an averaging process in which the static and dynamic characteristics (i.e. heterogeneous properties) of a fine-scale model are to be approximated by an equivalent homogeneous region made up of a coarse-scale model with an effective property value. For the upscaling process, we used a built-in algorithm of Petrel based on geometric mapping method and an arithmetic average algorithm for continuous properties.

3.3 Reservoir Flow Equations

The base of reservoir simulation is fluid flow in porous media, and the flow equations are based on a set of mass, momentum, and energy conservation equations and constitutive relations. These governing equations can be expressed by a set of partial differential equations (PDE), and ensures the conservation of mass for different fluid phases. For a single phase flow, the flow equation will take the following form,

$$\frac{\partial(\rho\emptyset)}{\partial t} + \nabla.(\rho v) = q \ , \tag{3.1}$$

where, v is the superficial velocity,ρ is fluid density, ∇ operator is the gradient operator (i.e. $\frac{\partial}{\partial x} + \frac{\partial}{\partial y} + \frac{\partial}{\partial z}$ operation for space in 3D-Cartesian coordinate) and q denotes a fluid source/sink term used to model the wells (injector/producer). On the other hand, the fluid velocity 'v' is related to the fluid pressure p through an empirical relation named after the French engineer, Darcy (1856) which is:

$$v = -\frac{k}{\mu}(\nabla p - \rho g z), \tag{3.2}$$

where k is the permeability, μ is the fluid viscosity, and g the gravity vector. Introducing the constitutive relations for porous material and fluid which includes the rock and fluid compressibilities, $c_r = \emptyset^{-1}(d\emptyset/dp)$ and $c_f = \rho^{-1}(d\rho/dp)$ respectively, Eqs. (3.1) and (3.2) can be combined to form a parabolic equation for the fluid pressure:

$$\emptyset\rho(c_r + c_f)\frac{\partial \rho}{\partial t} - \nabla.\left(\rho\frac{k}{\mu}(\nabla p - \rho g z)\right) = q\ . \tag{3.3}$$

In the special case of incompressible rock and fluid, Eq. (3.3) simplifies to Poisson's equation with variable coefficients,

$$-\nabla.(k\nabla\psi) = \frac{q\mu}{\rho}, \tag{3.4}$$

where $\psi = p - \rho|g|z$, is the fluid potential.

However, in general, the void space in a reservoir will generally be filled by both hydrocarbons and (salt) water. Also, water is frequently injected into the reservoir during a secondary recovery mechanism to improve hydrocarbon recovery. If the fluids are immiscible and separated by a sharp interface, they are referred to as phases. A two-phase system is commonly divided into a wetting and a non-wetting phase, given by the contact angle between the solid surface and the fluid-fluid interface on the microscale (acute angle implies wetting phase). On the macroscale, the fluids are assumed to be present at the same location, and the volume fraction occupied by each phase is called the saturation of that phase, and for a two-phase system the saturation of the wetting (Sw) and non-wetting phases (Sn) therefore sum to unity, Sn + Sw = 1.

In this section we will discuss the black oil formulation of multi-phase i.e., three phase flow (oil, gas, and water) in porous media (Fig. 3.6), and most of the equations and their solutions presented here are based on the textbook by Ertekin (2001), Chen et al. (2006) and Kleppe (2011).

In the absence of phase transitions, the saturations change when one phase displaces the other. During the displacement, the ability of one phase to move is affected by the interaction with the other phase at the pore scale. In the macroscopic model, this effect is represented by the relative permeability $k_{r\alpha}$ (α = oil (o), water (w), gas (g)), which is a dimensionless scaling factor that depends on the saturation and modifies the absolute permeability to account for the rock's reduced ability to transmit each fluid in the presence of the other. The multiphase extension is mathematically straightforward, but defining parameters such as relative permeability becomes more challenging. The multiphase extension of Darcy's law reads:

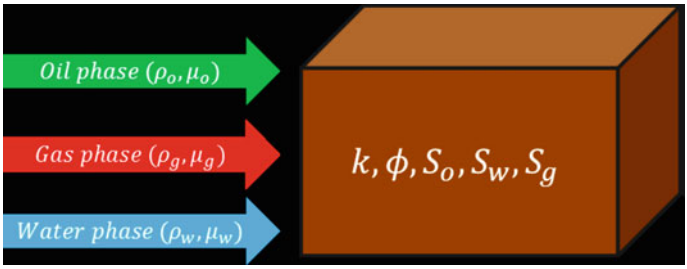

Fig. 3.6 Schematic illustration of multiphase flow through porous media. The *arrows* indicate at different phases in the reservoir

$$v_\alpha = -\frac{kk_{r\alpha}}{\mu_\alpha}(\nabla p_\alpha - \rho_\alpha g z), \tag{3.5}$$

which together with mass conservation of each phase forms the basic equation which is given by:

$$\frac{\partial(\rho_\alpha \emptyset S_\alpha)}{\partial t} + \nabla.(\rho_\alpha v_\alpha) = q_\alpha. \tag{3.6}$$

The partial differential equation of three phase flow is shown below:
Oil flow equation is:

$$\nabla.\left[\frac{\rho_o k k_{ro}}{\mu_o}(\nabla p_o - \rho_o g \nabla z)\right] = \frac{\partial(\rho_o \emptyset S_o)}{\partial t} + q_o, \tag{3.7}$$

Water flow equation is:

$$\nabla.\left[\frac{\rho_w k k_{rw}}{\mu_w}(\nabla p_w - \rho_w g \nabla z)\right] = \frac{\partial(\rho_w \emptyset S_w)}{\partial t} + q_w, \tag{3.8}$$

Gas flow equation is:

$$\nabla.\left[\frac{\rho_{Go} k k_{ro}}{\mu_{Go}}(\nabla p_o - \rho_o g \nabla z) + \frac{\rho_g k k_{rg}}{\mu_g}\left(\nabla p_g - \rho_g g \nabla z\right)\right] = \frac{\partial\left((\rho_{Go} S_o + \rho_g S_g)\emptyset\right)}{\partial t} + q_g, \tag{3.9}$$

where ρ_{Go} represents the part of gas at surface condition and others have their usual meaning as described earlier. Because of the interfacial tension, the pressure in the phases will differ. The pressure difference is called *capillary pressure*, $p_{cnw} = p_n - p_w$, and $S_o + S_w + S_g = 1$. The capillary pressure is usually assumed to be a function of saturation on macroscale.

After substituting black oil fluid properties, and including well rate terms, the flow equations i.e. (3.7), (3.8) and (3.9) become (3.10), (3.11) and (3.12), respectively as given by:

$$\nabla.[k\lambda_o(\nabla p_o - g\nabla z)] = \frac{\partial}{\partial t}\left(\frac{\emptyset S_o}{B_o}\right) + q_o, \tag{3.10}$$

$$\nabla.[k\lambda_w(\nabla p_w - g\nabla z)] = \frac{\partial}{\partial t}\left(\frac{\emptyset S_w}{B_w}\right) + q_w, \tag{3.11}$$

$$\begin{aligned}\nabla.\left[k\lambda_g\left(\nabla p_g - g\nabla z\right) + kR_{SO}\lambda_o(\nabla p_o - g\nabla z)\right] \\ = \frac{\partial}{\partial t}\left(\frac{R_{SO}\emptyset S_o}{B_o} + \frac{\emptyset S_g}{B_g}\right) + q_g + q_o R_{SO},\end{aligned} \tag{3.12}$$

where R_{SO} is solution gas-oil ratio, $\lambda_o = \frac{k_{ro}}{B_o\mu_o}$, $\lambda_w = \frac{k_{rw}}{B_w\mu_w}$, $\lambda_g = \frac{k_{rg}}{B_g\mu_g}$, B_o, B_w, B_g are the mobility and formation volume factor for oil, water and gas, respectively.

3.4 Numerical Solution

As these mathematical models become increasingly more complex, analytical solutions to reservoir flow equations are only obtainable after making simplified assumptions in regard to geometry, properties and boundary conditions that severely restrict the applicability of the solution. For mimicking the real reservoir conditions, such simplifications are not encouragable. Because of this, we need to solve these equations numerically. In general, the equations are spatially and temporally approximated for making them applicable in a computer solution scheme, where they are discretized and solution values calculated at computational nodes throughout a simulation grid, rather than as continuous functions (Aziz and Settari 1979; Dake 1983; Islam and Sepehrnoori 2013).

3.4.1 Discretization

Discretization is done with the help of grid system in which the computational nodes are placed (Fig. 3.7). The whole idea behind this is to divide the geological model into a number of cells, in which the solution variables such as pressure and saturation are held constant. The placement of computational nodes in the grid and discretisation methods of the governing PDEs are done in accordance with the specific numerical solution method applied in the simulation software.

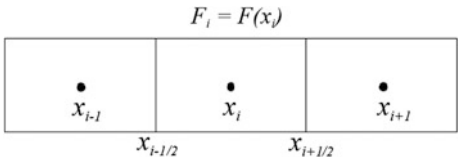

Fig. 3.7 Discretization notation

In the following, we will now use the discretization formulas of standard finite difference approximations to solve the PDEs appeared in the flow equations. In this context, we are interested in the transport term for all the phases α (=o, w, g; oil, water and gas, respectively) in the flow equations, i.e., $\nabla.[k\lambda_\alpha(\nabla p_\alpha - g\nabla z)]$. At this point, we restrict ourselves to 1D flow, and drop the time index for unknown pressures, so that if no time index is specified, $t + \Delta t$ is implied. Thus, we seek a finite difference approximation of the term:

$$\frac{\partial}{\partial x}\left(k\lambda\frac{\partial P}{\partial x}\right) = \frac{\partial}{\partial x}(F(x))(say), \tag{3.13}$$

where $k\lambda$ is known as "*transmissibility*", a measure of how easily fluid can flow between two grids since it is meaningless to represent "permeability at a point". From numerical analysis, it is known that central difference $\Delta F_i = F_{i+1} - F_{i-1}$, works better than forward and backward differences (Dimri 1992; Iserles 1996).

Using the central finite difference scheme, we finally obtain,

$$\frac{\partial}{\partial x}\left(k\lambda\frac{\partial P}{\partial x}\right) = \frac{1}{\Delta x_i}\left[(k\lambda)_{i+\frac{1}{2}}\left(\frac{P_{i+1} - P_i}{x_{i+1} - x_i}\right) - (k\lambda)_{i-\frac{1}{2}}\left(\frac{P_i - P_{i-1}}{x_i - x_{i-1}}\right)\right], \tag{3.14}$$

Equation (3.14) includes permeability and mobility evaluated at the *half-points*, hence permeability can be computed from two cell centres by treating as conductivity between the two cell centres. On the other hand, pressure is evaluated at the cell centre itself. Further, in three dimensions, and in terms of fluid potential (ψ), Eq. (3.14) becomes (only x-direction term is shown here):

$$\frac{1}{\Delta x_i}\left[\left(\frac{k_x\lambda}{\Delta x}\right)_{i+\frac{1}{2}}(\psi_{i+1} - \psi_i) - \left(\frac{k_x\lambda}{\Delta x}\right)_{i-\frac{1}{2}}(\psi_1 - \psi_{i-1})\right]\Delta y_j \Delta z_k = \Delta_x T_x \Delta_x \psi(say) \tag{3.15}$$

Similarly, Eq. (3.15) can also be written for y- and z-direction by cycling x, y, and z in the definition, and the total flow term can be given by,

$$\Delta T \Delta \psi = \Delta_x T_x \Delta_x \psi + \Delta_y T_y \Delta_y \psi + \Delta_z T_z \Delta_z \psi. \tag{3.16}$$

The black oil difference equations can be written as,

$$\Delta T_\alpha \Delta \psi_\alpha + q_{\alpha,ijk} = C_{ijk}\Delta_t(\emptyset S_\alpha B_\alpha), \quad \alpha = o, w \tag{3.17}$$

$$\Delta T_g \Delta \psi_g + \Delta R_{so} T_o \Delta \psi_o + q_{g,ijk} = C_{ijk}\Delta_t\left(\emptyset S_g B_g + \emptyset R_{so} S_o B_o\right), \tag{3.18}$$

Thus, we can see that the derived black oil equations are actually complex as it contains strongly non-linear terms such as mobility. To solve the system of equations, we need powerful technique such as Newton-Raphson method, The Gaussian elimination technique, Gauss-Seidel method, etc., but we will concentrate on Newton-Raphson method for this purpose which will be discussed in the Sect. 3.4.3.

3.4.2 Boundary Conditions

To obtain the solution, we must impose specific boundary conditions. We can assign two types of boundary conditions, the pressure specifications (Dirichlet-type conditions), and the flow rate specifications (Neumann-type conditions). In reservoir simulation, a pressure solution will normally be specified as a bottom-hole pressure of a production or injection well, at some position of the reservoir. However, practically this is not a boundary condition, but the treatment of this type of condition is quite similar to the treatment of a boundary pressure condition.

Alternatively, we would specify the reservoir flow rates at the end of the faces of the system. Using Darcy's equation at the end of the face of a simple 1D system for a reservoir of length L, this condition becomes,

$$Q_L = -\frac{kA}{\mu}\left(\frac{\partial P}{\partial x}\right)_{x=0} \quad \text{and} \quad Q_R = -\frac{kA}{\mu}\left(\frac{\partial P}{\partial x}\right)_{x=L}. \tag{3.19}$$

The flow rate condition may be specified as a production or injection rate of a well at some position of the reservoir, or it is designated as zero rates across a sealed boundary or fault, or between non-communicating horizons. No flow conditions at the boundaries are assigned by giving the respective transmissibility a zero value at that particular point.

3.4.3 Solution of Black Oil Equations—The Newton-Raphson Method

As noted, the black oil equations are strongly non-linear in terms of three linearly independent principal unknowns (most often one phase pressure and two

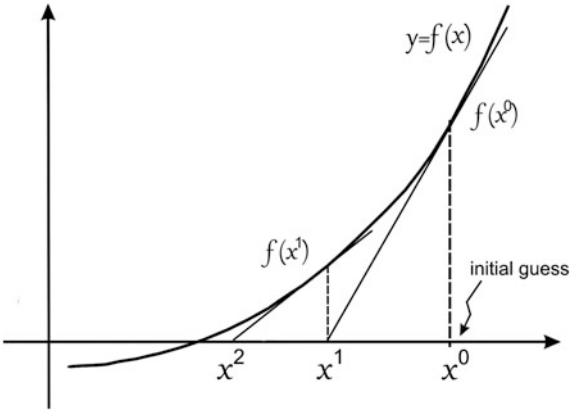

Fig. 3.8 An illustration of the Newton-Raphson method to solve a non-linear problem

saturations), therefore standard techniques are not applicable to solve these equations. We can linearize these equations using the generalized Newton-Raphson technique, such that we can implement a Newtonian iteration. This approximation implies that there exist an error, and it can be represented as a residual function whose derivative can be calculated with respect to each principal unknown to construct the Jacobian. The elements of the Jacobian matrix will be obtained using a numerical differentiation scheme.

Consider a non-linear equation $f(x) = 0$, where $y = f(x)$ is some function, e.g. one as shown in Fig. 3.8. The Newton-Raphson method can be best described by an algorithm as following,

1. Choose an initial guess or arbitrary starting point x^0, then find $y^0 = f(x^0)$.
2. Find the tangent to $y = f(x)$ at the point (x^0, y^0).
3. After that find the intersection x^1 between the tangents as evaluated from point (2) and the axis.
4. If $f(x^1) = 0$, or close to zero, then x^1 is the desired solution.
5. Else, continue procedure as in (2), (3), (4) until convergence is reached, defining points x^2, x^3,… approaching the solution.

We can see how the points x^0, x^1, x^2 approach the zero of $y = f(x)$, and easily satisfy ourselves that the solution is found (Fig. 3.7).

The tangent equation is $y = f(x^0) + f'(x^0) \cdot (x - x^0)$, and the point x^1 is found by setting $y = 0$ in this equation, so that we get,

$$x^1 = x^0 - \frac{f(x^0)}{f'(x^0)}. \tag{3.20}$$

At each iteration, we can define the difference between "present" and "previous" x as Δx^k. Then Eq. (3.20) can be written as:

$$f'\left(x^k\right)\Delta x^k + f\left(x^k\right) = 0. \tag{3.21}$$

This is the more suitable expression to generalize to several dimensions.

To get the difference form of the black oil equations, we rewrite Eqs. (3.17) and (3.18) by defining in slightly different way as given by,

$$\mathrm{F_1} = \Delta \mathrm{T_o} \Delta \psi_\mathrm{o} + \mathrm{q_{o,ijk}} - \mathrm{C_{ijk}} \Delta_\mathrm{t} (\emptyset \mathrm{S_o B_o}), \tag{3.22}$$

$$\mathrm{F_2} = \Delta \mathrm{T_w} \Delta \psi_\mathrm{w} + \mathrm{q_{w,ijk}} - \mathrm{C_{ijk}} \Delta_\mathrm{t} (\emptyset \mathrm{S_w B_w}), \tag{3.23}$$

$$\mathrm{F_3} = \Delta \mathrm{T_g} \Delta \psi_\mathrm{g} + \Delta \mathrm{R_{so}} \mathrm{T_o} \Delta \psi_\mathrm{o} + \mathrm{q_{g,ijk}} - \mathrm{C_{ijk}} \Delta_\mathrm{t} \left(\emptyset \mathrm{S_g B_g} + \emptyset \mathrm{R_{so} S_o B_o}\right), \tag{3.24}$$

Thus, the Eqs. (3.22)–(3.24) are now formulated equivalently as a system of equation such as $\mathrm{F_i} = 0,\ \mathrm{i} = 1, 2, 3$. In general, phase pressures and fluid saturations for the three phases (oil, water and gas) are considered as primary unknowns. The implementation step of Newton-Raphson technique has been shown in the form of flowchart in Fig. 3.9. The residual equations (R) can be obtained by simply the left hand side minus right hand side term of flow equation of each phase.

After the formulation of the residual of oil, water and gas flow equation, the Jacobian can be evaluated in order to form the linearized equation for solving the unknowns. The solution will be fully implicit in this case, and the problem can be set up as following,

Define the residual vector $R = \begin{bmatrix} R_o \\ R_w \\ R_g \end{bmatrix}$ and unknown vector

$$U = \begin{bmatrix} P \\ S_w \\ S_g \end{bmatrix}, \tag{3.25}$$

and the Jacobian matrix takes the form,

$$J = \frac{\partial R}{\partial U} = \begin{bmatrix} \frac{\partial R_o}{\partial P} & \frac{\partial R_o}{\partial S_w} & \frac{\partial R_o}{\partial S_g} \\ \frac{\partial R_w}{\partial P} & \frac{\partial R_w}{\partial S_w} & \frac{\partial R_w}{\partial S_g} \\ \frac{\partial R_g}{\partial P} & \frac{\partial R_g}{\partial S_w} & \frac{\partial R_g}{\partial S_g} \end{bmatrix}$$

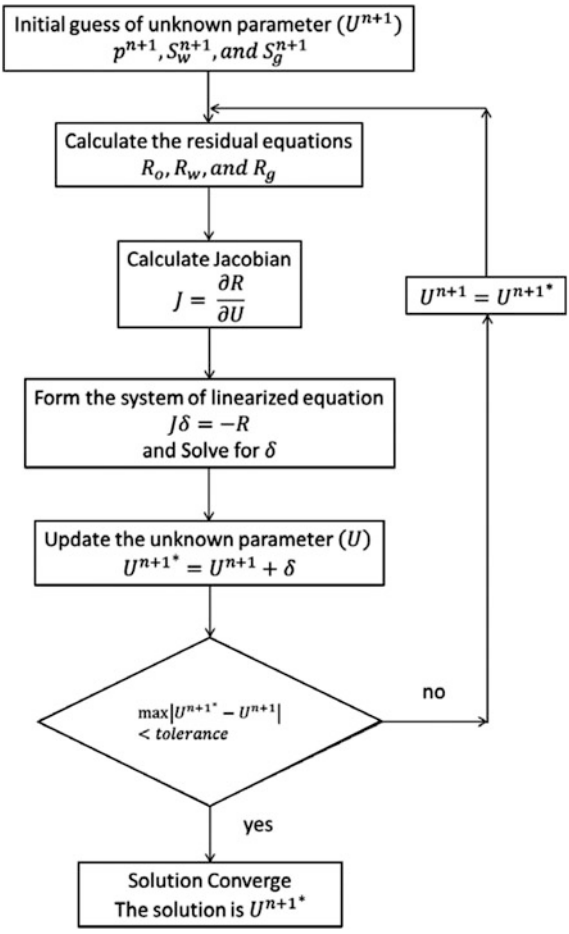

Fig. 3.9 Flowchart explaining the Newton-Raphson method used to solve the black oil system of equations

The Newton-Raphson iteration is,

$$J^{n+1*}\partial U = -R^{n+1*}$$

$$U^{n+1*} = U^{n+1} + \partial U. \tag{3.26}$$

The iteration will continue until the solutions are converged. When the solution is converged the norm of ∂U will approach to zero or smaller than some tolerance value. The mass change during the time step dt is, then proportional to $dM = M_{t+dt} - M_t$ with

$$M = PV \begin{bmatrix} \frac{S_o}{B_o} + \frac{R_{so}S_g}{B_g} \\ \frac{S_w}{B_w} \\ \frac{S_g}{B_g} + \frac{R_{so}S_o}{B_o} \end{bmatrix}, \tag{3.27}$$

where PV is the pore volume, and the other notations has their usual meanings as described earlier. When S_g is zero the solution variable becomes R_{so} (under saturated oil) and when S_o is zero it will become R_v, the vapour gas-oil ratio (under saturated gas).

3.5 Reservoir Flow Models

Efficiency of EOR practices relies profoundly on accurate reservoir models. Different types of flow simulation models are used to define various oil recovery mechanisms (Coats 1982). The most widely used flow models in reservoir simulations are black oil, compositional, thermal, and chemical model. In our study, we have used black oil and compositional model for reservoir simulation. The black oil model uses a simple PVT description in which the hydrocarbon chemical species are lumped together to form two components at surface conditions: a heavy hydrocarbon component called "oil" and a light hydrocarbon component called "gas", for which the chemical composition remains constant for all times. A typical lumping of the components can be CO_2, $N_2 + C_1$, $C_2 + C_3$, $C_4 + C_5$, C_6, C_7+ (where C_7+ includes all the remaining components of the fluid). Also, it is assumed that no mass transfer occurs between the water phase and the other two phases. At reservoir conditions, the gas component may be partially or completely dissolved in the oil phase, forming one or two phases (liquid and vapour) that do not dissolve in the water phase. In more general models, oil can be dissolved in the gas phase, the hydrocarbon components are allowed to be dissolved in the water (aqueous) phase, and the water component may be dissolved in the two hydrocarbon phases.

The black-oil model is often formulated as conservation of volumes at standard conditions rather than conservation of component masses by introducing formation volume factors $B_\alpha = V_\alpha / V_{\alpha s}$ (V_α and $V_{\alpha s}$ are volumes occupied by a bulk of component α at reservoir, and surface conditions) and a gas solubility factor $R_{so} = V_{gs}/V_{os}$, which is the volume of gas, measured at standard conditions, dissolved at reservoir conditions in a unit of stock-tank oil (at surface conditions). This type of simulator is very stable, common, and probably good starting practise in reservoir simulation.

On the contrary, compositional simulation model is analogous to black oil model as far as solution of flow equations is concerned. However, they differ significantly in their technique for mass balance as the later considers mass balance for each

component hydrocarbon component, such as methane, ethane, butane, propane, etc. For reservoirs containing light oil, the hydrocarbon component as well as pressure affects fluid properties. Compositional simulators use an equation of state with fugacity constraints and equilibrium flash calculations using *K*-values to determine hydrocarbon phase compositions. In practice, users sometime restrict the use of number of lighter components, and group heavier components into a pseudo-component. Thus, black oil model can be treated as *pseudo-compositional model* with two components (oil and gas, neglecting water).

The results from the compositional simulation are more reliable provided PVT characterization is very efficiently tuned by an expertise. However, one has to compromise with the computational cost as compositional simulation need huge computational time compared to the black oil simulation. Some of the important studies like CO_2-EOR and sequestration involve reaction of CO_2 with the reservoir pore space and fluid. For such studies, compositional simulation plays a crucial role, especially in the design of CO_2 recycling strategies including study of assessment of CO_2 breakthrough time and rate, and composition of produced fluids.

3.6 Fluid Flow Simulation Set up

Reservoir simulations were conducted to improve the understanding of the reservoir performance with respect to CO_2 injection. This process includes the calibration of an Equation-of-State (EOS) to describe the phase behaviour of reservoir fluid; necessary input data (e.g. fluid property description, pressure, Petrophysical properties, etc.); initialization of simulation model to access the volume of original hydrocarbon in place and prepare the model to predict future reservoir performance under CO_2-EOR operation. For the present study, we have used *Eclipse 100 and 300 (E-100, E-300)*, and *PVTi*, commercial software packages from Ms Schlumberger, and PVTSim by Calsep to conduct all the reservoir flow simulations, and to generate PVT characteristics of the compositional oil.

3.6.1 Reservoir Description and Fluid Properties

As discussed earlier, Ankleshwar is a mature and multi-layered anticline oil reservoir, which consists of 11 producing sandstones and alternating shale layer, located in Cambay Basin, Western India. It spreads over an area of $\sim$32.27 km^2 with the length of the reservoir structure of $\sim$17 km and width of $\sim$3 km. A summary of the Ankleshwar reservoir and the fluid properties are listed in the Table 3.1.

However, the reservoir properties for S3+4 horizons, the potential zone for CO_2-EOR, are slightly different from the average reservoir properties of

Table 3.1 Summary of Ankleshwar reservoir and fluid properties (ONGC report 2010)

Reservoir and fluid properties of the field (Operator report)		
Field/input data	Units	Values
Reservoir temperature	°C	78
Reservoir pressure	Bar	117.8
Saturation pressure	Bar	102.41
Average permeability	mD	500
Average porosity	%	23
Oil water contact	m	1190–1214
Gas oil contact	m	1050
Target zone depth	m	1113
Oil viscosity	Cp	0.36
Water viscosity	Cp	0.343
Density of stock tank oil	kg/Sm^3	820
GOR	lt/lt	23
B_o	Rm^3/Sm^3	1.44
Gas density	kg/Sm^3	0.739

Table 3.2 Summary of the reservoir properties of S3+4 horizons of Ankleshwar reservoir unit (ONGC report 2010)

Reservoir properties of S3+4 sand zone (Operator report)						
Field/input data	S4-1	S4-2	S4-3	S4-4	S3-1	S3-2
Effective thickness (m)	3.19	3.69	6.85	3.65	4.0	3.8
Porosity (%)	24.7	24.9	23.5	23.5	23.9	21.7
Permeability (mD)	540	1013	938	630	945	1953

Ankleshwar oil field (Table 3.2). The S3+4 layers have average porosity of 23% and permeability of 1000 mD respectively. The total thickness of the S3+4 sand zone is 26 ± 1.5 m.

3.6.2 Equation-of-State (EOS) Characterization

An essential part of a compositional simulation of miscible CO_2-EOR method is to predict the phase equilibria during EOR process. The aim is to tune an EOS that would simply reproduce the observed fluid behaviour and production characteristics seen in field operations, and helps to predict the CO_2/oil phase behaviour during compositional simulation study. It can also be used in the evaluation of minimum miscibility pressure for multiple contact miscibility. Cubic EOSs are used widely in

Table 3.3 Summary of the reservoir fluid composition, mol-fraction, molecular weight, and density of each component (ONGC report 2010)

Component	Mol-fraction	Molecular weight (g/mol)	Liquid density (g/cm^3)
N_2	2.280	28.014	0.2600
CO_2	0.850	44.010	0.4200
C1	79.310	16.043	0.2600
C2	7.480	30.070	0.3580
C3	5.980	44.097	0.5076
iC4	1.120	58.124	0.5633
nC4	1.580	58.124	0.5847
iC5	0.75	72.151	0.6246
nC5	0.75	72.151	0.6309
C6	15.98	86.178	0.6635
C7	16.36	96.000	0.7380
C8	13.73	107.000	0.7650
C9	8.10	121.000	0.7810
C10	6.03	133.000	0.7920
C11	4.29	145.000	0.7960
C12	4.10	158.000	0.8100
C13	3.53	171.000	0.8250
C14	2.86	185.000	0.8360
C15	2.05	198.000	0.8420
C16	1.56	209.000	0.8490
C17	1.54	226.000	0.8450
C18	0.95	242.000	0.8480
C19	0.80	251.000	0.8580
C20+	3.545	407.000	0.9000

the industry as it offers convenient and flexible calculation of the phase behaviour of reservoir fluids (Merrill and Hartman 1994; Pedersen et al. 2014).

Ankleshwar formation oil sample analysis data has been gathered through personal communication to ONGC. The reservoir oil in this field is very light to near volatile and the composition of the oil is illustrated in Table 3.3. Studies suggest that the swelling in the oil due to pure CO_2 injection is about 1.2 times of the volume (Dimri et al. 2012; Srivastava et al. 2015).

Due to the light hydrocarbon composition (average 46.3 API gravity), we preferred to use a 6-component Soave-Redlich-Kwong (SRK) EOS described in Table 3.4. SRK-EOS is used to obtain Z-factors and phase fugacities which are further used to define inter-phase equilibrium and fluid densities. PVT laboratory sample data including differential liberation experiments, constant composition expansion, swelling and separator test of Ankleshwar oil field were used in the tuning of the EOS for making it capable of characterizing the CO_2/oil system above the MMP.

Table 3.4 A six-component SRK-EOS model for Ankleshwar oil (46.3 API) with components

Component	Mw (g/gmole)	Pc (atm)	Tc (^{0}K)	Omega A	Omega B	Acentric factor
CO_2	44.0098	73.7646	304.200	0.4274800	0.0866400	0.22500
C1 + N2	16.3774	45.4252	187.522	0.4274800	0.0866400	0.00953
C2 + C3	36.3017	45.3936	340.155	0.4274800	0.0866400	0.12714
C4-C5	66.6494	35.0130	449.091	0.4274800	0.0866400	0.22119
C6	86.6619	29.6882	507.400	0.4274800	0.0866400	0.29600
C7+	138.4669	24.4821	617.857	0.4274803	0.0866404	0.64105

3.6.3 Calculation of Minimum Miscibility Pressure (MMP)

Whether the CO_2-EOR operation ensues in immiscible or miscible flood mode is decided by the MMP, and consequently estimation of the MMP is crucial.

In this case, we estimated the MMP through slim-tube simulations using E-300. The combined condensing and vaporizing drive mechanism was used in the MMP calculation at 78 °C. We identified that the MMP is around 134 bar (Fig. 3.10a), suggests that Ankleshwar oil is not miscible with pure CO_2 at the reservoir temperature and pressure (102 bar, and 78 °C). Thus, to lower the MMP, we developed a new injection fluid composition, consisting of 40% mole volume of CO_2, 10% methane, 20% ethane, 20% propane and 10% butane. The slim-tube simulation results shows that with the use of this injection fluid, the MMP was reduced from 134 to 93 bar (Fig. 3.10b).

3.6.4 Rock-Fluid Properties

Relative permeability is an important factor while describing multi-phase phenomena in a reservoir since the presence of multiple mobile fluids, viz., oil, water, and gas leads to reduction in flow capability. In general, relative permeability curves can be obtained by measurements on core samples in a laboratory. In case of non-availability of laboratory data, two phase relative permeability curves were generated using Corey's (Corey 1954; Stone 1970; Sigmund and McCaffery 1979) empirical correlations. The assigned residual oil saturations in water-oil (S_{orw}) and gas-oil (S_{org}) system were 0.25 and 0.2 respectively, and connate water and critical gas saturation were 0.18 and 0.005 respectively. Further it is assumed that there is no effect of hysteresis on the relative permeability. Capillary pressure was also neglected. The rock compressibility was taken as 2.16e-5 psi. The water-oil and gas-oil relative permeability curves illustrated in Fig. 3.11, were constructed using these values.

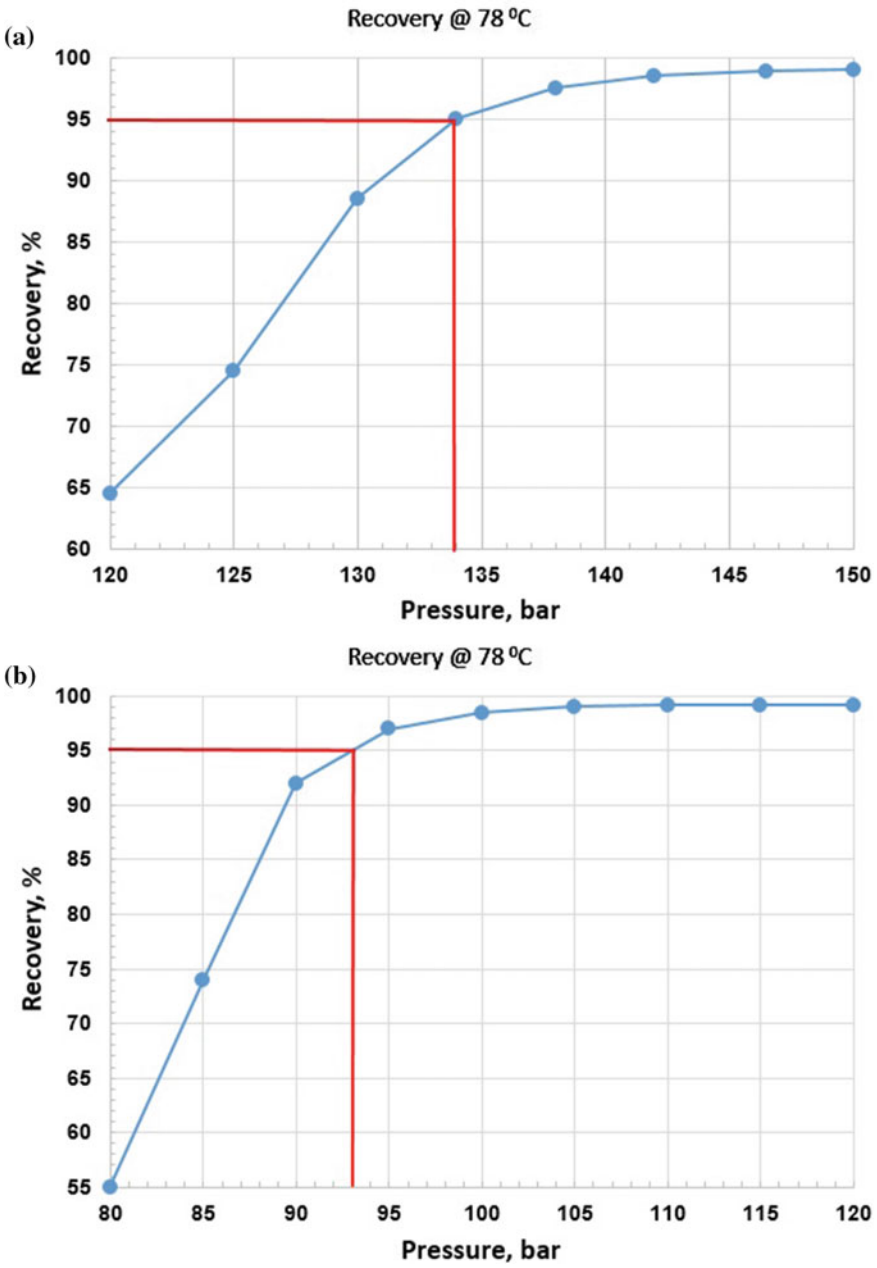

Fig. 3.10 Estimation of MMP at reservoir conditions: **a** before and **b** after introducing the new injection fluid composition, respectively

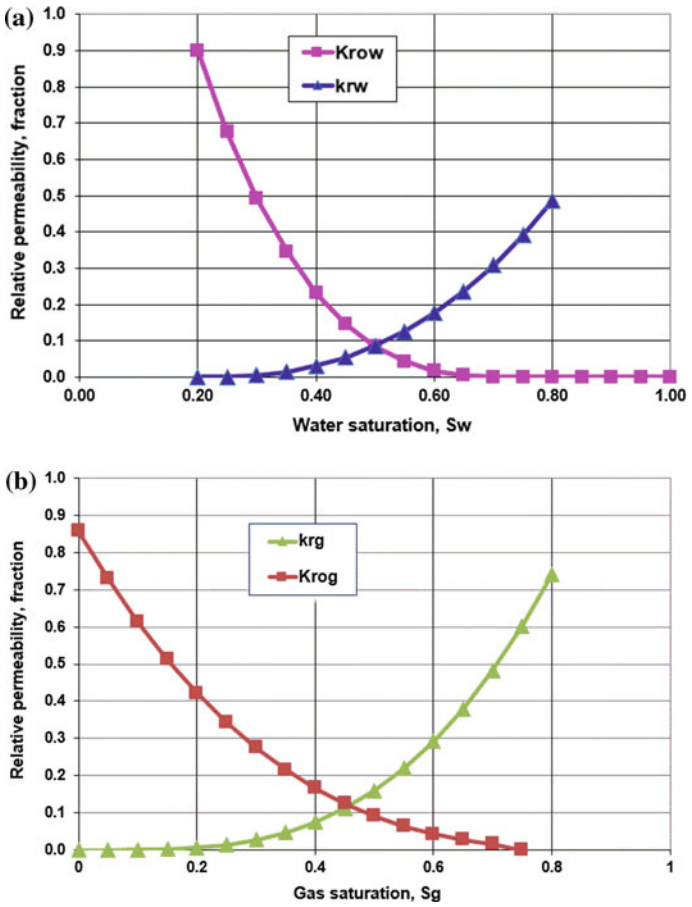

Fig. 3.11 Illustration of **a** Drainage oil/water relative permeability curves as a function of water saturation, and **b** Drainage gas/oil relative permeability curves as a function of gas saturation

3.6.5 Model Initialization and Validation

The model is initialized for reservoir simulation with reservoir temperature 78 °C and average reservoir pressure of 117.8 bar at a reference depth of 1113 m. Saturation pressure of the reservoir oil is 102.4 bar, and we considered the simulation model with under-saturated oil (no gas-cap condition) with oil API gravity of 47, and an enclosed aquifer with oil-water-contact (OWC) at 1202 m and gas-oil-contact (GOC) at 1050 m. The model is tuned to match the reported initial oil in place of 552 MMbbls. The wells were kept on production rate control for all the simulations.

3.7 Simulation Results and Discussion

We conducted several simulations broadly for three models as described in the previous Sect. 3.2.2. We started with the base case simulation bearing in mind the full field complex model that includes primary production for 2 years, and subsequent peripheral water injection for ~40 years to mimic the original field production scenario. This has been followed by performing the simulations for other two models, viz., sector and conceptual simulation model. The results from these models are described as following.

3.7.1 History Matching

In general, the validation of a reservoir model is obtained by simulating the past performance of the reservoir, and comparing the results with historical performance. In this case, history matching was performed using historical oil production rates as a constraint, and comparing the simulation results from the full field model to match historical cumulative oil production for water flooding period. The quality of the history matched has been judged by analysing how well the simulated oil and water production rates and reservoir pressure matched to the historical data.

Figure 3.12 depicts the results from the history matching. We observed that total cumulative field oil production (Sm^3) from the simulation of the complex full-field model is in good agreement with historical cumulative field oil production in Ankleshwar field. The match between simulated field oil production rate (Sm^3/day) and the oil production rate of Ankleshwar field is fairly good (Bottom: Fig. 3.12). However, the simulation model over predicts the total cumulative water produced in the field, and the water-cut scenario represents an opposite scenario during history matching (Top: Fig. 3.12). In addition to this, the simulation model under predicts the Ankleshwar field pressure. This is relevant since we have constrained the model with very limited pressure data provided by the operator. In the absence of required information from this old field, we couldn't do proper history matching but we managed to mimic the production curve based on random choice of producers and injectors. In order to overcome these limitations, we decided to develop a simulation model focusing on S3+4, the most productive horizons of the reservoir.

3.7.2 CO_2-WAG Injection Study from Sector Model

As per the present study's aim, we developed a sector model by constraining it with the properties of S3+4, major oil bearing sand horizons of the reservoir holding 552 MMbbls oil in-place. We conducted a feasibility study to evaluate the potential of CO_2-WAG injection for the recovery of residual oil from this mature field. The

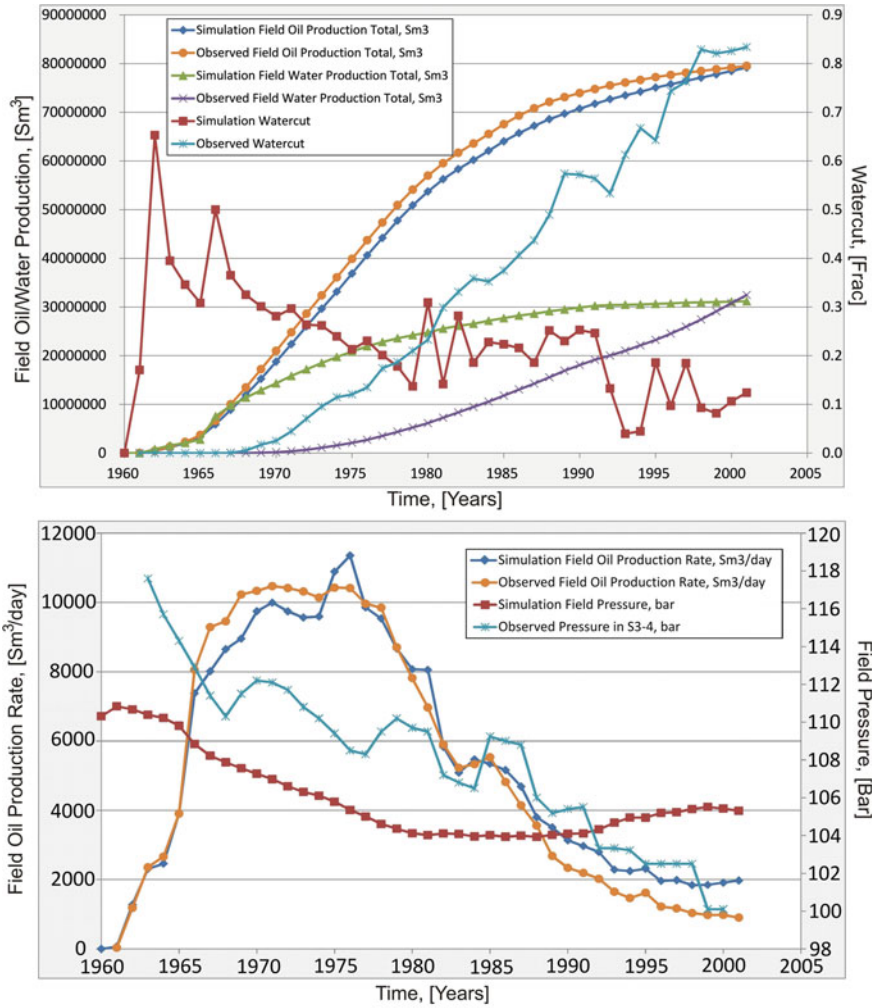

Fig. 3.12 Results from history matching, comparison of the simulated and observed data: total cumulative field oil and water production and water-cut scenario (*Top*), and the field oil production rate and field pressure behaviour (*Bottom*)

CO_2-WAG process involves alternating cycles of equal volumes of CO_2 and water at constant CO_2/water ratio, resulting in efficient displacement of oil towards the production wells by overriding gas and under riding water fronts.

All the wells used in this simulation study are vertical with an effective wellbore radius of 10.2 in. The skin factor at the wellbore was assigned zero value. Initially, the well placement pattern was adopted following the patterns implemented by the

operator (Fig. 3.4). However, some of the injection wells were drilled selectively, keeping in view the permeability variation and heterogeneity of reservoir sands.

The results from the sector simulation are shown in Fig. 3.13. It is interesting to note a significant increase in field oil production, from 200 to 1100 Sm^3/day after the implementation of CO_2-WAG (started in the year of 2005) with 1-month cycle of alternating water and CO_2 injection (at reservoir conditions). A noticeable decrease in water production, from 5800 to 3000 Sm^3/day, is also observed.

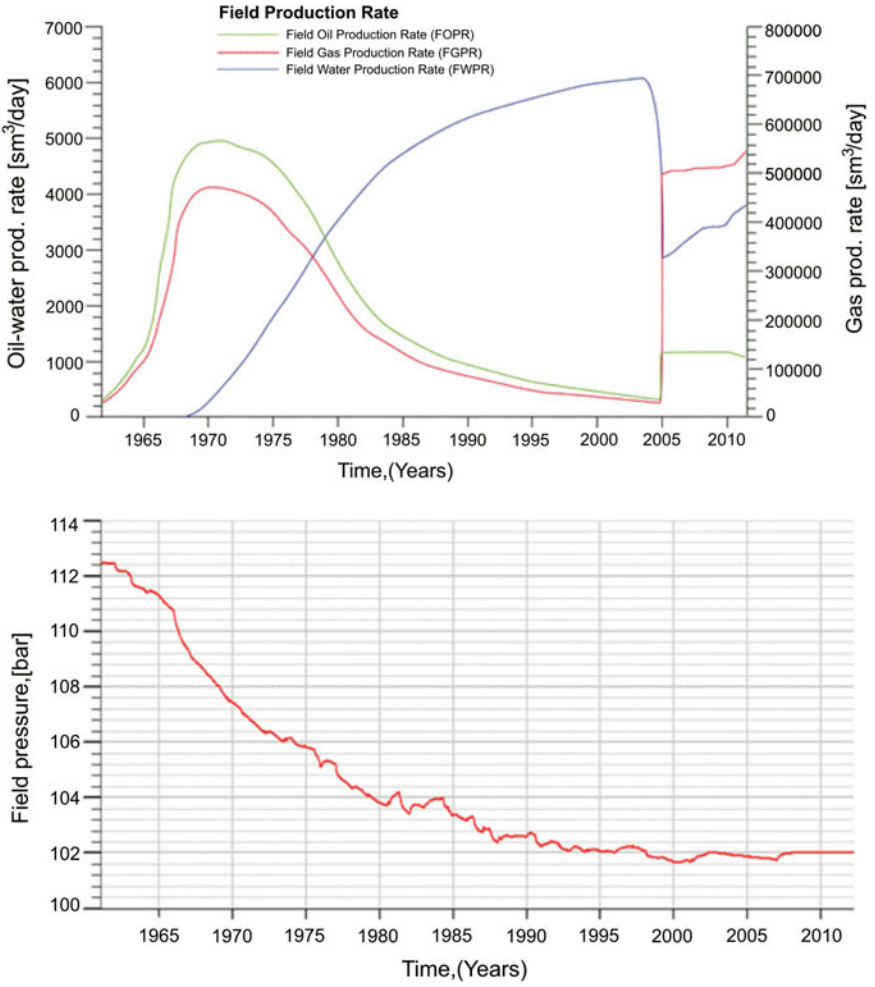

Fig. 3.13 The production profile of the reservoir in response to massive water flooding followed by CO_2-WAG process: oil, water and gas production (*Top*) and simulated reservoir pressure behaviour for the whole process (*Bottom*). The primary oil production (*green curve*) started in 1961 and peaked in the year 1967. Later, water flooding started which results in more water production (*blue curve*) with little oil production, continued until the end of 2004. This has been followed by CO_2-WAG technique with 1-month cycle of alternating water and CO_2 injection, showing significant oil production (*green curve*) after 2005

Increased oil production sustains a plateau for period of five years before declination in 2010; however water production increases steadily after initial drop in 2005. The preliminary analysis from the sector simulation model indicates ~5% of incremental oil recovery with the implementation of CO_2-WAG process.

3.7.3 *Feasibility of CO_2-EOR from Conceptual Model*

In order to optimize the CO_2 flooding technique for Ankleshwar reservoir, two different injection mechanisms viz., CO_2-WAG and continuous CO_2 injection have been incorporated in this study. As discussed in the previous Sect. 3.7.2, the CO_2-WAG scheme reports in total oil recovery factor of ~5% which is comparatively less than the recovery efficiency (~11.8%) reported by the operator from laboratory experiments. On the other hand, it has been seen that CO_2-WAG schemes do not contribute to maximize CO_2 storage, since some of the pore space is allocated for the water that otherwise could be occupied by CO_2 (Kovscek and Cakici 2005). Therefore, for long term project including EOR followed by CO_2 storage, we need to perform a systematic study. In the view of this, we developed a conceptual simulation model with one injector and one producer, and conducted sensitivity analysis of various operational parameters such as grid size, Corey exponent for oil and water, etc. Also, we have investigated the possibility of miscible flood displacement by tuning the Todd-Longstaff (T&L) mixing parameter for attaining optimized recovery factor from this mature oil field. The bottom-hole-pressure (BHP) of the producer was maintained at 102.9 bar, which is above the bubble point pressure. To mimic the reservoir conditions, the conceptual model was subjected to water flooding for about 50 years followed by continuous gas injection for next 30 years.

3.7.3.1 Grid Sensitivity Analysis

It is well-known that there is always a tradeoff between computational time and accuracy while performing simulations. In general, very fine grid simulations are more accurate than coarser ones, but computational time is more for fine grid models. Hence, to select optimum grid size for simulation, four cases were tested with grid sizes ranging from very fine scale, viz. 12.5 m (155 × 140 × 23) to coarse scale, i.e.100 m (19 × 17 × 23). The petrophysical properties like permeability and porosity were upscaled accordingly for each grid resolution. Our aim is to recommend an optimum grid size for the model, which can adequately represent the reservoir geometry and correctly describe the reservoir behavior with a good agreement with the fine scale compositional oil model.

The field oil production rates (FOPRs) for various grid sizes are shown in Fig. 3.14. About two years after the CO_2 injection in 2016, the oil production increases rapidly for 12.5 m grid model (green line) and 25 m grid size grid model

(red line), but these models are very expensive in terms of the computational cost. The field oil recovery efficiency (FOE) also follows the trend similar to oil production rate (Fig. 3.14b).

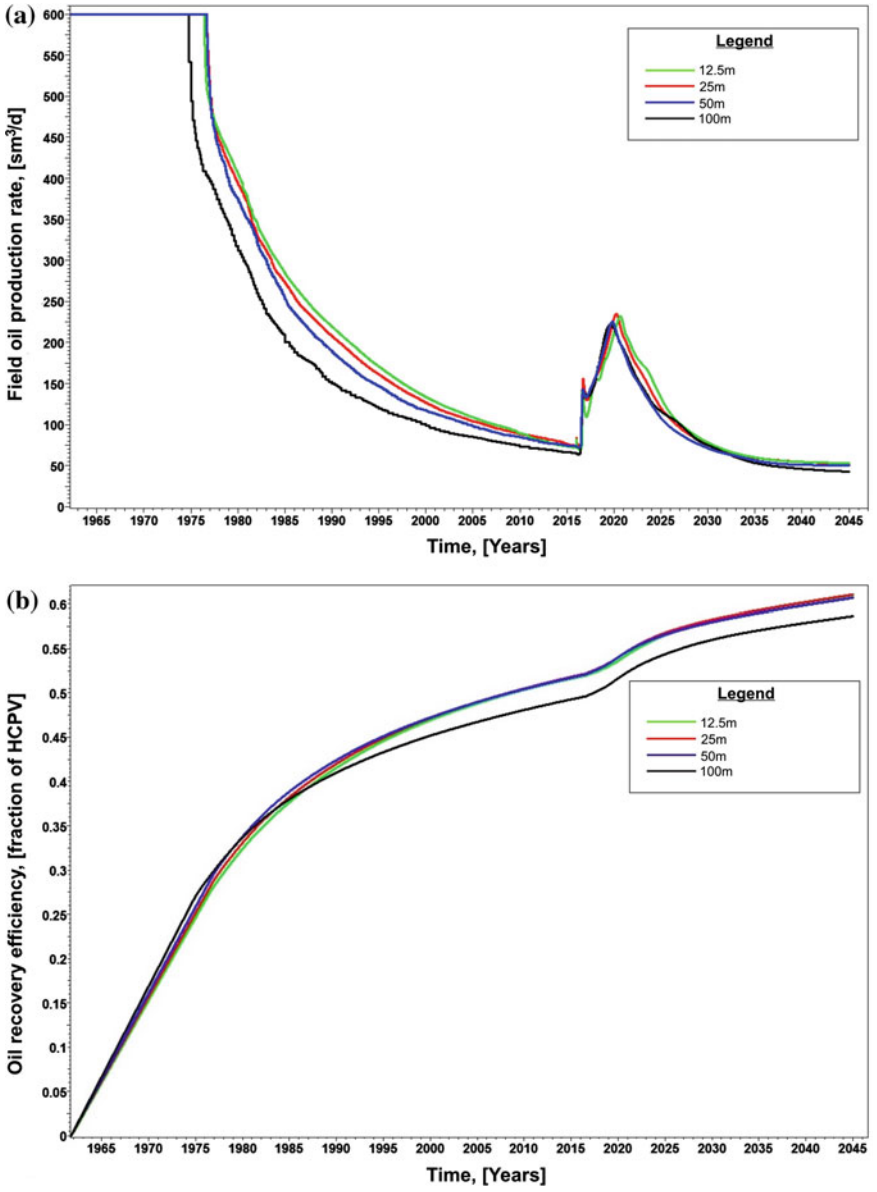

Fig. 3.14 The oil production and recovery profile from the simulation of conceptual model: production (*Top*) and recovery efficiency (*Bottom*). Legend represents the different values of grid size in X and Y direction; where *green curve*, *red curve*, *blue curve* and the *black curve* represents 12.5, 25, 50 and 100 m grid resolution, respectively

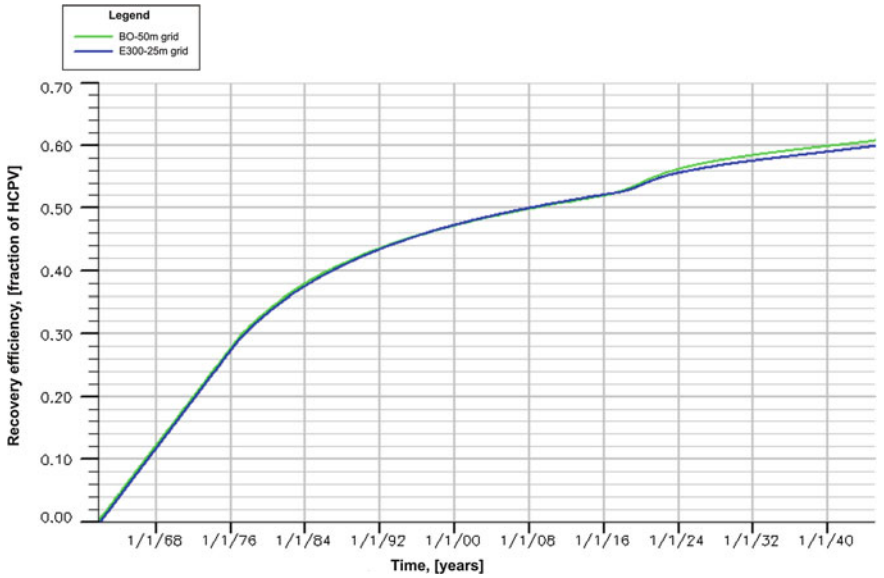

Fig. 3.15 Comparison between fine grid compositional (25 m) and medium grid black oil simulation model (50 m) for estimating the oil recovery efficiency. *Blue curve* and *green curve* represents compositional model with 25 m grid size, and black oil simulation model with 50 m grid size in X- and Y direction, respectively

We also found that the recovery factor obtained from the simulation of 50 m grid black oil model is in good agreement with the recovery factor of 25 m compositional model (Fig. 3.15), which is widely accepted for its accuracy. Therefore, we decided to choose 50 m grid black oil model as the optimized model to describe the reservoir behaviour in response to CO_2-EOR, and further analysis are conducted based on this model.

3.7.3.2 Sensitivity Analysis of Corey Exponent for Oil and Water

Relative permeability, between constrained end-points, is controlled by the Corey exponents, N_w (water) and N_o (oil). In general, Corey's exponents are obtained from the relative permeability curves generated using laboratory studies. In case of non-availability of laboratory data, two phase relative permeability curves can be generated by considering the empirical correlations (Corey 1954; Stone 1970; Sigmund and McCaffery 1979).

For unconsolidated sands, oil-water Corey exponents of 3.0 and 3.5 have been proposed in literature (Honarpour et al. 1986). It is noteworthy that lower Corey exponent values result in more concave relative permeability curve, thus lower the

relative permeability, indicates more sand heterogeneity, while higher exponent values result in comparatively a less concave curve, indicates more homogeneous sand (Kevin 2002). Corey's exponents are reservoir specific, hence its value must be adjusted based on simulation results. To analyze the effect of Corey water exponent (N_w) and oil exponent (N_o) on reservoir performance, we selected values of N_w and N_o typically as 3, 4, and 5 in a consistent manner by keeping one fixed at a time, which covers wide range of heterogeneity of the sand layers. Hence, we assumed that the wetting phase is water and non-wetting phase is oil.

We observed that the field oil production rate (FOPR) and field oil recovery efficiency (FOE) decreases drastically with the increase of value of N_o (Fig. 3.16a, b). These results are reasonable as previous studies suggest that the oil permeability and recovery decrease with an increase in N_o (Corey 1954). However, an opposite scenario is seen for N_w. We observed increase in FOPR and FOE with increase in the exponent (Fig. 3.16c, d). We selected the values of $N_o = 3$ (red solid line) and $N_w = 5$ (green curve) as for these values reservoir performance was found to be better.

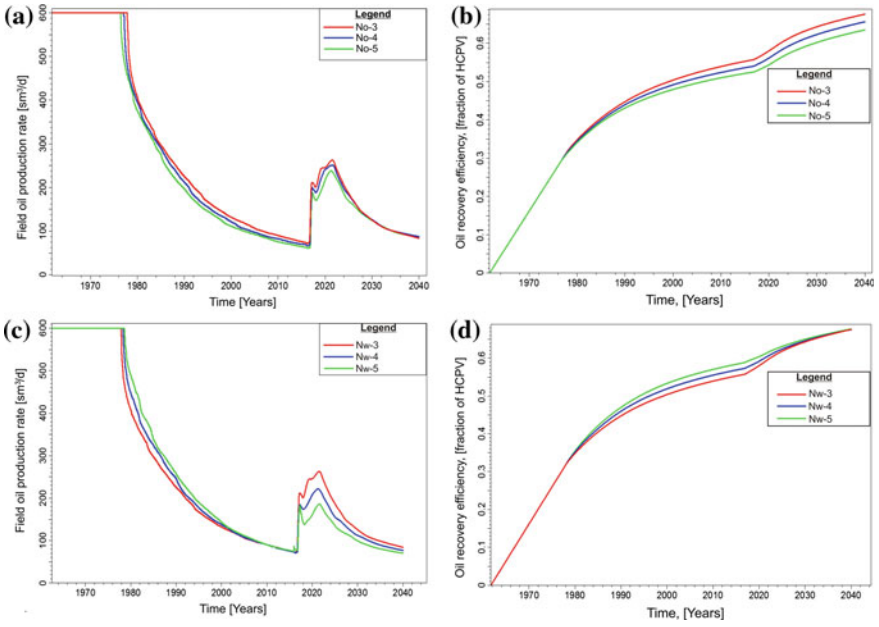

Fig. 3.16 Sensitivity analysis of different Corey exponents for oil (N_o) and water (N_w) on production scenario: field oil production rate (*Left*) and the field oil recovery efficiency (*Right*). *Red curve*, *blue curve* and *green curve* represents the value of Corey exponents for oil and water as 3, 4 and 5, respectively

3.7.3.3 Sensitivity Analysis of Todd-Longstaff (T&L) Parameter

Todd and Longstaff (1972) have proposed an empirical mixing parameter (ω), known as T&L mixing parameters, particularly for viscosity and density calculations to define the effective properties during miscible displacement. These parameters are generally used for field scale miscible flood simulations, particularly, for CO_2 flooding in a reservoir. Use of these parameters can circumvent intensive computations for the compositional simulation, without compromising the accuracy level. The values of ω lie between 0 and 1, and control the degree of injected fluid mixing within each grid cell. The value ω = 1 suggests that the fluids are miscible in each grid cell and if ω = 0, the fluids are immiscible (Todd and Longstaff 1972). These parameters are also adjusted on the basis of simulation results. Thus, to analyse all possible scenarios, we considered different combinations of values of ω for viscosity and density computations, demonstrated in Table 3.5.

Figure 3.17 depicts the sensitivity of T&L mixing parameters on reservoir performance. We observed promising results for 'ω' = 1, 0.67 for viscosity and density computations, respectively (brown curve). However, for ω = 1, 0.33, the field oil production peaked during gas injection period (pink curve), but the field oil recovery efficiency curve was not satisfactory. Hence, the optimum values of 'ω' for viscosity and density computation were selected as 1 and 0.67 respectively. Miscible CO_2 injection can be possible by considering the optimum T&L parameters suggested by this sensitivity analysis. This allows more injection of gas into the reservoir, and hence results in incremental oil recovery.

3.7.3.4 Estimation of CO_2-EOR Potential

After performing the simulations using 3D conceptual model, we estimated an additional oil recovery of about 10.4% of OOIP can be achieved from this field as a

Table 3.5 Different T&L mixing parameters (ω) used for the viscosity and density calculations during miscible displacement

T&L parameter for viscosity	T&L parameter for density
0.33	1
0.67	1
0.33	0.67
1	0.33
0.67	0
0.67	0.67
0.33	0.33
1	0.67
0	0.33
0.33	0
1	0
0	0.67

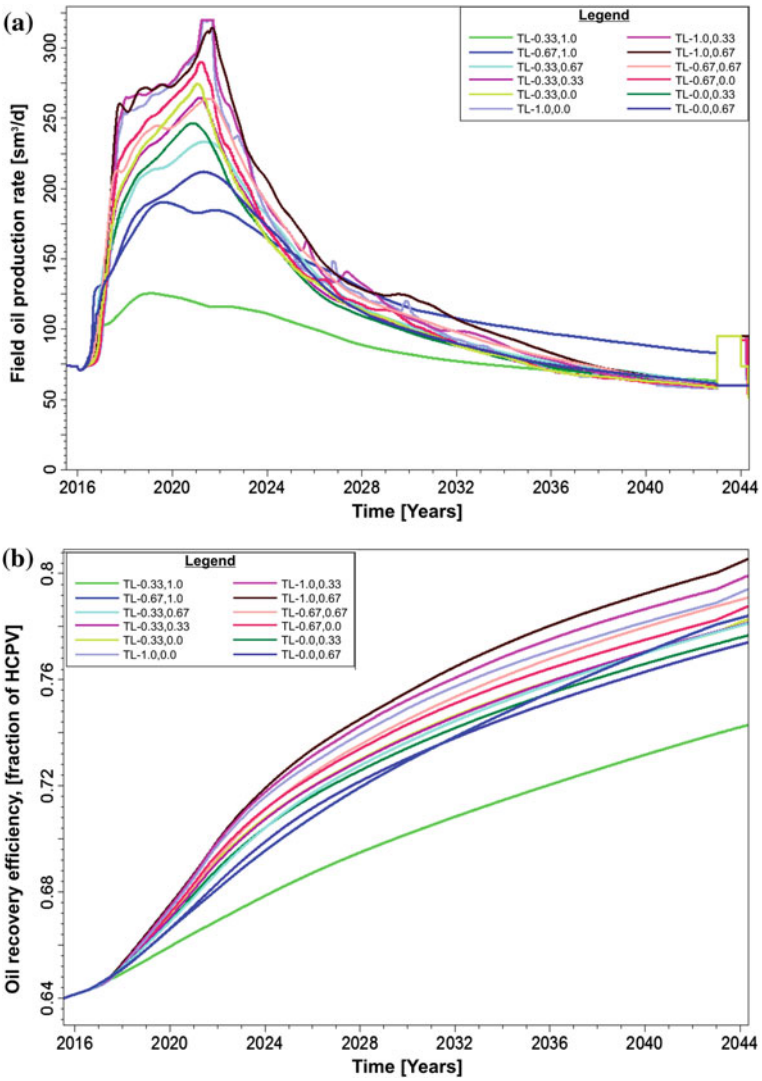

Fig. 3.17 The effect of various T&L parameters on: the field oil production rate (*Top*), and the oil recovery efficiency (*Bottom*) for the conceptual CO_2-EOR model. *Colour bar* represents the different combination of the T&L mixing parameters for viscosity and density calculations

result of CO_2-EOR. At the end of 2044, one could determine the incremental oil attributable to CO_2-EOR by calculating the difference in production rate and recovery factor between the projected decline rates without CO_2 injection (i.e., continuous water injection, represented by solid curve) and continuous CO_2 injection (dash-dot curve), illustrated in Fig. 3.18.

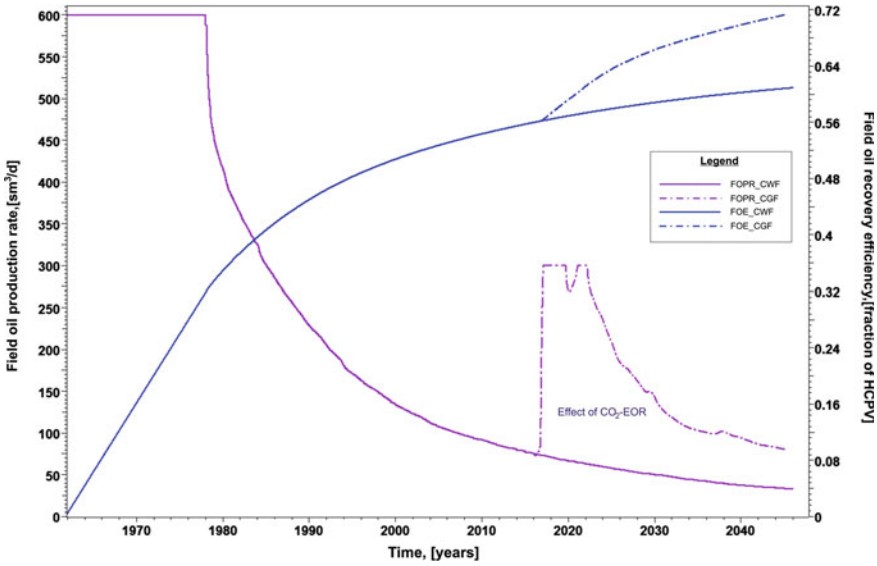

Fig. 3.18 The quantitative estimation of CO_2-EOR potential for Ankleshwar oil field in Cambay Basin, India. The field oil production rate (*magenta curve*) and oil recovery efficiency (*blue curve*) has been plotted as a function of time. The solid line represents the result from continuous CO_2 flooding, while *dashed-dotted line* represents continuous water flooding. The difference in results from continuous CO_2 flooding and water flooding helps to estimate the incremental oil recovery from this field

3.7.3.5 CO_2 Distribution in the Reservoir

Once the operational parameters are adjusted, we carried out simulations using E-100 (Black oil simulator). The conceptual model was subjected to water flooding for about 50 years followed by continuous gas injection for next 30 years. Changes in the lateral spreading of CO_2 with time in the reservoir can provide qualitative insights into the plume dynamics. Simulation results indicate patchy CO_2 distribution, with highest saturation in the top-most layer of the reservoir (Fig. 3.19).

The saturation of reservoir fluids at different stages i.e. from beginning to till the end of CO_2 injection period is shown in Fig. 3.20. We also noticed that the oil saturation is comparatively less near the high gas (CO_2) saturated zones, which suggests that CO_2 has successfully dragged the residual oil towards the production well for incremental oil recovery. Results from the simulation not only demarcated reservoir areas with high oil saturation, but also revealed that the mobility ratio needs to be improved for better incremental oil recovery. This information can be useful for the production engineers to plan the drilling strategy for optimum tertiary oil recovery.

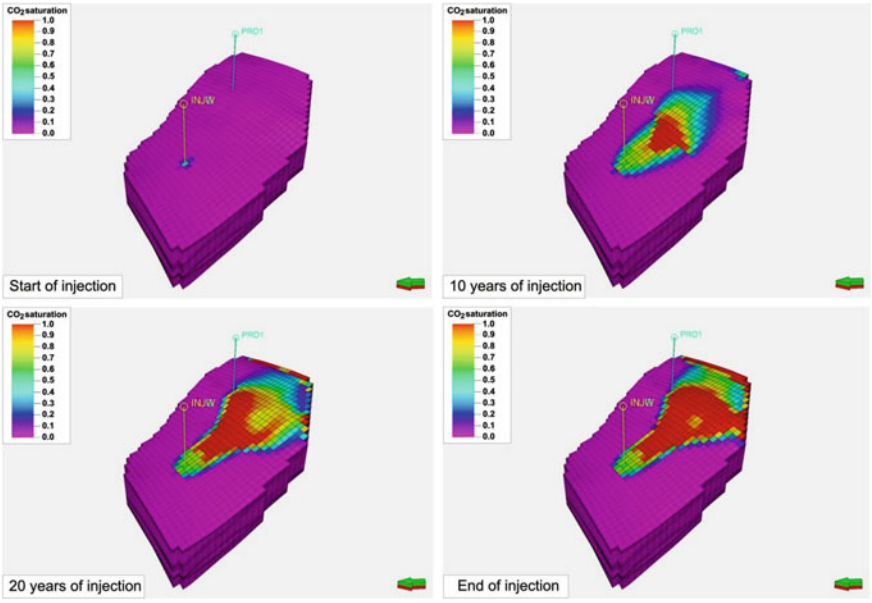

Fig. 3.19 Time lapse CO_2 saturation in the reservoir as a consequence of CO_2 flooding for EOR. The *colour bar* represents the CO_2 saturation, where *red* and *pink* represents maximum and minimum CO_2 saturation, respectively. Note that as the time spent, layer edges are comparatively found to be accumulated more CO_2 than other part of the reservoir

3.7.4 Calculation of Theoretical CO_2 Sequestration Capacity of Ankleshwar Oil Field

In case of high water cut reservoirs, the theoretical CO_2 sequestration capacity includes three parts, theoretical sequestration capacity (a) in free space of oil reservoir, (b) dissolving in water, and (c) dissolving in oil (Bachu et al. 2007; Zhao et al. 2014). The theoretical sequestration capacity (M_{co_2t}) can be represented by

$$M_{co_2t} = M_{co_2displace} + M_{co_2inoil} + M_{co_2inwater}. \tag{3.28}$$

In this case, $M_{co_2displace}$ is the sequestration capacity in the process of CO_2 flooding, M_{co_2inoil} and $M_{co_2inwater}$ are the sequestration capacities of CO_2 dissolved in crude oil and water, respectively. The sequestration capacity in the process of CO_2 flooding can be obtained by,

$$M_{co_2displace} = \rho_{co_2r}(R_f \times POIP - V_{iw} + V_{pw}), \tag{3.29}$$

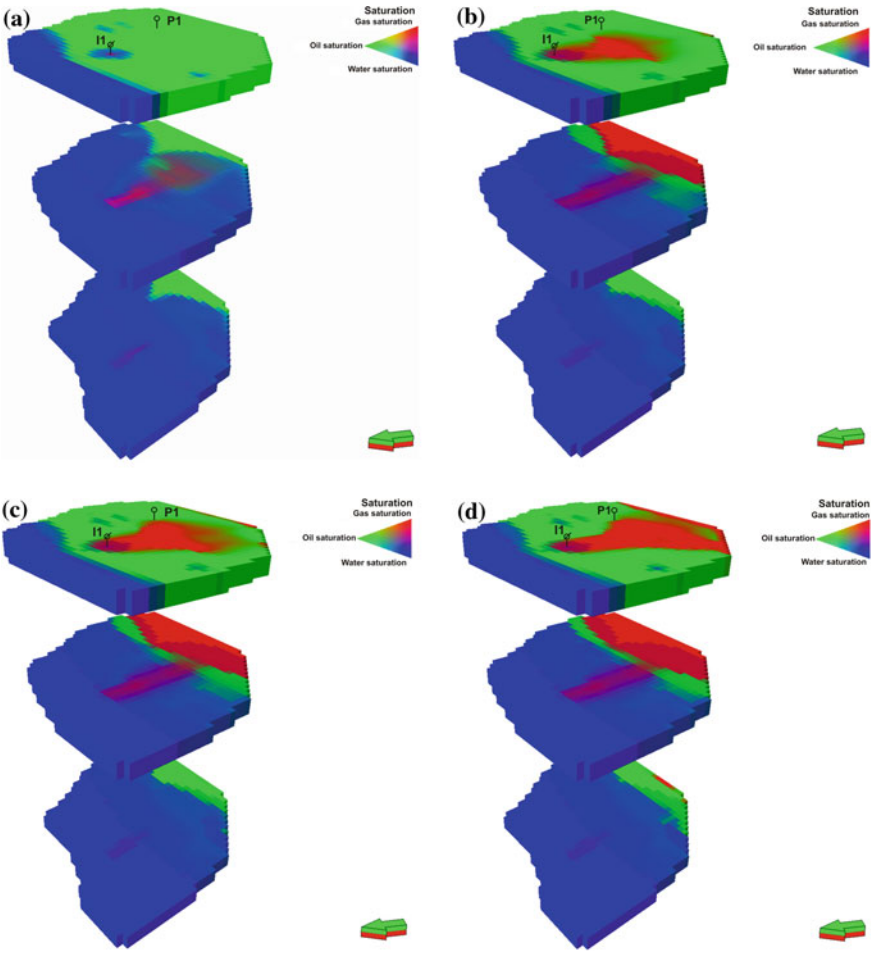

Fig. 3.20 Time lapse ternary diagram of saturation of reservoir fluids at different time scales due to CO_2 flooding in the reservoir: **a** after gas breakthrough, **b** after 10 years, **c** after 15 years and **d** at the end of CO_2 injection, respectively. The *colour bar* represents the saturation of various reservoir fluids, where *red*, *green* and *blue* represents CO_2 saturation, oil saturation and water saturation respectively

here, ρ_{co_2r} is the density of CO_2 at Ankleshwar reservoir temperature and pressure conditions; R_f is the oil recovery factor as obtained from the simulation; POIP is the amount of oil in the reservoir after water flooding; V_{iw} and V_{pw} are the volumes of injected and produced water, respectively.

$$M_{co_2 displace} = 0.233 \times 10^3 \times \left[(0.53 \times 169.017 \times 10^6) - 87.22 \times 10^6 + 45.03 \times 10^6\right]$$
$$= 0.233 \times 10^3 \times (47.554) \times 10^6 = 11.079 \times 10^6 \text{ metric ton (Mt)}$$

The sequestration capacity of CO_2 dissolved in crude oil ($M_{co_2 \text{ in oil}}$) can be evaluated using the following equation

$$M_{co_2 inoil} = E_f \times \rho_{co_2 r} \times POIP \times (1 - R_f) \times m_{co_2 inoil}, \tag{3.30}$$

where $m_{co_2 inoil}$ is the solubility of CO_2 in oil, and E_f is the sweep efficiency of CO_2 displacement, which can be obtained by:

$$E_f = \left[\frac{\text{oil formation volume factor} \times \text{cumulative oil produced}}{(\text{Pore Volume}) \times (1 - \text{irreducible water saturation} - \text{residual oil saturation})} + \frac{\text{initial gas saturation}}{(1 - \text{irreducible water saturation} - \text{residual oil saturation})}\right]$$
$$= \frac{1.44 \times 0.4761 \times 10^9}{(2415.172) \times 10^9 \times (1 - 0.18 - 0.25)} + \frac{0.15}{(1 - 0.18 - 0.25)} = 0.498 + 0.2631 = 0.761$$

Hence, $M_{co_2 \text{ in oil}} = 0.761 \times 0.233 \times 10^3 \times 169.017 \times 10^6 \times (1 - 0.53) \times 0.238 = 3.355 \times 10^6$Mt.

Also, the sequestration capacity of CO_2 dissolved in water ($M_{co_2 inwater}$) is given by:

$$M_{co_2 inwater} = E_f \times \rho_{co_2 r}(PWIP + V_{iw} - V_{pw}) \times m_{co_2 inwater}, \tag{3.31}$$

here $m_{co_2 inwater}$ is the solubility of CO_2 in water, and PWIP is the amount of water in the reservoir after water flooding, respectively. The values of $m_{co_2 inoil}$ and $m_{co_2 inwater}$ were computed using the empirical formulas suggested by Emera and Sarma (2006).

$$M_{co_2 inwater} = 0.761 \times 0.233 \times 10^3 \times [(42.19 + 87.22 - 45.03) \times 10^6] \times 0.0409$$
$$= 0.761 \times 0.233 \times 10^3 \times 3.451 \times 10^6 = 0.612 \times 10^6 \text{Mt}$$

Thus, $M_{co_2 t} = (11.079 + 0.612 + 3.355) \times 10^6$ Mt $= 15.046 \times 10^6$ Mt.

Therefore, from the conceptual model we found that Ankleshwar reservoir has the potential to sequestrate 15.04 million metric ton of CO_2. However, the amount of storage capacity will increase to ~150.4 million metric tons if the full field reservoir is considered since the full-field model is about 10 times in size than this conceptual model. In this way if we can identify 10 to 15 more potential reservoirs for CO_2 storage in India, then we could restrict the CO_2 emission by sequestrating ~2256 million metric tons in sedimentary formation.

3.8 Conclusions

In order to test the feasibility of the CO_2-EOR pilot project at Ankleshwar oil field, we developed various 3D reservoir models and performed fluid flow simulations. The following conclusions were reached:

- In total, three reservoir models of various sizes were developed based on the structural contour maps, well-logs, well-tops, etc., and reservoir properties such as porosity, permeability, saturation, etc., were incorporated in the geomodels to mimic the reservoir conditions for predicting the reservoir response with respect to CO_2 injection. Basically, two injection schemes including WAG and continuous CO_2 injection were considered to recommend better scheme for enhanced oil recovery from this mature field. We identified that continuous CO_2 injection option is better for both, EOR and storage, providing $\sim$10.4% of additional oil recovery which is close to the estimate primarily made by the operator (ONGC) in the laboratory and CO_2 sequestration of 15.04 million metric ton.
- History matching study suggests that more pressure data and water production data constraints from additional wells have to be integrated for better match between the projected and actual production profiles. However, the projected oil production rate (Sm^3/day) is in good agreement with the actual production rate from the most productive zone (S3+4 sand layers) of the reservoir.
- During the sensitivity analysis, we studied the impact of various operational parameters such as grid size, Corey exponent for oil and water, and T&L mixing parameters for miscible flood displacement on reservoir performance. Results suggest that the reservoir performance during CO_2 flooding was influenced by several factors, and accordingly optimum parameters were recommended for improved oil recovery.
- We propose a 50 m grid size (horizontal x-and y directions) black oil model with the optimized parameters for industrial scale simulations. This model is in good agreement with the fine scale (25 m grid) compositional simulation model of high accuracy. For miscible displacement, optimum values of T&L mixing parameter for viscosity and density calculations were selected as 1 and 0.67 respectively. We also synthesized a new injection fluid, which can reduce the MMP for miscible and more efficient displacement of CO_2.

Thus, the present study shows interesting and optimistic results for the possible CO_2-EOR and storage in Ankleshwar oil field. However, keeping in mind the age of platform, the operator should evaluate the proposal very carefully before initializing a field scale CO_2-EOR. Since CO_2 is corrosive in nature, the operator has to assess the cost of well work-overs and CO_2 transport compared with the gain due to incremental oil recovery.

References

Akervoll I, Bergmo PE (2010) CO_2-EOR from representative North Sea oil reservoirs. SPE International conference on CO_2 capture, storage and utilization, New Orleans, Louisiana, USA, 139765 pp

Aziz K, Settari A (1979) Petroleum reservoir simulation. Elsevier Applied Science Publishers, London

Bachu S, Bonijoly D, Bradshaw J, Burruss R, Holloway S, Christensen NP, Mathiassen OM (2007) CO_2 storage capacity estimation: methodology and gaps. Int J Greenhouse Gas Control 1(4):430–443

Bondor PL (1992) Applications of carbon dioxide in enhanced oil recovery. Energy Convers Manage 33:579–586

Caers J (2005) Petroleum geostatistics. Society of Petroleum Engineers Publishers, p 104, ISBN-13: 978-1555631062

Chen Z, Huan G, Ma Y (2006) Computational methods for multiphase flows in porous media. Southern Methodist University, Dallas, Texas, Society for Industrial and Applied Mathematics (SIAM), p 531

Clark NJ, Shearin HM, Schultz WP, Garms K, Moore JL (1958) Miscible drive—its theory and application. J Petrol Technol 10:11–20

Coats KH (1982) Reservoir simulation: state of the art. SPE publishers, SPE, Distinguished author series 10020

Corey AT (1954) The interrelation between gas and oil relative permeabilities. Prod Mon 19:38–41

Dake LP (1983) Fundamentals of reservoir engineering (Developments in petroleum science). Elsevier Science publishers, p 462

Darcy H (1856) Les Fontaines Publiques de la Ville de Dijon. Dalmont, Paris

Dimri VP (1992) Deconvolution and inverse theory: application to geophysical problems. Elsevier Science Publishers, Amsterdam, p 230

Dimri VP, Srivastava RP, Vedanti N (2012) Fractal models in exploration geophysics, vol 41, Elsevier Science Publishers, Amsterdam, p 165

Emera MK, Sarma HK (2006) Genetic algorithm (GA)—based correlations offer more reliable prediction of CO_2 oil physical properties. Canadian international petroleum conference, Calgary, Alberta, Canada, 13–15 June

Ertekin T, Abou-Kassem JH, King GR (2001) Basic applied reservoir simulation. Textbook Series, SPE, Richardson, Texas

Honarpour M, Koederitz LF, Harvey AH (1986) Relative permeability of petroleum reservoir. CRC Press, Boca Raton

Iserles A (1996) Numerical analysis of differential equations. Cambridge University Press, Cambridge

Islam AW, Sepehrnoori K (2013) A review on SPE's comparative solution projects (CSPs). J Petrol Sci Res 2(4):167–180

Kevin B (2002) Development of an integrated model for compaction/water driven reservoirs and its application to the J1 and J2 sands at Bullwinkle, Green Canyon Block 65, Deepwater Gulf of Mexico. MS Thesis, The University of Texas at Austin

Kleppe J (2011) Lecture notes on reservoir recovery technique. Norwegian University for Science and Technology, personal communication

Kovscek AR, Cakici MD (2005) Geologic storage of carbon dioxide and enhanced oil recovery. II. Cooptimization of storage and recovery. Energy Convers Manage 46:1941–1956

Merrill RC, Hartman KJ (1994) A comparison of equation of state tuning methods. SPE-28589-MS, New Orleans, Louisiana, p 259

Michelena R, Gringarten E (2009) An introduction to this special section: reservoir modeling constrained by seismic. Lead Edge 28(12):1429

Muggeridge A, Cockin A, Webb K, Frampton H, Collins I, Moulds T, Salino P (2014) Recovery rates, enhanced oil recovery and technological limits. Phil Trans R Soc A 372

Mukherjee MK (1981) Evolution of Ankleshwar Anticline, Cambay Basin. India Geol Notes, AAPG, pp 336–345

Oil and Natural Gas Corporation of India (ONGC) (2010) Annual report of Ankleshwar asset for the year 2009–2010 by Sub-surface team. Ankleshwar asset, ONGC

Orr FM, Taber JJ (1984) Use of carbon dioxide in enhanced oil recovery. Science 224(4649): 563–569

Pedersen KS, Christensen PL, Shaikh JA (2014) Phase behavior of petroleum reservoir fluids, 2nd edn, CRS Press, Bocoa Raton, p 465

Sigmund PM, McCaffery FG (1979) An improved unsteady-state procedure for determining the relative-permeability characteristics of heterogeneous porous media. SPE J 19(1):15–28

Srivastava RP, Vedanti N, Akervoll I, Bergmo P, Yerramilli RC, Yerramilli SS, Dimri VP (2015) Study of CO_2 EOR in a sector model from mature oil field, Cambay Basin, India. In: Mukherjee S (ed), Petroleum geosciences: Indian contexts. Springer, Berlin, pp 87–98

Stone HL (1970) Probability model for estimating three-phase relative permeability. J Petrol Technol 22(2):218–241

Todd M, Longstaff W (1972) The development, testing and application of a numerical simulator for predicting miscible flood performance. J Petrol Technol 24:874–882

Zhao DF, Liao XW, Yin DD (2014) Evaluation of CO_2 enhanced oil recovery and sequestration potential in low permeability reservoirs, Yanchang Oilfield. Chin J Energy Inst 87:306–313

Chapter 4
Acoustic Properties of Reservoir Fluids-CO_2 System

4.1 Introduction

One of the crucial objectives of any successful EOR project is to evaluate the changes in reservoir seismic properties due to the injection of foreign fluid, e.g. CO_2. Monitoring the changes of seismic properties with the changes in fluid properties will help to enhance the reservoir production performance. Estimation of the reservoir fluid saturations from the reservoir simulation at the time of the baseline and monitor survey is utilized together with the acoustic properties of the fluid phases to obtain the effective bulk moduli and density of the reservoir fluids. These data are necessary to envisage the changes in acoustic properties of the reservoir due to the changes in fluid pressure, composition, and saturation. This chapter details models for the acoustic properties of the reservoir fluids at reservoir temperature and pressure conditions.

The physical properties of pore fluids have an influence on seismic response of porous rock comprising those fluids. Hence, fluid properties at reservoir conditions are used in calculating the elastic stiffness matrix of the rock-fluid system, as suggested by Gassmann's (1951) or Brown and Korringa's (1975) equations. Reservoir fluids affect the compressional-wave velocity, V_p, of the rock-fluid system by influencing the density, ρ, and bulk modulus, K:

$$V_p = \sqrt{\frac{K + \frac{4}{3}G}{\rho}}, \tag{4.1}$$

where G is the shear modulus. The low-frequency (<100 Hz) Gassmann's approach is a simple model to analyse seismic velocities of a rock subjected to various fluid conditions, a well-known problem of "fluid substitution". This approach is based on three major assumptions: the rock is homogenous, monomineralic and isotropic, the

S.S. Ganguli, *Integrated Reservoir Studies for CO_2-Enhanced Oil Recovery and Sequestration*, Springer Theses,
DOI 10.1007/978-3-319-55843-1_4

pore space is completely connected and the fluids can freely move in the pore space. A very well-known form of it (Smith et al. 2003) is:

$$K_{sat} = K_{fr} + \frac{\left(1 - \frac{K_{fr}}{K_{ma}}\right)^2}{\frac{\emptyset}{K_{fl}} + \frac{1-\emptyset}{K_{ma}} - \frac{K_{fr}}{K_{ma}^2}}, \tag{4.2}$$

where, K_{sat} is the saturated rock bulk modulus to be used in Eq. (4.1), K_{fr} is the frame or dry rock bulk modulus, K_{ma} is the mineral modulus making up rock, K_{fl} is effective fluid bulk modulus, and $\emptyset$ is the porosity. It is to be noted that the "dry-modulus" is not completely dry, but slightly moist or wet rock modulus is used for fluid substitution analysis (Mavko et al. 1998). Since fluid has no effect on the shear modulus (G), and has minor influence on shear wave velocity, hence, remain constant during fluid substitution (Smith et al. 2003; Mavko et al. 1998).

Therefore, to evaluate the influence of fluid on acoustic response using Gassmann's equations, the bulk density and fluid bulk modulus must be modelled as a function of composition and pressure using Batzle and Wang (1992).

4.2 Ankleshwar Fluid Properties

The CO_2-Enhanced Oil Recovery (EOR) operation will alter the composition and saturation of the pore fluids at Ankleshwar oil field in Cambay Basin, India, especially in S3+4 sand layers. The fluid phases in this unit are brine, oil, CO_2, and mixtures of oil and CO_2. The following data on reservoir fluids provided by the operator (ONGC), will be used in this study. The average reservoir temperature is 78 °C, and the initial reservoir pressure is estimated as 12 MPa. During water flooding, the pore pressure in the reservoir is estimated to vary from 8 to 14 MPa.

For the modeling purposes, the expected pore pressure range is assumed to be 8–18 MPa under CO_2 flooding, with an average of 14 MPa. It is noteworthy that higher pressure may happen close to the injector wells, but pressure should decrease a short distance away from the injectors, due to faulted and permeable nature of the reservoir.

4.2.1 Brine Properties

The most common pore fluid is brine, and its composition may vary from pure water to saturated saline solutions. Also, the brine salinity is simplest variable to model in a specific reservoir condition since brine resistivities are routinely calculated during well-logging. There are some simple relationships by which one can convert brine resistivities into salinity (Edwards et al. 1963; Schlumberger 1989). Sodium chloride

(Nacl) is the only solid dissolved is considered. The brine phase calculations can be performed using the equations provided by Batzle and Wang (1992).

The density of brine (ρ_{br}) of salinity (S) of Nacl at reservoir temperature, T and pressure, P is given by:

$$\begin{aligned}\rho_{br} =& \rho_w + S\{0.668 + 0.44S + 10^{-6}[300P - 2400PS \\ &+ T(80 + 3T - 3300S - 13P + 47PS)]\},\end{aligned} \tag{4.3}$$

where the density of pure water (ρ_w), in g/cm^3 is

$$\begin{aligned}\rho_w = 1 + 10^{-6}&\left(-80T - 3.3T^2 + 0.00175T^3 + 489P - 2TP + 0.016T^2P\right. \\ &\left. - \left(1.3 \times 10^{-5}\right)T^3P - 0.333P^2 - 0.002TP^2\right),\end{aligned} \tag{4.4}$$

The acoustic velocity of pure water, V_w, in m/s:

$$V_w = \sum_{i=0}^{4}\sum_{j=0}^{3} W_{ij}T^iP^j, \tag{4.5}$$

where, the constants W_{ij} are provided in Table 4.1.

And the acoustic velocity of brine, V_{br}, in m/s

$$\begin{aligned}V_{br} = V_w &+ S\left(1170 - 9.6T + 0.055T^2 - 8.5 \times 10^{-5}T^3 + 2.6P - 0.0029TP - 0.0476P^2\right) \\ &+ S^{3/2}\left(780 - 10P + 0.16P^2\right) - 1820S^2.\end{aligned} \tag{4.6}$$

Also, the modulus of gas-free brine can be obtained as,

$$K_{br} = \rho_{br}V_{br}^2, \tag{4.7}$$

According to the ONGC report (2010), the Ankleshwar formation has average salinity of 33,000 ppm total dissolved solids (TDS) after approximately 50 years of massive water flooding in the field. We expect a change in salinity due to

Table 4.1 Coefficients for the calculation of velocity of water (V_w)

$W_{00} = 1402.85$	$W_{02} = 3.437 \times 10^{-3}$
$W_{10} = 4.871$	$W_{12} = 1.739 \times 10^{-4}$
$W_{20} = -0.04783$	$W_{22} = -2.135 \times 10^{-6}$
$W_{30} = -1.487 \times 10^{-4}$	$W_{32} = -1.455 \times 10^{-8}$
$W_{40} = -2.197 \times 10^{-7}$	$W_{42} = 5.230 \times 10^{-11}$
$W_{01} = 1.524$	$W_{03} = -1.197 \times 10^{-5}$
$W_{11} = -0.0111$	$W_{13} = -1.628 \times 10^{-6}$
$W_{21} = 2.747 \times 10^{-4}$	$W_{23} = 1.237 \times 10^{-8}$
$W_{31} = -6.503 \times 10^{-7}$	$W_{33} = 1.327 \times 10^{-10}$
$W_{41} = 7.987 \times 10^{-10}$	$W_{43} = -4.614 \times 10^{-13}$

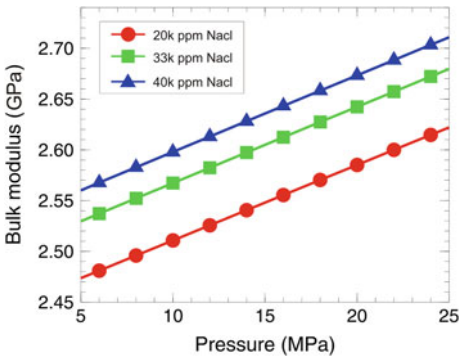

Fig. 4.1 Bulk modulus of brine as a function of salinity and pressure, at an average reservoir temperature of 78 °C

non-uniformity of the water flooding. Therefore, to model the brine properties at Ankleshwar reservoir conditions, we consider that the salinity varies from 20,000 to 40,000 ppm TDS and pore pressures from 8 to 14 MPa.

We found that under the above stated conditions, the bulk modulus of reservoir brine is expected to vary from 2.55 to 2.60 GPa (Fig. 4.1), the density ranges from 1.000 to 1.003 g/cc, and the acoustic velocity ranges from 1.596 to 1.609 km/s (Fig. 4.2).

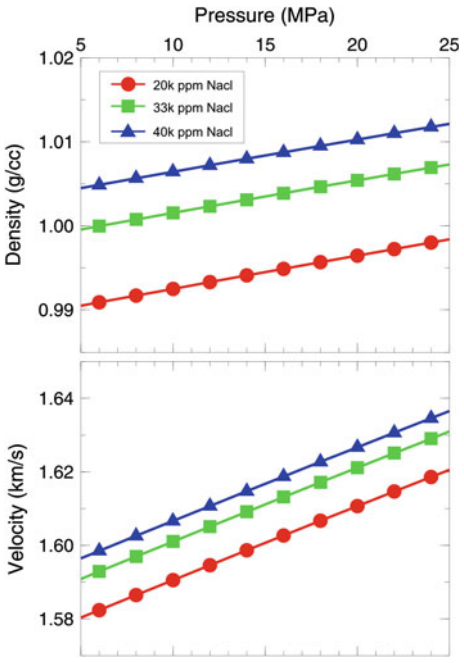

Fig. 4.2 Density and acoustic velocity of brine as a function of salinity and pressure, at an average reservoir temperature of 78 °C

4.2.2 Oil Properties

Crude oils may range from light liquids (condensates) to very heavy tars, and the American Petroleum Institute (API) gravity is widely used to classify crude oils. An API gravity of 5 signifies very heavy tar like crude, and an API gravity value near to 80 represents a very light condensate. Large amounts of hydrocarbon gases can be dissolved in oils under pressure, characterized by the gas-to-oil ratio (GOR) value can significantly decrease the bulk density and modulus for live oils. Similar to hydrocarbon gas, oil density and bulk modulus depend on the temperature, pressure, GOR, and the type of oil.

The density of live oil, ρ_{oil}, in g/cc, can be written as (Wang and Nur 1990; Batzle and Wang 1992):

$$\rho_{oil} = \frac{\rho_{pl}}{\left[0.972 + (3.81 \times 10^{-4})(T + 17.78)^{1.175}\right]}, \tag{4.8}$$

where

$$\rho_{pl} = \left(\rho_{gl} + 0.00277P - 1.71 \times 10^{-7}P^3\right)\left(\rho_{gl} - 1.15\right)^2 + \left(3.49 \times 10^{-4}\right)P\ ,$$

$$\rho_{gl} = \frac{(\rho_0 + 0.0012R_gG)}{B_{oil}},$$

$$B_{oil} = 0.972 + 0.0003812\left[2.4955R_g\left(\frac{G}{\rho_0}\right)^{0.5} + T + 17.778\right]^{1.175}.$$

And, the velocity of live oil, V_{oil}, in m/s:

$$V_{oil} = 2096\left(\frac{\rho_{dl}}{2.6 - \rho_{dl}}\right)^{0.5} - 3.7T + 4.64P + 0.0115\left[4.12\left(\frac{1.08}{\rho_{dl}} - 1\right)^{0.5} - 1\right]TP\,, \tag{4.9}$$

$$\rho_{dl} = \frac{\rho_o}{B_{oil}}(1 + 0.001R_g)^{-1}.$$

Once the velocity and density is known, the bulk modulus of live oil can be calculated as:

$$K_{oil} = \rho_{oil}V_{oil}^2. \tag{4.10}$$

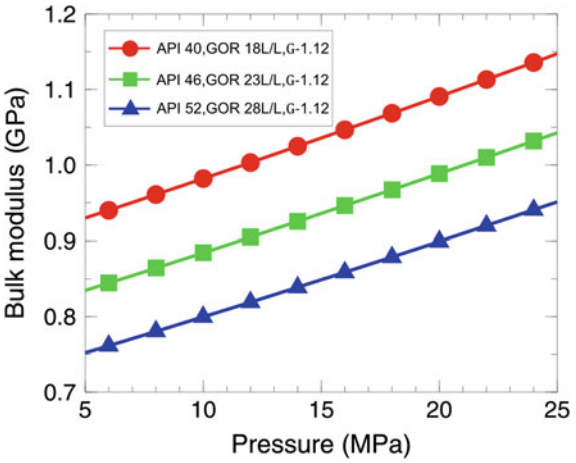

Fig. 4.3 Bulk modulus of the live crude oil of Ankleshwar as a function of composition and pressure, at an average reservoir temperature of 78 °C

According to the ONGC report (2010), Ankleshwar crude oil is a light crude oil with average oil properties e.g. 46.3 API gravity, 23 L/L gas-to-oil ratio (GOR), and bubble point pressure of 9.3 MPa. Also, the average gas gravity (G) is assumed to be 1.12, the value of sample tested at ONGC (personal communication). For modeling purpose, we consider the range as 40–52 API gravity, 18–28 L/L GOR with a constant G = 1.12.

Figures 4.3 and 4.4 illustrate the bulk modulus, density and velocity of live Ankleshwar crude oil, respectively. We observed that the bulk modulus, density

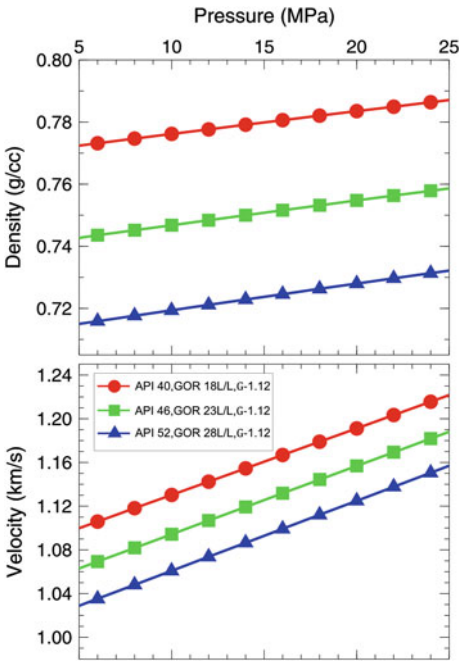

Fig. 4.4 Density and acoustic velocity of Ankleshwar crude oil as a function of composition and pressure, at an average reservoir temperature of 78 °C

and velocity increases with decreasing API gravity, decreasing GOR and increasing pressure.

The enhanced oil recovery operations at Ankleshwar are designed to keep the pressure above the bubble point pressure to avoid the gas coming out of solution in the oil. For the Ankleshwar field, the bulk modulus of crude oil is expected to vary from 0.75 to 0.94 GPa (Fig. 4.3); the density ranges from 0.710 to 0.774 g/cc, and the acoustic velocity ranges from 1.03 to 1.10 km/s (Fig. 4.4). The physical properties of crude oil experiences more change compare to the physical properties of brine at Ankleshwar reservoir conditions.

4.2.3 CO_2 Properties

CO_2 is injected into hydrocarbon reservoirs for enhanced oil recovery operations, and seismic can be used to monitor the injected CO_2 and displacement process. Hence, the properties of CO_2 are equally important to know for a successful EOR project. The physical properties of CO_2 can be computed using some of the many equations of state (EoS) developed for real gases such as Van der Waals (vW) equation (Van der Waals 1873), Peng and Robinson (PR) equation (Peng and Robinson 1976), etc.

The EoS for an ideal gas at absolute pressure P, and absolute temperature T is given by:

$$PV = RT, \tag{4.11}$$

where V is molar volume and R (=8.314472 J mol^{-1} K^{-1}) is the Universal gas constant. But ideal gas law doesn't follow the range of pressures and temperatures encountered in hydrocarbon reservoirs because of finite volume of gas molecules and intermolecular attraction. Van der Waals equation improves upon the ideal gas law, which is:

$$P = \frac{RT}{V - b} - \frac{a}{V^2}. \tag{4.12}$$

This equation referred as 'cubic' equation since it takes the form of a cubic polynomial to solve for volume:

$$PV^3 - (RT + bP)V^2 + aV - ab = 0. \tag{4.13}$$

The most popular EoS used in the industry and scientific purpose is, the Peng-Robinson EoS (1976), which is:

$$P = \frac{RT}{V - b_i} - \frac{a_i(T)}{V(V + b_i) + b_i(V - b_i)}, \tag{4.14}$$

where,$a_i(T) = \Omega_{a_0}[1 + (0.37464 + 1.54226w_j - 0.26992w_j^2)(1 - (\frac{T}{T_c})^{0.5})]^2 \frac{R^2T_c^2}{P_c}$, $b_i = \Omega_{b_0}\frac{RT_c}{P_c}$. T_c and P_c are critical temperature and pressure, Ω_{a_0} and Ω_{b_0} are 0.457235529 and 0.07796074, respectively.

This can be optionally modified for a large acentric factor (w_j), e.g. $w_j > 0.491$, using the factor $(0.379642 + 1.48503w_j - 0.164423w_j^2 + 0.016666w_j^3)$ rather than $\left(0.37464 + 1.54226w_j - 0.26992w_j^2\right)$.

To apply such EoS to mixture of various components, mixing rules are necessary to consider, and one of the widely used method is Van der Waals one fluid mixing rules and the classic combination rules (Privat and Jaubert 2014).

The density of gas with known molecular weight can be estimated as a function of pressure and temperature using the relationship for density, ρ, molecular weight, m_w, and molar volume, V, $\rho = \frac{m_w}{V}$.

The bulk modulus, K, is defined as:

$$K = \frac{1}{V}\frac{\partial P}{\partial V}. \tag{4.15}$$

The acoustic velocity, V_p, is related to bulk modulus and density as:

$$V_p = \sqrt{\frac{K}{\rho}}. \tag{4.16}$$

At Ankleshwar reservoir conditions, CO_2 is above critical point of 7.4 MPa pressure and 31 °C temperature. Hence it will behave as a supercritical fluid, i.e., a dense fluid without any distinction between liquid and gas. Also the expected temperature changes in the reservoir are negligible since compared to the reservoir volume, small amount of CO_2 injection is considered. With these settings, the physical properties of CO_2 at reservoir conditions are estimated, and depicted in Fig. 4.5.

We found that, for expected pore pressure range, 8–18 MPa, the bulk modulus, density, and velocity of CO_2 is 0.011–0.055 GPa, 0.166–0.521 g/cc, and 0.288–0.357 km/s (Fig. 4.5), respectively. It is noteworthy to mention that unlike the case for brine and oil at reservoir conditions, the sensitivity of velocity change of pure CO_2 is more than the bulk modulus and density. This behaviour of CO_2 will make it distinguish from other fluids within the reservoir, and a velocity contrast is expected after CO_2 injection. This suggests time-lapse seismic monitoring of injected CO_2 could provide information about changes in seismic wave velocity. Nevertheless, the direction and magnitude of the velocity change will depend on the time since injection.

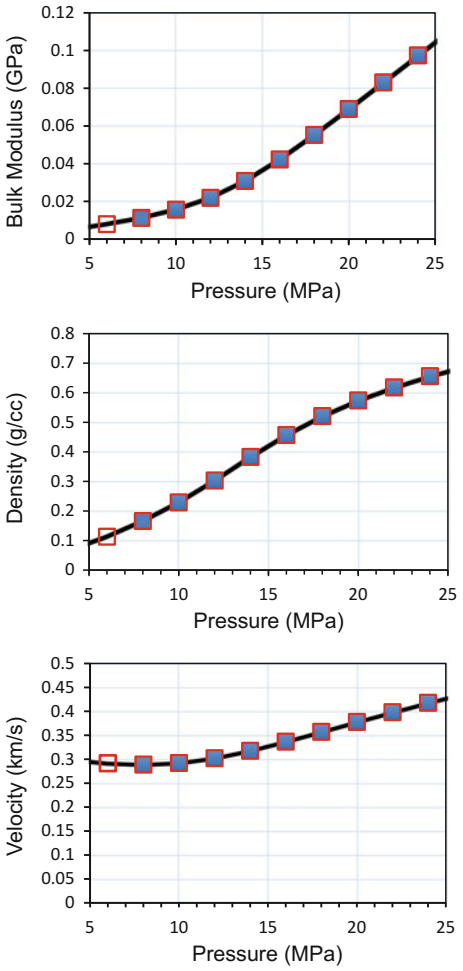

Fig. 4.5 The bulk modulus, density and acoustic velocity of pure CO_2 as a function of pressure, respectively at an average reservoir temperature of 78 °C. The *filled boxes* represent the values above the critical point of CO_2

4.2.4 Oil + CO_2 Mixtures

The injected CO_2 will not attain a pure separate phase in the reservoir. Basically it will extract hydrocarbons from the oil until it attains a composition that may lead to miscible displacement above MMP. As discussed in Chap. 3, the MMP was too high, and hence a new injection scheme, consisting of 40 mole-% CO_2, 10% methane, 20% ethane, 20% propane and 10% butane, was developed for miscible CO_2 flooding. Literature suggests that up to approximately 0.66 mol fraction of CO_2 can dissolve in the crude oil above the MMP and if more CO_2 is present, a CO_2-rich phase with dissolved light hydrocarbons will be formed (Brown 2002). Of course, this phase will be more mobile than the live oil, it will flow faster. Thus, a mixture of both live oil and CO_2 at Ankleshwar reservoir conditions also needs to be calculated.

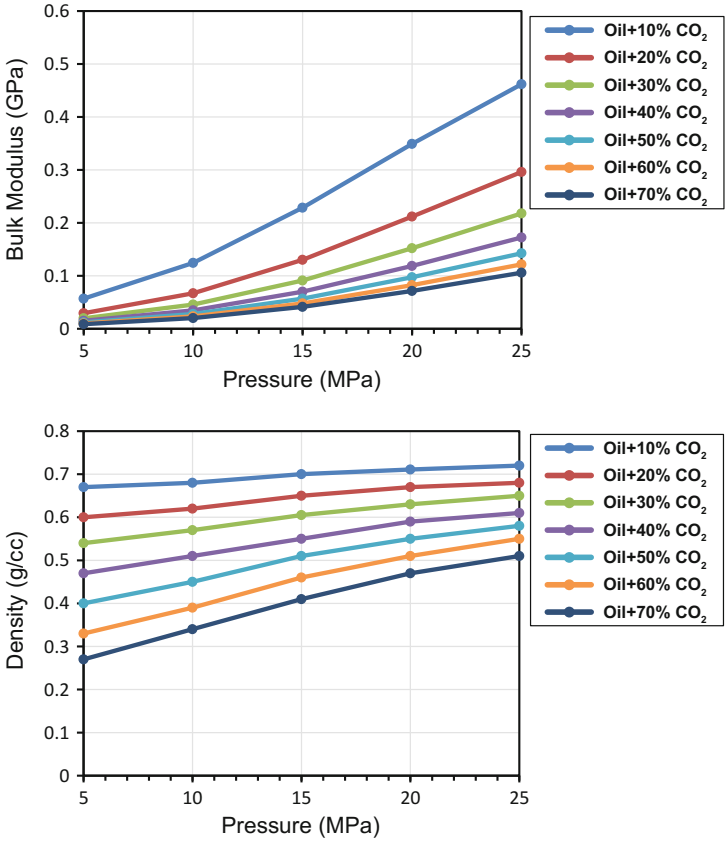

Fig. 4.6 The bulk modulus (*Top*) and bulk density (*Bottom*) of oil and CO_2 mixture as a function of composition and pressure, at an average reservoir temperature of 78 °C. The legend represents the various proportions of mixture of CO_2 with the oil at reservoir conditions

The effective properties of oil and CO_2 mixtures can be modeled using mixing law, such as Wood's (1955) relation. According to this, the effective bulk modulus, K_{eff}, can be expressed as:

$$K_{eff} = \frac{1}{\left(\frac{S_{oil}}{K_{oil}} + \frac{S_{co_2}}{K_{co_2}} + \frac{S_{br}}{K_{br}}\right)}. \tag{4.17}$$

The density of the fluid mixture can be estimated by arithmetic averaging of densities (i.e., mass balance) of the separate fluid phases:

$$\rho_{eff} = S_{oil}\rho_{oil} + S_{co_2}\rho_{co_2} + S_{br}\rho_{br}, \tag{4.18}$$

here S_{oil}, S_{co_2} and S_{br} are the saturation values (as fraction) of oil, CO_2 and brine, respectively.

The addition of CO_2 to live oil has the effect of increasing GOR and the gas gravity. For modeling, the average properties of Ankleshwar oil is taken as 46.3 API gravity, 23 L/L GOR, and G = 1.12. The acoustic properties of individual phases such as oil, and CO_2 are estimated as described in the previous sections, and the resultant bulk modulus and density of mixture of oil and CO_2 are computed using Eqs. (4.17) and (4.18) as shown in Fig. 4.6. A significant difference in the acoustic properties is observed between the original oil composition of the field, and the oil and CO_2 mixtures (Compare Figs. 4.3 and 4.4 with Fig. 4.6).

We observe that the bulk modulus and density of the mixture of oil and CO_2 is decreasing with the increase in mole percentages of CO_2 which is true since the addition of CO_2 to live Ankleshwar oil increases the GOR, but increases significantly with the increase in pressure. However, the change in bulk modulus with increasing pressure is very abrupt for low mole percentages of CO_2.

The expected bulk modulus and density of the mixture of oil and CO_2 at pore pressures of 8–18 MPa is 0.02–0.07 GPa (Fig. 4.6), and 0.33–0.47 g/cc (Fig. 4.6), respectively.

4.3 Conclusions

We have studied how the reservoir fluids and CO_2 will behave in Ankleshwar reservoir conditions, and examined the feasibility of CO_2 monitoring on the basis of Batzle and Wang (1992) model. The acoustic properties, such as bulk modulus, density and velocity for Ankleshwar under expected reservoir pressure and temperature conditions are examined and presented in each section under Ankleshwar fluid properties. This will help to use seismic data more effectively during CO_2-EOR and storage. The acoustic properties of the fluids such as brine, oil and CO_2 can be used for fluid substitution study to determine the maximum fluid effects on seismic properties of a rock saturated with a particular fluid. The following conclusions were reached:

- We provide an avenue to calculate values at reservoir conditions (irreducible water saturation conditions) from logging conditions (saturated or residual oil conditions), and acoustic properties modeling for Ankleshwar oil field can be used to determine expected seismic responses during the enhanced oil production from this reservoir.
- The acoustic properties of crude oil experiences more change compare to the properties of brine at Ankleshwar reservoir conditions. The increase in gas-oil ratio has significant impact on crude oil properties, it decreases the bulk density, modulus and velocity. The decrease in acoustic velocity with the increase in API

gravity could be due to the increase in compressibility. A noteworthy change in acoustic properties is observed while modeling the mixture of oil and CO_2 and oil alone.

- As depicted in Fig. 4.5, CO_2 will no longer be in pure gaseous form at Ankleshwar reservoir conditions, rather behave as a supercritical fluid, hence strong seismic response is expected in field data as a result of CO_2-EOR.

References

Batzle M, Wang Z (1992) Seismic properties of pore fluids. Geophysics 57(11):1396–1408

Brown LT (2002) Integration of rock physics and reservoir simulation for the interpretation of time-lapse seismic data at Weyburn Field, Saskatchewan. M.Sc. thesis, Reservoir Characterization Proj., Colorado School of Mines

Brown RJS, Korringa J (1975) On the dependence of the elastic properties of a porous rock on the compressibility of a pore fluid. Geophysics 40:608–616

Edwards DP, Lacour-Gayet PJ, Suan J (1963) Log evaluation in wells drilled with inverted oil emulsion mud. SPE-10206-MS, San Anthonio 313–318

Gassmann F (1951) Über die elastizität poröser medien: Vierteljahrss-chrift der Naturforschenden Gesellschaft in Zurich, 96, 1–23. The English translation of this paper is available at http://sepwww.stanford.edu/sep/berryman/PS/gassmann.pdf

Mavko G, Mukerji T, Dvorkin J (1998) The rock physics handbook: tools for seismic analysis in porous media. Cambridge University Press, Cambridge, New York, USA

Oil and Natural Gas Corporation of India (ONGC) (2010) Annual report of Ankleshwar asset for the year 2009–2010 by Sub-surface team. Ankleshwar asset, ONGC

Peng DY, Robinson DR (1976) A new two-constant equation of state. Ind Eng Chem Fundam 15 (1):59–64

Privat R, Jean-Noël Jaubert (2014) Predicting the phase equilibria of carbon dioxide containing mixtures involved in CCS processes using the PPR78 Model. In: CO_2 Sequestration and valorization, esteves, V.P.P (Ed.), InTechOpen, 443–462

Schlumberger (1989) Log Interpretation principles 8–9

Smith TM, Sondergeld CH, Rai CS (2003) Gassmann fluid substitutions: a tutorial. Geophysics 68:430–440

Van der Waals JD (1873) Over de continuiteit van den gas en vloeistoftoestand. Dissertation, Leiden

Wang Z, Nur AM, Batzle ML (1990) Acoustic velocities in petroleum oils. J Petrol Technol 42:192–200

Wood AW (1955) A textbook of sound. The MacMillan Co., New York, p 360

Chapter 5
Rock Physics Modeling of Ankleshwar Reservoir: A CO_2-EOR Perspective

5.1 Introduction

Enhanced oil recovery (EOR) operations offer a fundamental challenge in the study of reservoir characterization primarily due to the lack of understanding of inherent complexity in the estimation of reservoir parameters. Rock physics models play a crucial role in solving production problems and reducing the ambiguities of fluids within reservoir. In recent years, oil and gas industries prefer these models to reduce exploration risks by estimating the lithology and fluid content of undrilled areas provided that the undrilled area has the same geological depositional environment as a drilled area (Chi and Han 2009). Central to most rock physics studies is the application of theoretical models to the selected borehole logs by adjusting the parameters of the model which helps in understanding the reservoir behaviour due to the changes in elastic properties.

As discussed in the previous Chaps. 2–4, Ankleshwar oil field is a mature oil field situated in Cambay Basin (Western India). Due to massive water flooding for long duration in this oil field, it has witnessed sufficient changes in reservoir parameters which can be quantitatively mapped through the application of rock physics models. Moreover, initiative of CO_2-EOR operations at this old field will lead to significant changes in the reservoir property, hence, rock physics modeling can be used to improve the understanding and interpretation of seismic signatures by providing a fundamental relationship between the lithology, fluid, and geological depositional environment of the reservoir.

In this chapter, we report establishment of an isotropic rock physics model of Ankleshwar sands which can be a useful input prior to field scale CO_2-EOR operation in this mature oil field. In this perspective, we conducted rock physics diagnostic, fluid replacement modeling and rock physics template (RPT) analysis to well log data from the four wells drilled through the sands of Ankleshwar formation

S.S. Ganguli, *Integrated Reservoir Studies for CO_2-Enhanced Oil Recovery and Sequestration*, Springer Theses,
DOI 10.1007/978-3-319-55843-1_5

in Cambay Basin which were provided by the operator, ONGC. Also, we extended these studies to predict the time-lapse response of the elastic attributes subjected to the CO_2 injection for EOR.

5.2 Well-Log Analysis of Ankleshwar Oil Field

Well-log analysis is essential to understand the petrophysical properties of reservoir and estimate elastic parameter prior to conduct rock physics modeling. Although, there are hundreds of wells within a few km radius of Ankleshwar oil field, unfortunately only four well logs, ANKL-1, ANKL-2, ANKL-3 and ANKL-4 were provided by the operator that penetrates Ankleshwar formation and adjacent rock layers. In general, well-log data are subjected to many sources of error, which could influence our interpretation. For this, we performed quality check for all the well data by evaluating the caliper log which is good indicator of washout zones affecting the log measurements.

Petrophysical analysis and well correlation of all the four logs were performed and illustrated in Figs. 5.1 and 5.2. The main working interval for the analysis and rock physics modeling was focused within the most productive pay sands of Ankleshwar reservoir, S3+4, which was decided as the target zone for possible CO_2-EOR as described in Chap. 3. The gamma-ray log was used as source log to evaluate the shale volume of the formation.

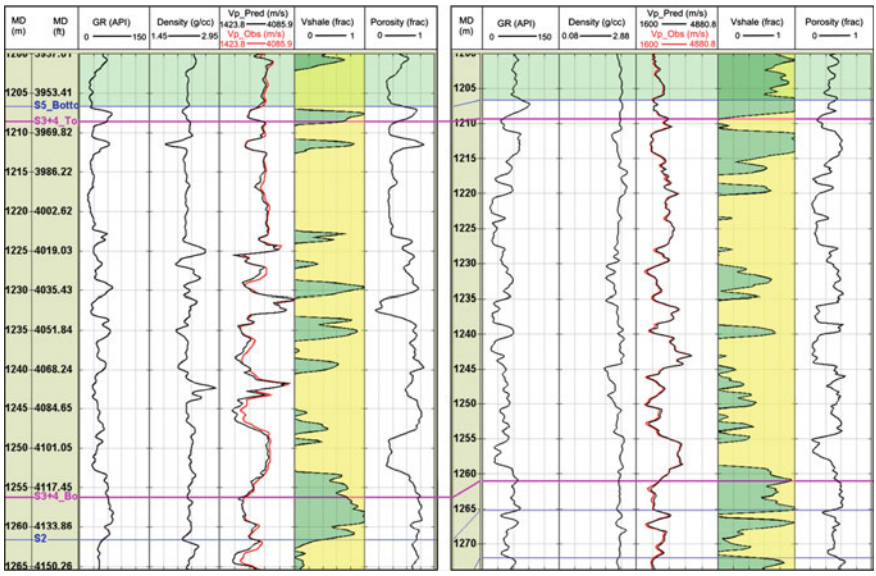

Fig. 5.1 Gamma ray, density, P-wave velocity (Vp), shale volume, and porosity logs of Wells, ANKL-1 (*Left*) and 2 (*Right*). *Black colour curve* indicates the predicted Vp log using Gassmann's equation, while *red colour* indicates the observed Vp log. The target reservoir zone for CO_2-EOR, S3+4, is demarcated by *magenta curve*

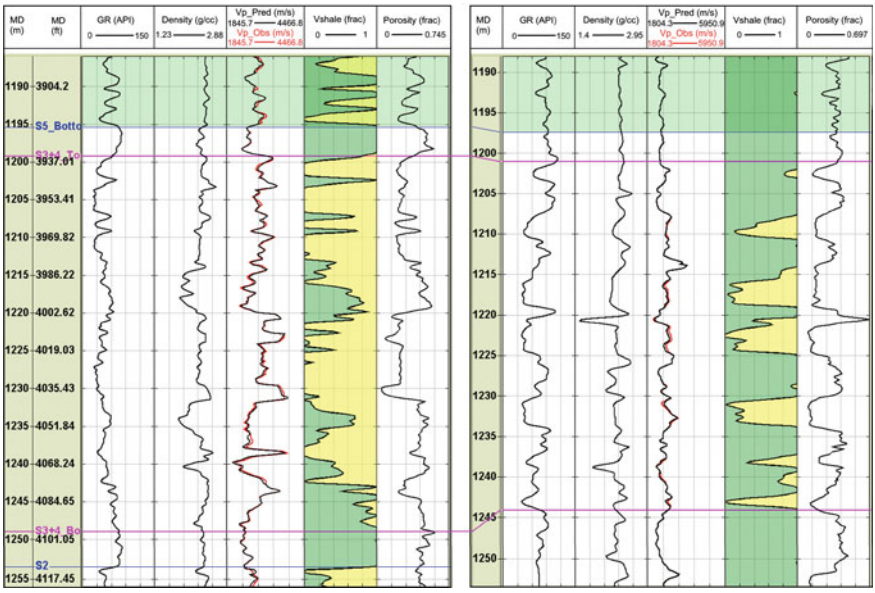

Fig. 5.2 Gamma ray, density, P-wave velocity (Vp), shale volume, and porosity logs of Wells, ANKL-3 (*Left*) and 4 (*Right*). *Black colour curve* indicates the predicted Vp log using Gassmann's equation, while *red colour* indicates the observed Vp log. The target reservoir zone for CO_2-EOR is marked by *magenta curve*

We observed comparatively more gamma ray count in well ANKL-4 than the other wells. The main input logs, P-wave velocity (Vp), density (Rho), were corrected (e.g. spike removal) prior to conduct rock physics modeling. Also, we generated pseudo Vp logs (black curve in Figs. 5.1 and 5.2) for all the wells by considering Gassmann's equation (Gassmann 1951; Smith et al. 2003). The pseudo Vp logs were generated using Gassmann's equation and the saturation input were taken from the previous study on reservoir flow simulation as described in Chap. 3. We observed a good agreement between the observed (red curve) and predicted Vp logs (black curve) as depicted in Figs. 5.1 and 5.2.

Shear log is absent in all the provided logs. Therefore, in the present work, we estimated shear wave velocity (Vs) with various existing techniques such as Greenberg-Castagna's empirical relations (Castagna et al. 1985; Greenberg and Castagna 1992), Han's empirical relation (Han 1986), Krief's relations (Krief et al. 1990), Xu and White's relation (Xu and White 1995), G-method (Han and Batzle 2004), and suggested the most relevant Vs prediction method for the present study. We identified that predicted Vp log using G-method is correlated well with the observed data for Ankleshwar reservoir, while other models such as Krief's method overestimates the measurement in Vp, and Xu-white's method doesn't show any systematic correlations with the observations (Figs. 5.3 and 5.4). Hence, Vs log predicted by G-method was taken into consideration for further rock physics study in the following sections.

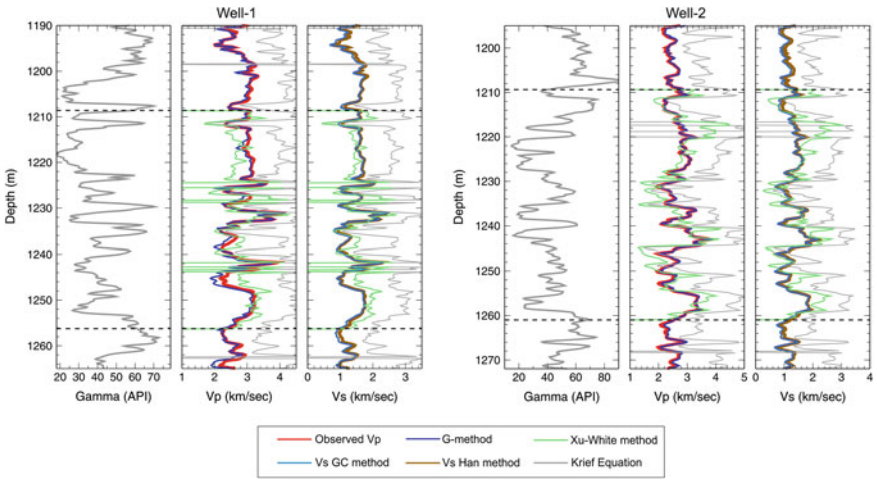

Fig. 5.3 A composite log with estimated P and S-wave logs using various models of ANKL-1 (*Left*) and ANKL-2 (*Right*). *Red curve* indicates the observed Vp log, *blue*, *green*, *cyan*, *brown* and *grey curve* represents predicted velocities (Vp & Vs) using G-method, Xu-white, Greenberg-Castagna (GC), Han, and Krief method, respectively. The target reservoir zone for CO_2-EOR, S3+4, is marked by *grey dotted curve*

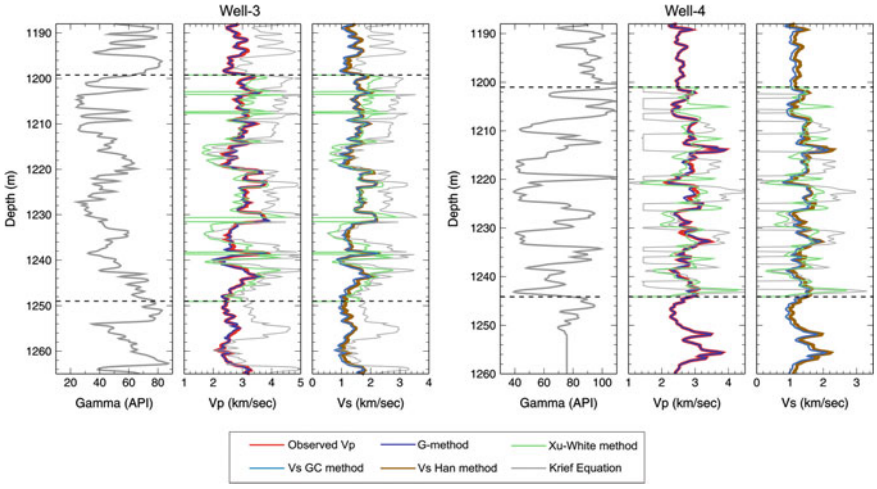

Fig. 5.4 A composite log with estimated P and S-wave logs using various models of Wells, ANKL-3 (*Left*) and ANKL-4 (*Right*). *Red curve* indicates the observed Vp log, *blue*, *green*, *cyan*, *brown* and *grey curve* represents predicted velocities (Vp and Vs) using G-method, Xu-white, Greenberg-Castagna (GC), Han, and Krief method, respectively. The target reservoir zone for CO_2-EOR, S3+4, is marked by *grey dotted curve*

5.3 Rock Physics Diagnostics—An Overview of Theory and Models

Rock physics diagnostic was introduced by Dvorkin and Nur (1996) as a technique to provide practically significant information about the rock properties, helps in establishing a velocity-porosity trend consistent with the local geological factors (Avseth et al. 2000, 2005). Velocity-porosity trends can help to infer about the rock microstructure by providing useful information about diagenetic or depositional processes (Avseth et al. 2010). Several workers (e.g., Han 1986; Klimentos 1991; Vernik and Nur 1992; Dvorkin and Nur 1996) explained the processes (e.g., compaction, cementation, sorting and clay content) that controls the wide scatter trend in velocity-porosity relations in sandstone.

In general, rock physics models can be divided into effective elastic medium or bound and mixing laws, granular media, fluid effect on wave propagation and empirical models (Hossain 2011). However, most of the theoretical rock physics models (RPM) are based on granular media concept, and granular media models used to infer rock microstructure by providing insights about porosity, sorting, cementation and stress effect of sandstones (Mavko et al. 2009). These models can be applied by adjusting effective elastic medium theoretical model curve to a trend in the data, assuming that the microstructure of the sediment is same to that used in the model (Avseth 2000). These models include Voigt and Reuss bounds (Voigt 1910; Reuss 1929), Hill average (Hill 1952), Hertz-Mindlin contact model (Mindlin 1949), Kuster and Toksöz approximations (Kuster and Toksöz 1974; Berryman 1980), Digby's model (Digby 1981), Walton model (Walton 1987), differential effective medium models (Zimmerman 1991; Mukerji et al. 1995a, b), the cemented sand model (Dvorkin and Nur 1996), the soft-sand model (Dvorkin and Nur 1996), the stiff-sand and intermediate stiff-sand models (Mavko et al. 2009). To analyse the effect of pore fluids on seismic wave propagations, the most widely used models include Biot's velocity relations (Biot 1956), Gassmann's equations (Gassmann 1951), and squirt flow model (Mavko and Jizba 1991). Due to the availability of numerous models, we confined to the most commonly used rock physics models and these are friable sand model (Dvorkin and Nur 1996), contact cement model (Dvorkin and Nur 1996), and constant cement model (Avseth 2000), briefly explained in the following sections. Figure 5.5 summarizes the work flow for conducting rock physics diagnostic where four main processes such as rock physics models, model calibration, static and dynamic modeling has been highlighted in yellow, green, blue, and pink, respectively.

5.3.1 The Friable-Sand Model

The well-known "friable or unconsolidated sand" model was developed by Dvorkin and Nur (1996) for high porosity sands, and it consists of finding the elastic moduli

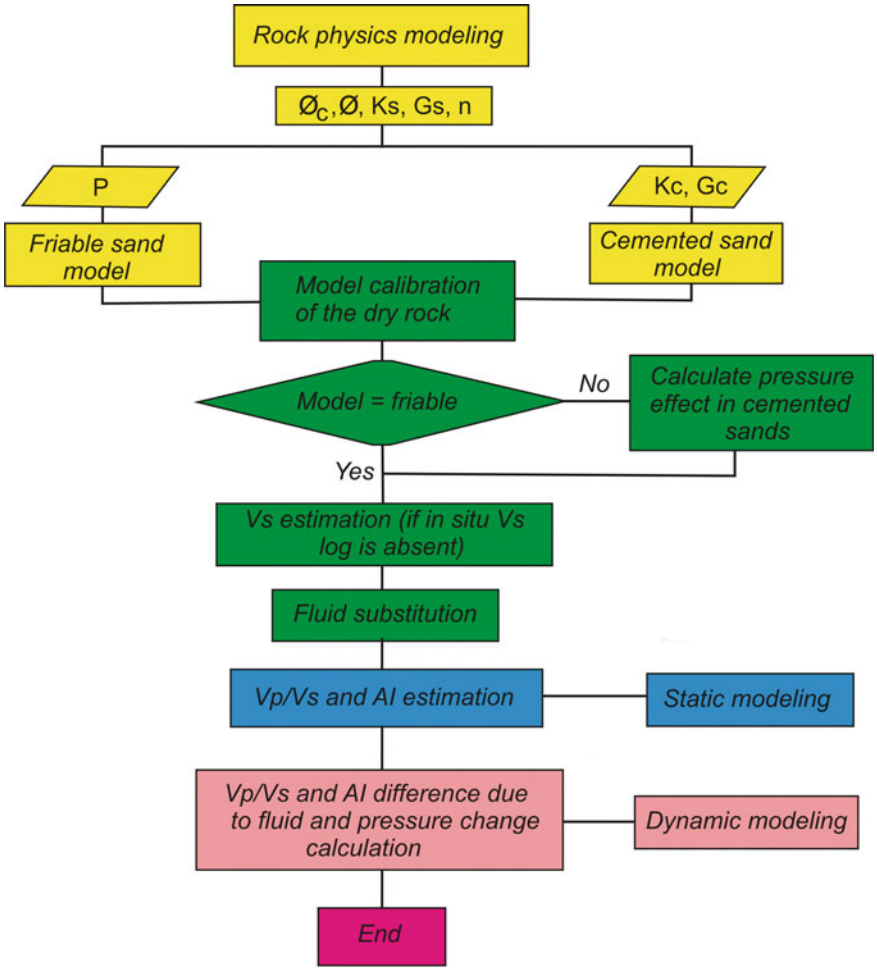

Fig. 5.5 Rock physics modeling workflow. Colors: *yellow*, *green*, *blue* and *pink* indicates the subsections: rock physics modeling, model calibration, static modeling and dynamic modeling, respectively (modified after Meneses 2013)

of the dry rock when there is no cement at the spherical grain contacts. This model describes how the velocity-porosity trend changes as the sorting changes by assuming the porosity reduction from well-sorted end member with critical porosity ($\emptyset_c \sim 40\%$) due to the deposition of solid matter away from the grain contacts that result in gradual stiffening of the rock. Such porosity reduction has been reported as a result of deteriorating grain sorting. The Hertz-Mindlin contact theory (Mindlin 1949) has been utilized to compute the elastic moduli of the dry well-sorted end member at critical porosity, and the zero porosity represents the mineral point. The effective moduli can be represented by:

$$K_{HM} = \left[\frac{n^2(1-\emptyset_c)^2 G_s^2}{18\pi^2(1-v_s)^2} P\right]^{1/3}, \tag{5.1}$$

$$G_{HM} = \frac{5-4v_s}{5(2-v_{s)}}\left[\frac{3n^2(1-\emptyset_c)^2 G_s^2}{2\pi^2(1-v_s)^2} P\right]^{1/3}, \tag{5.2}$$

where P, n, are the effective pressure, coordination number (i.e. number of contacts per grain), and v_s, G_s are Poisson's ratio and shear modulus of the mineral frame, respectively. Likewise, the moduli of the poorly sorted sands with porosities between 0 (mineral point) and $\emptyset_c$ (critical point) are computed by simple interpolation between these points using the modified lower Hashin-Shtrikman (MLHS) model (see detailed formulation in Hashin and Shtrikman 1963; Avseth 2000; Mavko et al. 2009). Then the bulk (K_{dry}) and shear (G_{dry}) moduli of the dry frame are:

$$K_{dry} = \left[\frac{\phi/\emptyset_c}{K_{HM}+\frac{4}{3}G_{HM}} + \frac{1-\phi/\emptyset_c}{K+\frac{4}{3}G_{HM}}\right]^{-1} - \frac{4}{3}G_{HM}, \tag{5.3}$$

$$G_{dry} = \left[\frac{\phi/\emptyset_c}{G_{HM}+C} + \frac{1-\phi/\emptyset_c}{G+C}\right]^{-1} - C, \quad C = \frac{G_{HM}}{6}\left(\frac{9K_{HM}+8G_{HM}}{K_{HM}+2G_{HM}}\right), \tag{5.4}$$

5.3.2 The Contact-Cement Model

This model was introduced by Dvorkin et al. (1994) and consists of calculating the elastic moduli of the dry rock when there is cement in the grain contacts, and the grains were considered to be spherical. The cementation can be in the form of quartz, calcite, or other minerals, is a product from diagenesis, and during burial sands are probable to become cemented sandstones, which result in increase in rock stiffness as the grain contact are connected together by cement. This model describes the reduction in porosity from the initial sand pack due to uniform deposition of cement layers on the grain surface (Fig. 5.6). The mathematical formulation of this model is based on rigorous contact-problem solution by Dvorkin et al. (1994). The effective bulk (K_{dry}) and shear (G_{dry}) moduli of the dry frame can be written as:

$$K_{dry} = \frac{n(1-\emptyset_c)M_c S_n}{6}, \tag{5.5}$$

$$G_{dry} = \frac{3}{5}K_{dry} + \frac{3n(1-\emptyset_c)G_c S_\tau}{20}, \tag{5.6}$$

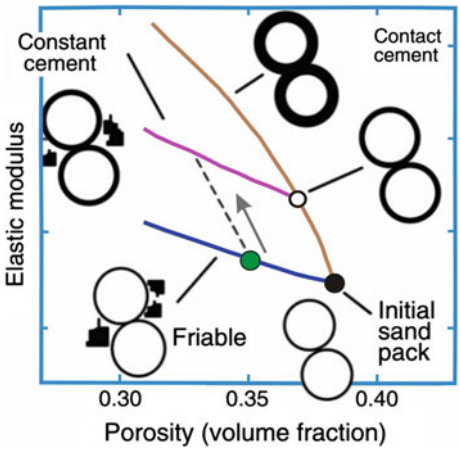

Fig. 5.6 Schematic illustration of the three well-known rock physics models (RPM) in the elastic modulus-porosity plane and corresponding rock microstructure characteristics. The elastic modulus can be compressional, bulk, or shear and porosity can total, or effective (modified after Dvorkin et al. 1994)

where G_c, $M_c = (K_c + \frac{4}{3}G_c)$ are the shear and compressional modulus, respectively, and K_c is the bulk modulus of the cement material. The terms S_n and S_τ corresponds to:

$$\begin{aligned} &S_n = A_n(\Lambda_n)\alpha^2 + B_n(\Lambda_n)\alpha + C_n(\Lambda_n), \quad A_n(\Lambda_n) = -0.024153.\Lambda_n^{-1.3646}, \\ &B_n(\Lambda_n) = 0.20405.\Lambda_n^{-0.89008}, \quad C_n(\Lambda_n) = 0.00024649.\Lambda_n^{-1.9864}; \end{aligned} \tag{5.7}$$

$$\begin{aligned} &S_\tau = A_\tau(\Lambda_\tau, v_s)\alpha^2 + B_\tau(\Lambda_\tau, v_s)\alpha + C_\tau(\Lambda_\tau, v_s), \\ &A_\tau(\Lambda_\tau, v_s) = -10^2.\left(2.26v_s^2 + 2.07v_s + 2.3\right).\Lambda_\tau^{0.079v_s^2 + 0.1754v_s - 1.342}, \\ &B_\tau(\Lambda_\tau, v_s) = \left(0.0573v_s^2 + 0.0937v_s + 0.202\right).\Lambda_\tau^{0.0274v_s^2 + 0.0529v_s - 0.8765}, \\ &C_\tau(\Lambda_\tau, v_s) = 10^{-4}.\left(9.654v_s^2 + 4.945v_s + 3.1\right).\Lambda_\tau^{0.01867v_s^2 + 0.4011v_s - 1.8186}; \end{aligned} \tag{5.8}$$

$$\Lambda_n = 2G_c(1 - v_s)(1 - v_c)/[\pi G_s(1 - 2v_c)], \quad \Lambda_\tau = G_c/(\pi G_s); \tag{5.9}$$

where, $\alpha = \left[\frac{2/3(\emptyset_c - \phi)}{1 - \emptyset_c}\right]^{0.5}$ is the amount of contact cement for cemented layer around the grain, and the terms v_s and v_c are the Poisson's ratio of the rock dry mineral frame and the cement, respectively. For detailed explanation of these equations and their derivation readers are referred to Dvorkin and Nur (1996).

5.3.3 The Constant-Cement Model

This model was introduced by Avseth et al. (2000), and is a combination of friable-sand model and the contact-sand model. It assumes that all sands have the same amount of cemented materials, but at different porosity. The porosity reduction is related to deteriorating sorting and cementation. This model can be used to calculate the effective dry moduli of the granular assembly by adjusting the well-sorted end-member porosity ($\emptyset_b$) and smaller porosity interpolated with the modified lower

Hashin-Shtrikman (1963) bound. Since the amount of cement is often related to the depth, it is sometimes known as "*the constant-cement depth model*" for clean sands. On the other hand, sorting is related to lateral variation in flow energy during sediment deposition. The effective dry moduli are given by:

$$K_{dry} = \left[\frac{\phi/\emptyset_b}{K_b + \frac{4}{3}G_b} + \frac{1-(\phi/\emptyset_b)}{K + \frac{4}{3}G_b}\right]^{-1} - \frac{4}{3}G_b, \tag{5.10}$$

$$G_{dry} = \left[\frac{\phi/\emptyset_b}{G_b + D} + \frac{1-(\phi/\emptyset_b)}{G + D}\right]^{-1} - D\ , \quad D = \frac{G_b}{6}\left(\frac{9K_b + 8G_b}{K_b + 2G_b}\right). \tag{5.11}$$

In this case, K_b, G_b and $\emptyset_b$ are the bulk, shear modulus and porosity, respectively, calculated in the contact cement model. The detailed mathematical derivation of this model can be accessed from Avseth et al. (2000). Figure 5.6 illustrates schematic representation of all the models explaining the geological processes that affects the elastic moduli of rocks.

5.4 Evaluating Rock Property Relationships Through Cross-Plot Analysis

Cross-plot analysis is the key to reservoir characterization study, helps to understand how the rock properties vary with fluid and lithology. In this section, we investigated the effect of geological factors such as compaction, cementation, sorting and clay content on rock elastic properties and fluid sensitivities in rocks. Figure 5.7 illustrates the elastic-attribute cross plot in Vp-versus-porosity domain

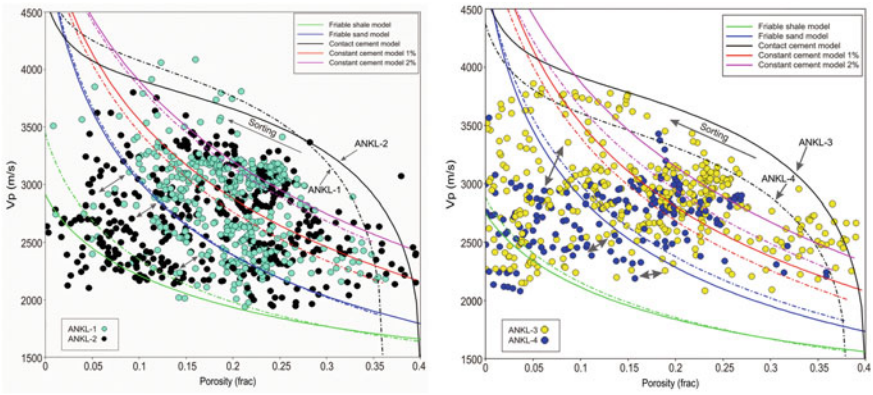

Fig. 5.7 P-wave velocity versus porosity crossplot for the major pay zone, S3+4, from Wells, ANKL-1, ANKL-2, ANKL-3, and ANKL-4 of Ankleshwar oil field with various rock physics model *curves* superimposed. The *arrow* shows the direction of deteriorating sorting and *small arrows* illustrate the differentiation in velocity in the two wells for the same porosity range. Note that the critical porosity for all the wells is different, indicating different diagenetic trend from same field

with rock physics models superimposed on available in situ data from the wells located ~1 and ~2 km within Ankleshwar area in Cambay Basin. The superimposed curves correspond to 85% quartz and 15% clay (except the friable shale model which corresponds to 90% clay and 10% quartz), were derived from the most common rock physics models (RPM), contact-cement, constant- cement and friable-sand models as discussed earlier in Sect. 5.3.

We can see preferential directions in sands to pure shale, and at shallow depth clean sands are not distinctive from the shales, but with the gradual increase in depth, the differentiation in velocity is dramatic in wells, ANKL-3 and ANKL-4 unlike Wells, ANKL-1 and ANKL-2, mainly due to the quartz cementation of the sands (Fig. 5.7). Yet, a difference in velocity is observed within the major pay-zone which corresponds to the same porosity range. This is most likely due to assemblage of shale packages around the clean sands (Fig. 5.8). Also, the porosity of initial sand pack is different for all the wells, e.g. wells ANKL-1, ANKL-2, ANKL-3 and ANKL-4 are with 36, 40, 40 and 38%, respectively. The initial contact cementation in wells ANKL-1 and ANKL-4 developed faster when compared to wells ANKL-2 and ANKL-3 which could be the reason for variation in elastic attributes, resulting in different diagenetic trend.

In addition to the above, different cementation schemes from unconsolidated sand to constant cement of 2% explain this data qualitatively. It is noteworthy that the bypassed oil sands (enclosed by brown circle) were located in the porosity range of about 23–28% which matches satisfactorily with the observed porosity (~23%) of Ankleshwar pay sands (Fig. 5.8). Nevertheless, due to sorting, the oil producing sands for both the wells fall into the constant-cement sand model with higher porosity than the brine sands.

A cross plot of compressional modulus (M)-versus-porosity with superimposed RPMs is also analysed, and we identified this as a better lithologic discriminator unlike velocity-porosity trend, satisfying the fact that clean sands are preferentially lies on constant-cement curve with a very small amount of contact-cement (Figs. 5.9 and 5.10).

Additionally, cross plot of bulk density and P-wave acoustic impedance was investigated, which suggest that this can be a powerful tool for fluid discriminator than a lithologic identifier (Figs. 5.11 and 5.12).

In Fig. 5.12, we observed differentiated sands (marked by dark brown ellipses) of low P-impedance/low density corresponds to bypassed oil zone which can be a potential target for CO_2-EOR operation. The porosity colour scale (Fig. 5.13) attached to these cross plots show a remarkable separation of reservoir oil facies (high porosity, low impedance and low density) from the brine facies (intermediate to low porosity, high impedance and high density). The model developed by these cross plots can be used to understand the reservoir quality in terms of enhanced production perspective.

Additionally, we also analysed the well data with one of the most widely used tool for fluid and mineralogy discrimination, Vp/Vs ratio versus porosity cross plot as depicted in Fig. 5.14.

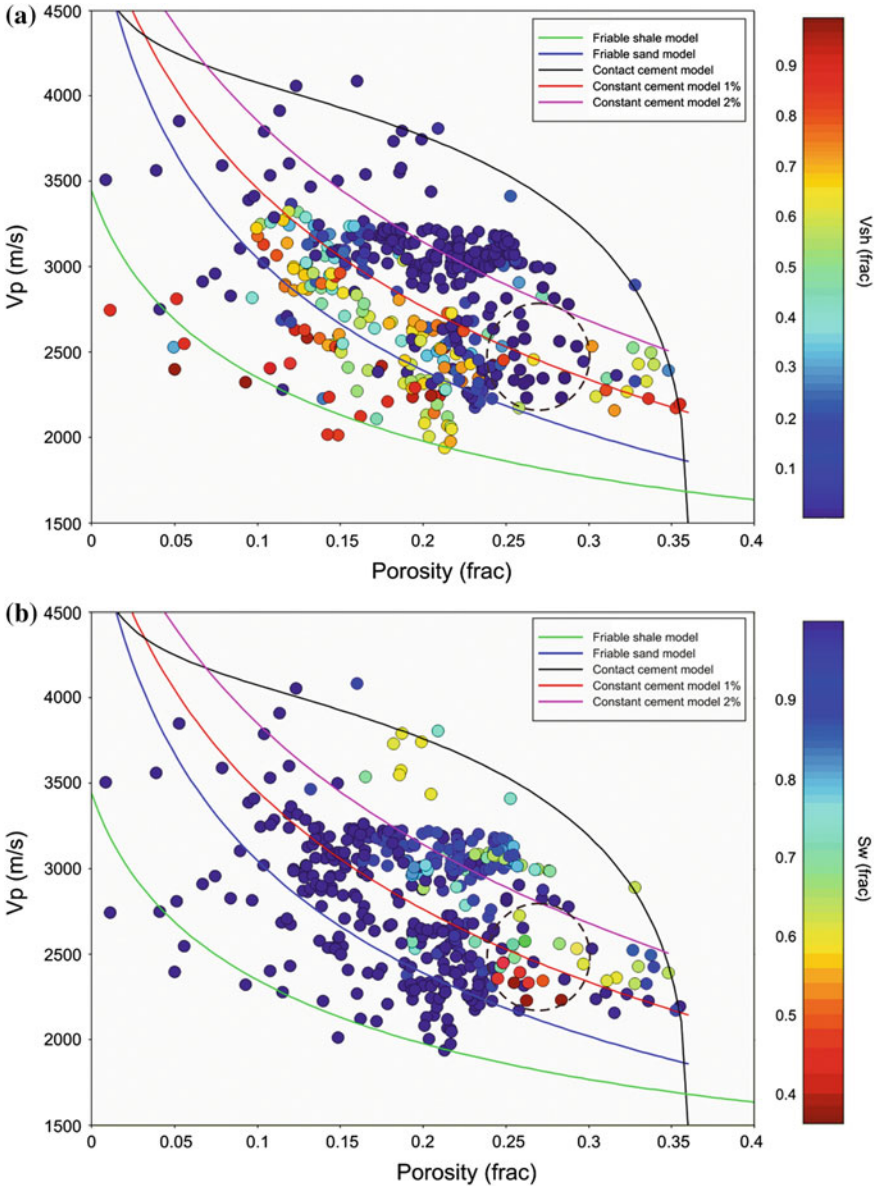

Fig. 5.8 P-wave velocity versus porosity cross plot for the major pay zone from Well ANKL-1 of Ankleshwar oil field, Cambay Basin with various rock physics model curves superimposed: **a** as a function of shale volume **b** as a function of brine saturation. *Dark brown circle* encloses clean sands with significant residual oil saturation

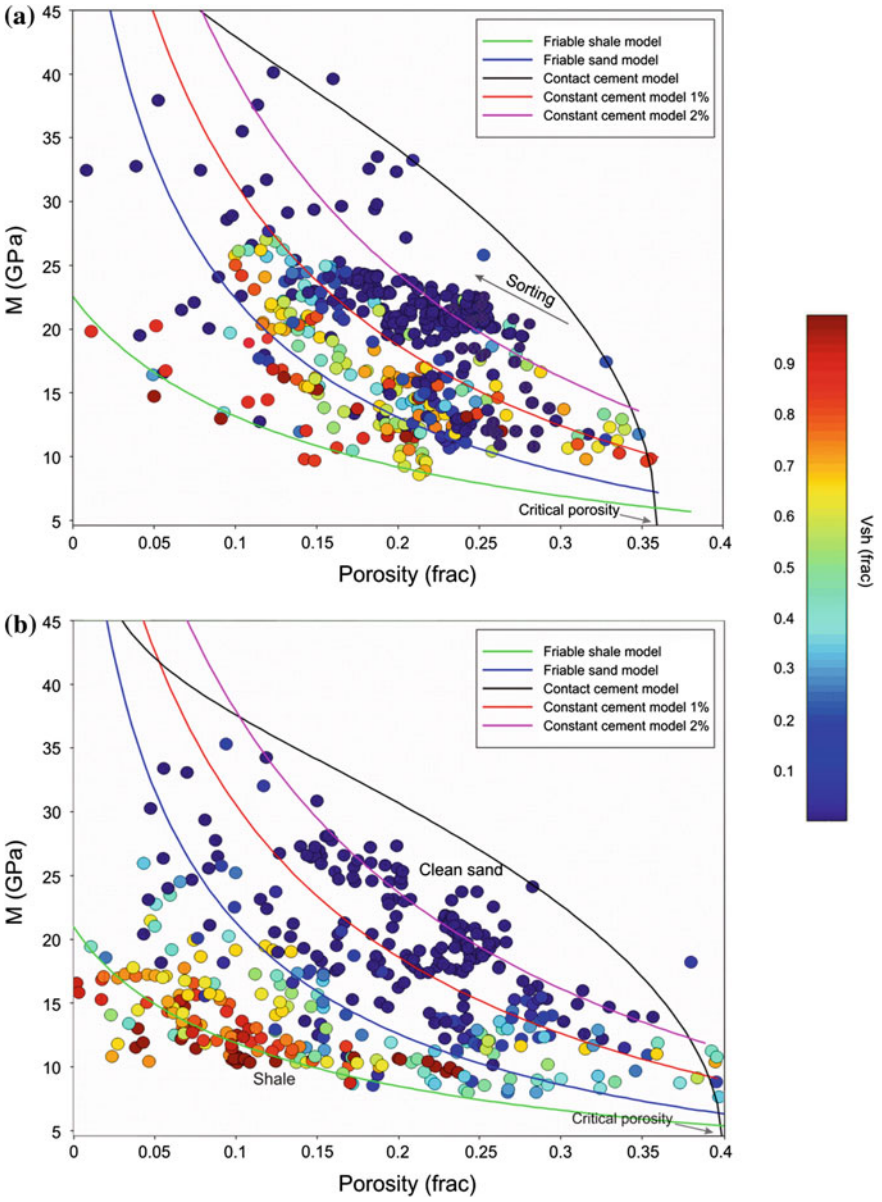

Fig. 5.9 Compressional modulus (M)-porosity cross plot for the major pay zone of Ankleshwar oil field in Cambay Basin: **a** Well ANKL-1, and **b** ANKL-2 and superimposed diagnostic RPMs. Note that the initial sand pack and sorting is different for both the well data. The *colour bar* indicates the shale volume in both the wells

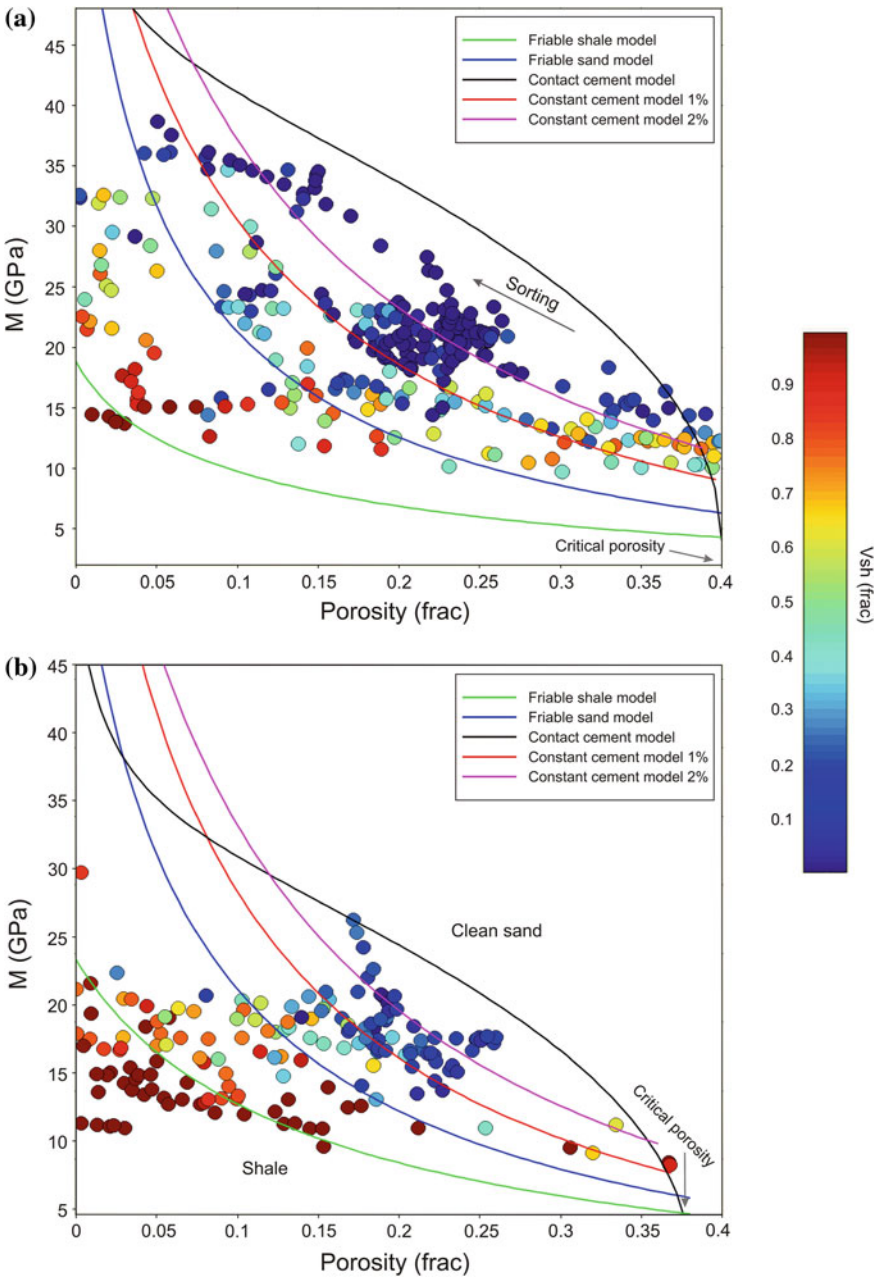

Fig. 5.10 Compressional modulus (M)-porosity cross plot for the major pay zone of Ankleshwar oil field in Cambay Basin: **a** Well ANKL-3, and **b** ANKL-4 and superimposed diagnostic RPMs. Note that the initial sand pack and sorting is different for both the well data. The *colour bar* indicates the shale volume in both the wells

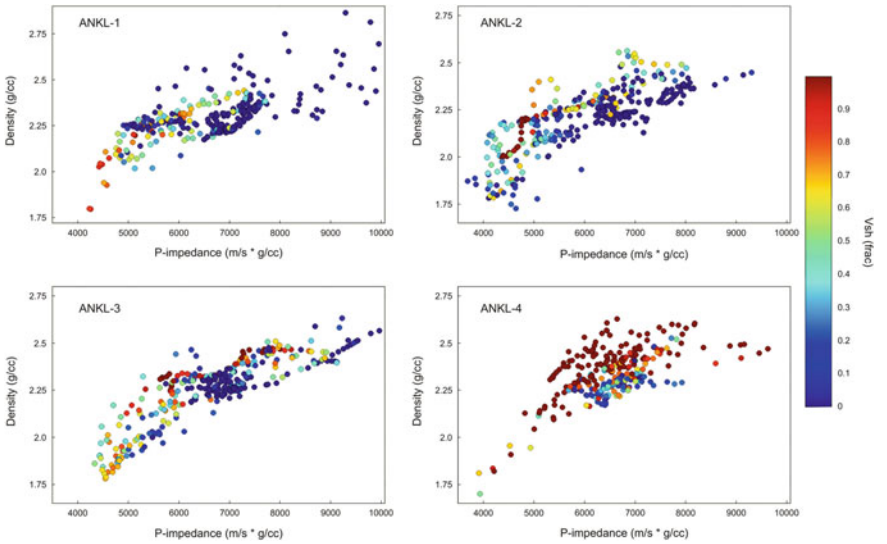

Fig. 5.11 Density-P-impedance cross plot for the major pay zone of Ankleshwar oil field in Cambay Basin: Wells, ANKL-1 and 2 (*Top*), ANKL-3 and 4 (*Bottom*). The *colour bar* indicates the shale volume in all the wells

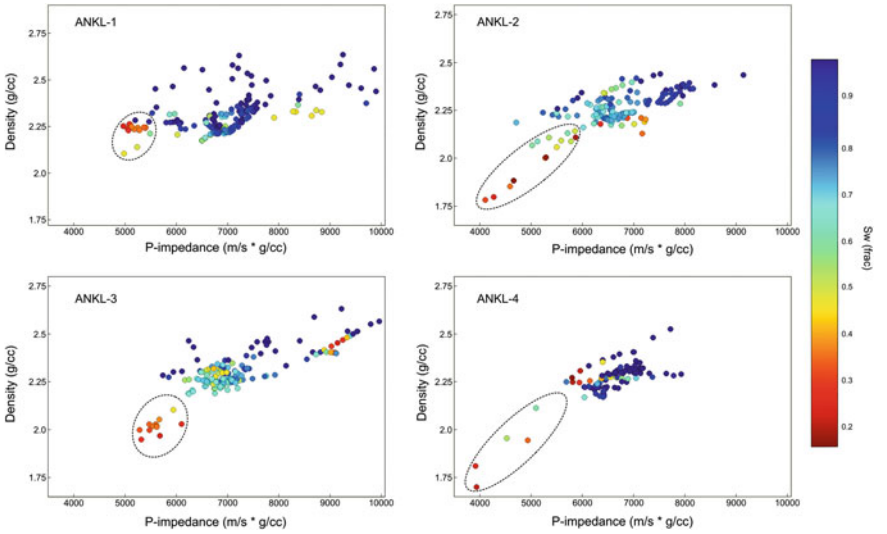

Fig. 5.12 Density-P-impedance cross plot for the major pay zone (*sands* only) of Ankleshwar oil field: Wells, ANKL-1 and 2 (*Top*), ANKL-3 and 4 (*Bottom*). The *colour bar* indicates the brine saturation (Sw) in all the wells. *Dark brown* ellipses enclose differentiated sands with significant residual oil saturation

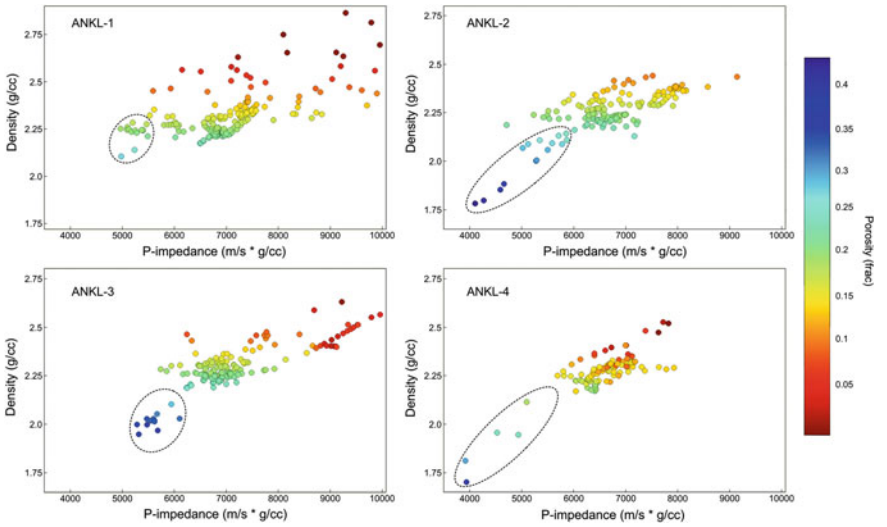

Fig. 5.13 Density-P-impedance cross plot for the major pay zone (*sands* only) of Ankleshwar oil field: Well ANKL-1 and 2 (*Top*), ANKL-3 and 4 (*Bottom*). The *colour bar* indicates the porosity. *Dark brown* ellipses enclose differentiated *sands* with relatively high porosity justifies the residual oil zone

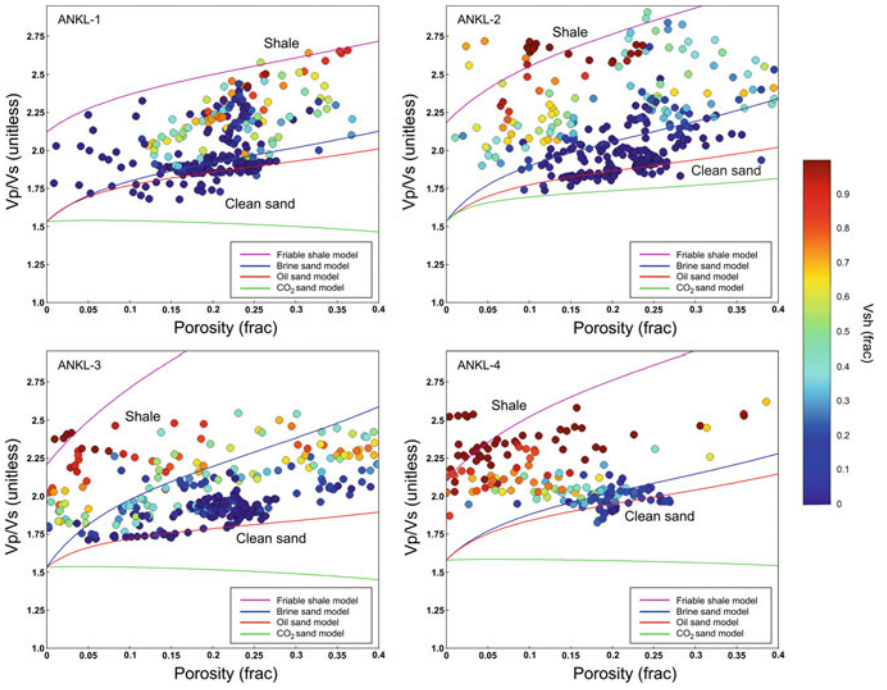

Fig. 5.14 Vp/Vs ratio versus porosity cross plot for the major pay zone of Ankleshwar oil field prior to CO_2 injection: Wells, ANKL-1 and 2 (*Top*), ANKL-3 and 4 (*Bottom*). The *colour bar* indicates the shale volume. The legend represents the models used to describe the data

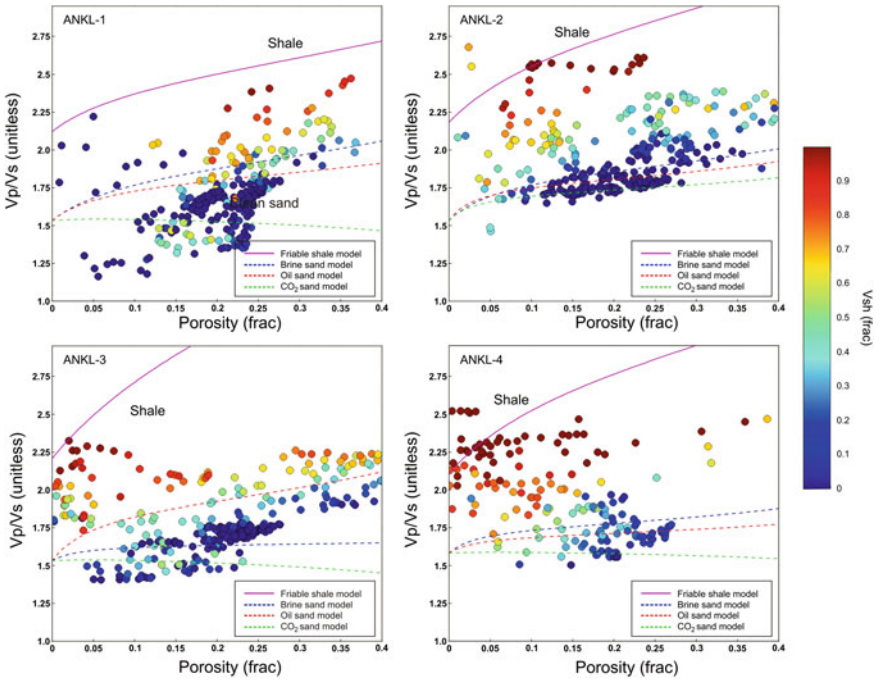

Fig. 5.15 Vp/Vs ratio versus porosity cross plot for the major pay zone of Ankleshwar oil field after CO_2 injection: Wells, ANKL-1 and 2 (*Top*), ANKL-3 and 4 (*Bottom*). The *colour bar* represents the shale volume. The legend represents the models used to describe the data

We observed the separation of clouds for shale and clean sands, and within the sandstone interval, various fluids are noticeably separated with oil sands plotting at comparatively lowest Vp/Vs ratio than brine sands from all the well data (Fig. 5.14). This analysis was done before CO_2 injection into the major pay zone (S3+4 sand horizons) of Ankleshwar formation, and we were interested to observe the effect of CO_2-EOR on the pay sands. As described earlier, constant cement model with 2% cementation scheme better explain this data, so we have used it to generate various sand models such as oil sand, brine sand and CO_2 sand models. It is noteworthy to mention that CO_2 sands correlated well to the model with distinguishably lower Vp/Vs ratio values (Fig. 5.15), suggesting a feasible CO_2-EOR operation at the field to recover bypassed oil. Also, we found that the effect of CO_2-EOR on Well ANKL-1 is comparatively larger than the other wells. This is mostly due to less assemblage of shale around sand packs, and pure sand occupied with CO_2 results in lower Vp/Vs ratio since CO_2 has lower bulk moduli compared to other reservoir fluids.

5.5 Time-Lapse Well Log Analysis, Fluid Substitution: Gassmann's Approach

Fluid substitution modeling is an effective tool in reservoir characterization, and can be understood as a short-term or immediate effect of CO_2-EOR and sequestration. The substitution of brine and oil by CO_2 during EOR operation can be interpreted from the seismic attributes such as velocity, impedance and elastic moduli using Gassmann's equations. Gassmann's approach is the low frequency limit (relaxed fluid-rock state) for wave propagation in saturated media, and it includes several assumptions; the rock is macroscopically homogeneous; all the pores are communicating and occupied with frictionless fluids (i.e. the viscosity of saturating fluid is close to zero); the rock-fluid system is closed (undrained) and there is no interaction between solid and fluid (Gassmann 1951; Smith et al. 2003; Mavko et al. 2009). Nevertheless, Gassmann's relations proved to be effective while studying sandstone reservoirs, and are fundamental process for reservoir fluid replacement problems. Therefore, Gassmann's approach was considered to study the CO_2 replacement effect on reservoir sands of Ankleshwar oil field. The fluid replacement modeling assumes that after dissolving in the residual oil, the supercritical CO_2 will effectively replace the oil. Gassmann proposed a relation to predict the changes in the elastic moduli due to pore fluid replacement in isotropic rocks:

$$\frac{K_{sat}}{K_{ma} - K_{sat}} = \frac{K_{dry}}{K_{ma} - K_{dry}} + \frac{K_{fl}}{\emptyset(K_{ma} - K_{fl})}, \tag{5.12}$$

$$G_{sat} = G_{dry}, \tag{5.13}$$

where, K_{sat}, K_{dry} are saturated and dry rock bulk modulus, and G_{sat}, G_{dry} are saturated and dry rock shear modulus, respectively. K_{ma}, K_{fl}, and $\emptyset$ are the mineral modulus making up rock, effective fluid bulk modulus, and porosity, respectively.

Gassmann's fluid replacement recipe is summarized below as described in Avseth et al. (2005) where it is proposed to initiate with an initial set of velocities and densities that usually comes from well logs (or might also be the results of inversion or theoretical models), corresponding to the rock with initial set of fluids, referred as "fluid (1)". Then fluid substitution can be performed in following steps as given by:

Step 1: Extract the dynamic elastic moduli from $V_p^{(1)}$, $V_s^{(1)}$, and $\rho^{(1)}$:

$$K^{(1)} = \rho^{(1)}\left[(V_p^{(1)})^2 - \frac{4}{3}(V_s^{(1)})^2\right], \quad G^{(1)} = \rho^{(1)}(V_s^{(1)})^2. \tag{5.14}$$

Step 2: Apply Gassmann's relation [Eq. (5.12)] to model the fluid replacement in the reservoir rock such that fluid (1) is replaced by a new fluid (2) with velocities of rock $V_p^{(2)}$, $V_s^{(2)}$, and bulk density $\rho^{(2)}$, respectively, and is given by:

$$\frac{K_{sat}^{(2)}}{K_{ma}-K_{sat}^{(2)}}-\frac{K_{fl}^{(2)}}{\emptyset(K_{ma}-K_{fl}^{(2)})}=\frac{K_{sat}^{(1)}}{K_{ma}-K_{sat}^{(1)}}-\frac{K_{fl}^{(1)}}{\emptyset(K_{ma}-K_{fl}^{(1)})}. \tag{5.15}$$

Step 3: Leave the shear modulus unchanged during fluid substitution:

$$G_{sat}^{(2)}=G_{sat}^{(1)}. \tag{5.16}$$

Step 4: Estimate the new rock bulk density for the fluid change:

$$\rho^{(2)}=\rho^{(1)}+\emptyset\left(\rho_{fluid}^{(2)}-\rho_{fluid}^{(1)}\right). \tag{5.17}$$

Step 5: Reassemble the velocities for the new fluid:

$$V_p^{(2)}=\sqrt{\left[K_{sat}^{(2)}+\frac{4}{3}G_{sat}^{(2)}\right]/\rho^{(2)}},\quad V_s^{(2)}=\sqrt{G_{sat}^{(2)}/\rho^{(2)}}. \tag{5.18}$$

CO_2 injection has not been started in the Ankleshwar oil field to date, therefore, in this study, we investigated the possibility of CO_2 drive through the whole oil leg, where in the residual oil was replaced by the injected CO_2. The residual oil saturation input was taken from the simulation results as discussed in Chap. 3, and correlated with the available well-log data. The new fluid mixture bulk modulus and density were calculated as a combination of arithmetic average (i.e. patchy saturation case), and the harmonic average (i.e. uniform saturation case) of fluid bulk moduli and densities (Mavko and Mukherjee 1998). The fluid properties utilized for fluid substitution modeling were calculated by considering Ankleshwar reservoir temperature and pressure conditions, and using Batzle and Wang's empirical relationships (Batzle and Wang 1992) as discussed in Chap. 4.

Figures 5.16 and 5.17 illustrate the results from fluid replacement modeling in wells ANKL-1, ANKL-2, ANKL-3 and ANKL-4. The velocity changes were estimated at 20% CO_2 saturation for uniform and patchy saturation within Ankleshwar formation. Higher saturations are likely to be present in the real case when implemented; consequently 20% saturation can be viewed as reasonable minimum.

We identified that the elastic properties of Ankleshwar formation were altered, resulted in changes in seismic velocities and densities due to CO_2 injection. P-wave velocity (Vp) and density changes before and after CO_2 injection are comparatively larger than S-wave velocity (Vs) changes, and the decrease in Vp in case of uniform saturation is significantly larger than in the case of patchy saturation, demonstrating an upper and lower bounds for Vp changes for the given saturation, respectively (Figs. 5.16 and 5.17).

It is noteworthy that Vs increases after CO_2 injection, in both the uniform- and patchy-saturation cases, due to density reduction at each depth level. Also, the dry modulus at each depth sample was calculated from the saturated modulus assuming

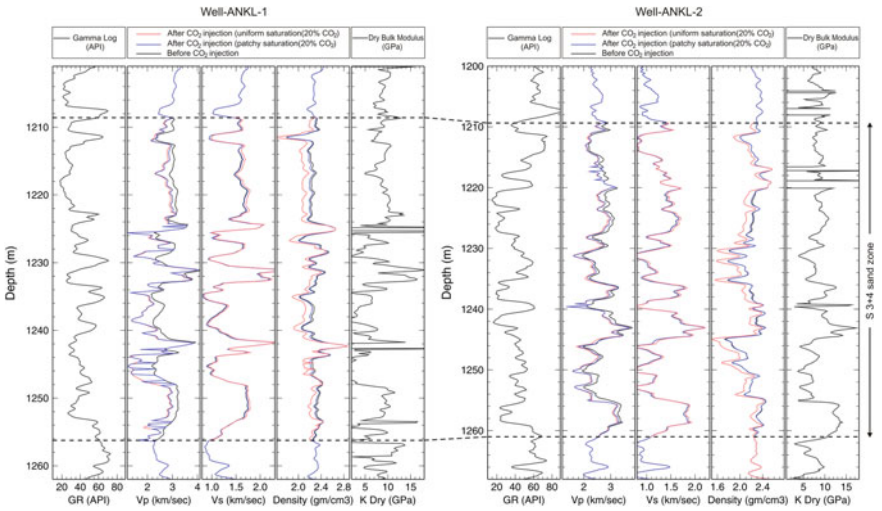

Fig. 5.16 Gamma log, fluid substituted Vp, Vs, and density logs for uniform-and patchy-saturation models at 20% CO_2 saturation, and dry bulk modulus log in Wells, ANKL-1 (*Left*) and ANKL-2 (*Right*), respectively. *Dashed black curve* represents the major pay sands (S3 +4) of Ankleshwar reservoir

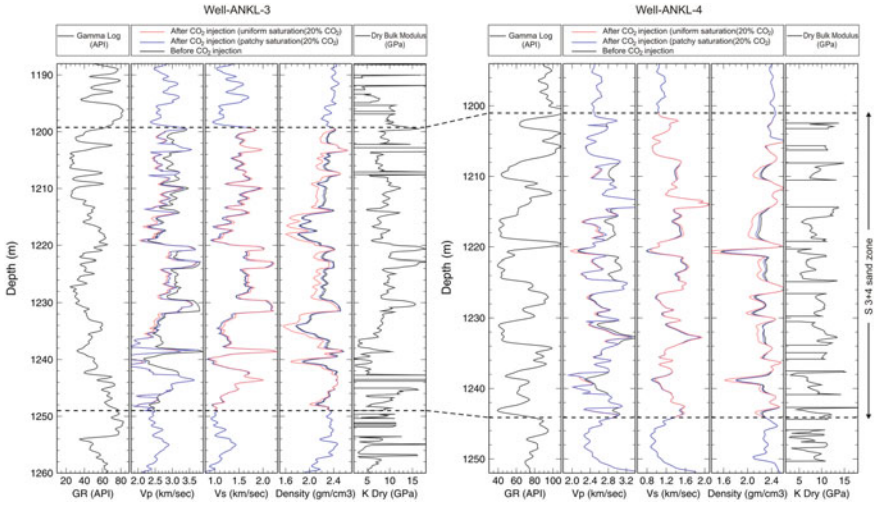

Fig. 5.17 Gamma log, fluid substituted Vp, Vs, and density logs for uniform- and patchy—saturation models at 20% CO_2 saturation, and dry bulk modulus log in Wells, ANKL-3 (*Left*) and ANKL-4 (*Right*), respectively. *Dashed black curve* represents the major pay sands (S3+4) of Ankleshwar reservoir

that matrix modulus is constant for the reservoir pay zone. We found that the dry bulk modulus ranges from 5 to 18 GPa. The variation in dry bulk modulus can be correlated to the increase in gamma reading, suggesting presence of pore filling clay particles within the medium.

5.6 Rock Physics Template (RPTs) Analysis

The *Rock Physics Templates* (RPTs) tool was introduced by Ødegaard and Avseth (2004) for effective reservoir characterization, which are rock physics models constrained by local geological factors (Avseth et al. 2005). In general, RPTs are field (basin) specific, and represented by a cross plot of elastic parameters obtained theoretically from various rock physics models constrained by the expected lithology for the area under investigation. The most widely used RPT is the cross plot between Vp/Vs ratio and P-wave acoustic impedance (AI), since combination of these two is a better indicator for lithology and fluid content from well logs (Avseth et al. 2005). The reliability of the rock physics template is highly dependent on the quality of input data and model assumption (Ødegaard and Avseth 2004).

Figure 5.18 demonstrates an example of RPT including the theoretical trends developed by assuming idealized siliciclastic lithologies, fluid along with its saturation, and porosity, which can be used when interpreting well data or seismically derived cross plot values (elastic properties inverted from seismic).This template helps to interpret and classify various fluid and geological trends from the data.

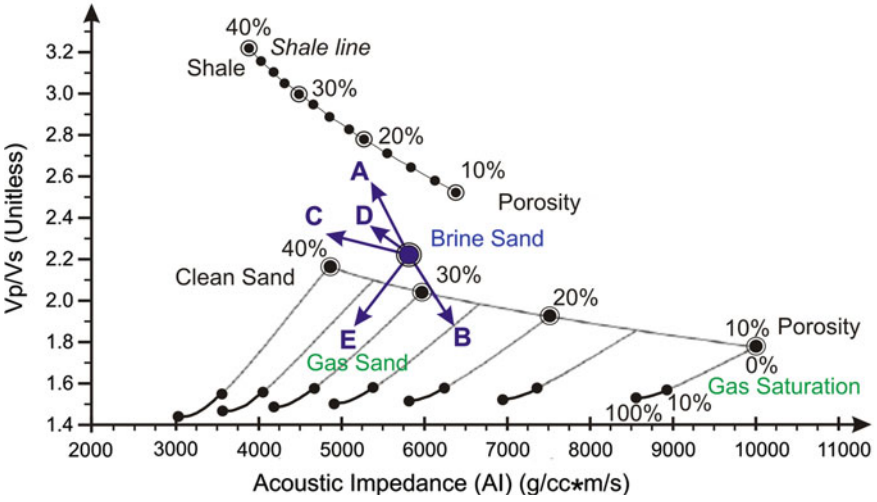

Fig. 5.18 Schematic of rock physics template (RPT) in terms of mineralogy, fluid content, and porosity made from the rock physics models in conjunction with Gassmann's fluid substitution approach (modified after Ødegaard and Avseth 2004). The theoretical trends are shown by assuming idealized siliciclastic lithologies, can be used when interpreting well data or seismically derived cross plot values

In the modeling of an RPT (Avseth et al. 2005), the first step is to establish velocity-porosity trends for the expected lithology at different burial depths. This is followed by the application of Hertz-Mindlin contact theory (Mindlin 1949) to calculate the dry modulus of the pressure dependency rock at the high-porosity end member. The other end member is calculated at the zero porosity and has the bulk and shear moduli of the solid mineral. These two points in the porosity-moduli plane are then connected by the curve based on Hashin-Shtrikman (1963) bounds, which gives theoretical predicted values of effective elastic moduli of the mixture of grains and pores. For unconsolidated sands, porosity reduction due to packing and sorting can be explained by the lower bound. On the other hand, for cemented rocks, the upper Hashin-Shtrikman bound or Dvorkin-Nur's model should be applied. The Hashin-Shtrikman bounds can be applied to mixtures of more than two phases with the assumption that each phase and the rocks are isotropic and elastic (Chi and Han 2009).

The dry rock properties calculated from the combined Hertz-Mindlin and Hashin-Shtrikman model are used as the inputs into Gassmann's equation to evaluate the effect of fluid substitution in RPT with various fluids (e.g. brine, oil/gas, CO_2) assuming either uniform or patchy saturation. It is important to note that during RPT modeling process, we need to know various acoustic properties of brine and hydrocarbons in the area of investigation which can be known by utilizing reservoir pressure, temperature, brine salinity, gas gravity, oil API gravity, saturation and gas-to-oil ratio (GOR), etc.

5.6.1 Static Rock Physics Template Analysis for Ankleshwar Oil Field

The static rock physics templates (SRPTs) are used widely in industry for reservoir characterization of producing reservoir at a fixed time of its life history (Meneses 2013). These can be developed to locate the bypassed oil zone, a potential target for CO_2-EOR operation. As we have seen that the constant cement model has described properly the in situ well data of the Ankleshwar reservoir (Fig. 5.8), so we decided to utilize constant cement model in SRPT analysis to investigate the bypassed oil zone. Nevertheless, friable shale model (magenta curve) was also developed to describe the shale content in the reservoir pay zone (Figs. 5.19 and 5.20). Vp/Vs ratio and P-wave acoustic impedance of the saturated rocks were estimated to build the SRPT. Additionally, the cross plots were colour coded to represent shale volume and brine saturation for reliable interpretation. Table 5.1 summarize the parameters used in the modeling of RPTs for Ankleshwar oil reservoir in Cambay Basin.

The results from the SRPT analysis for the major pay zone (S3+4) of Ankleshwar formation including all in situ well data are depicted in Figs. 5.19 and 5.20. We identified zone A (dark brown polygon) on all the Vp/Vs ratio versus

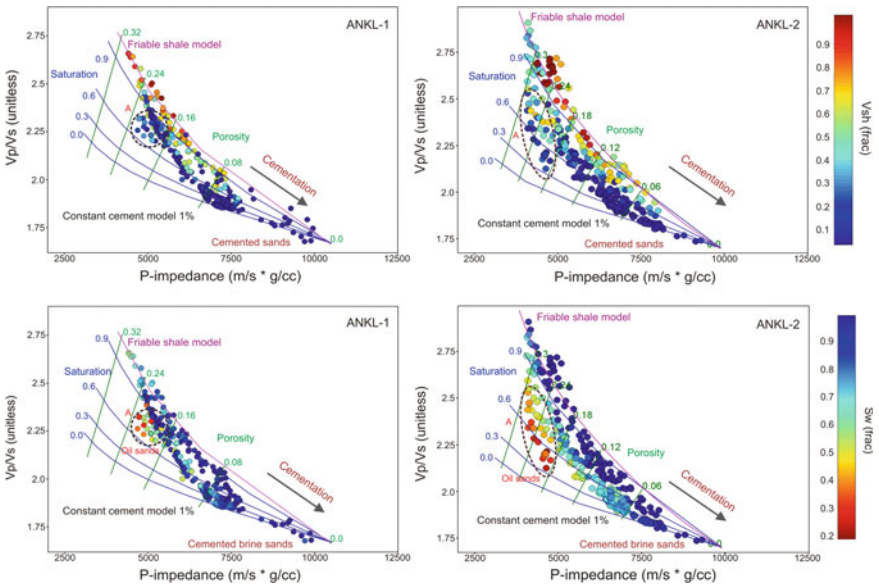

Fig. 5.19 A cross plot between Vp/Vs ratio and P-wave impedance from Wells, ANKL-1 (*Left*) and ANKL-2 (*Right*) of Ankleshwar oil field. The *colour bar* represents the shale volume (*Upper*), and brine saturation (*Lower*) in fraction. Different well data was superimposed on the constant cement model (1%) and friable shale model. The *dark brown* polygon (zone A) encompasses the clean sand with significant residual oil zone, a possible target for CO_2-EOR

P-impedance cross plots, where clean sand dominates with average brine saturation of more than 55% according to the SRPT which is not correlated reliably with the well data measurements, unlike from the well ANKL-2 where the well-log measured saturation points positioned close with the SRPT derived saturation lines. Therefore, SRPTs over predict the brine saturation. However, the bypassed oil sands were located in the average porosity of about 0.24 from the SRPT which matches with the observed porosity range of about 20–25% of Ankleshwar reservoir (Figs. 5.19 and 5.20). This can be referred as inherent non-uniqueness in RPT modeling while evaluating various reservoir parameters at a fixed production life. The source of these ambiguities can be sorting, clay content, lithology, etc. One way to solve these ambiguities would be the use of Vs log data which is not available with us for investigation.

Brine cemented regions have also been realized in the entire cross plots, unlike in well ANKL-4 where brine cemented sands are almost absent (Fig. 5.20). These brine cemented sand were validated with significantly low porosity and high P-impedance values, characterizes trend for increasing burial depth and subsequent compaction. Additionally, we found the shale assemblage in well ANKL-4 located at comparatively greater depth than the shale cluster from all the wells, probably has been subjected to high degree of compaction than the shales in other wells (Fig. 5.20).

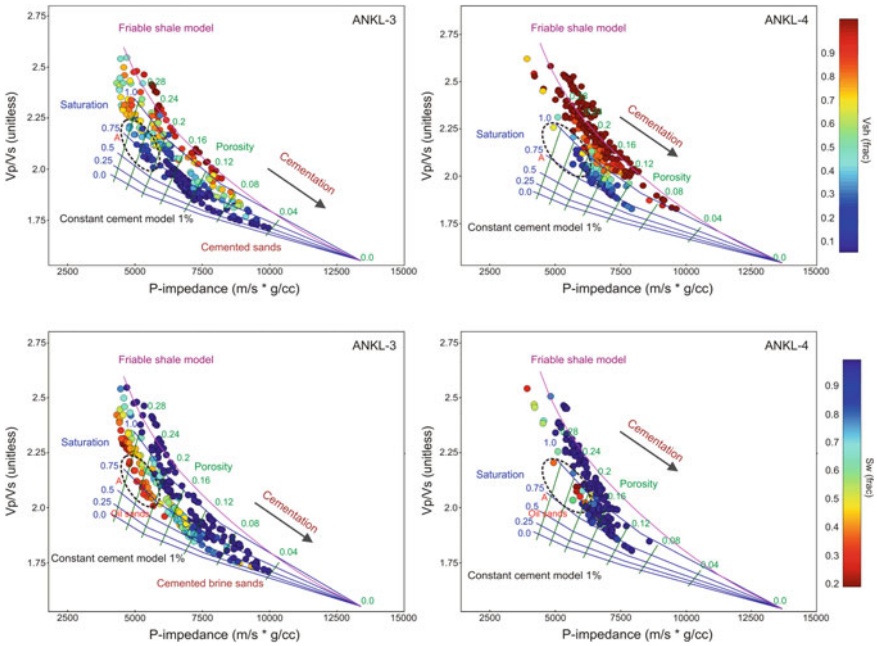

Fig. 5.20 A cross plot between Vp/Vs ratio and P-wave impedance from Wells, ANKL-3 (*Left*) and ANKL-4 (*Right*) of Ankleshwar oil field. The *colour bar* represents the shale volume (*Upper*), and brine saturation (*Lower*) in fraction. Different well data was superimposed on the constant cement model (1%) and friable shale model. The *dark brown* polygon (zone A) encompasses the clean sand with significant residual oil zone, a possible target for CO_2-EOR

Table 5.1 Input model parameters for RPTs forward modeling

Summary of parameters used in RPTs modeling	
Reservoir temperature = 78 °C	Gas gravity = 1.12 API
Effective pressure = 13.1 MPa	Co-ordination number = 8.65–10.3
Brine salinity = 33,000 ppm	Shear friction factor = 0.4
Oil gravity = 46.3 API	Critical porosity = 0.36–0.40

5.6.2 *Dynamic Rock Physics Template Analysis for Ankleshwar Oil Field*

The dynamic rock physics templates (DRPTs) relate the relative changes in elastic properties due to pore pressure and fluid saturation changes in its production life history (Andersen et al. 2009; Meneses 2013). The feasibility of dynamic rock physics modeling for Ankleshwar oil field comprises of quantifying the relative changes in reservoir property between the monitor surveys due to CO_2 injection for EOR operation. The relative changes can be represented by:

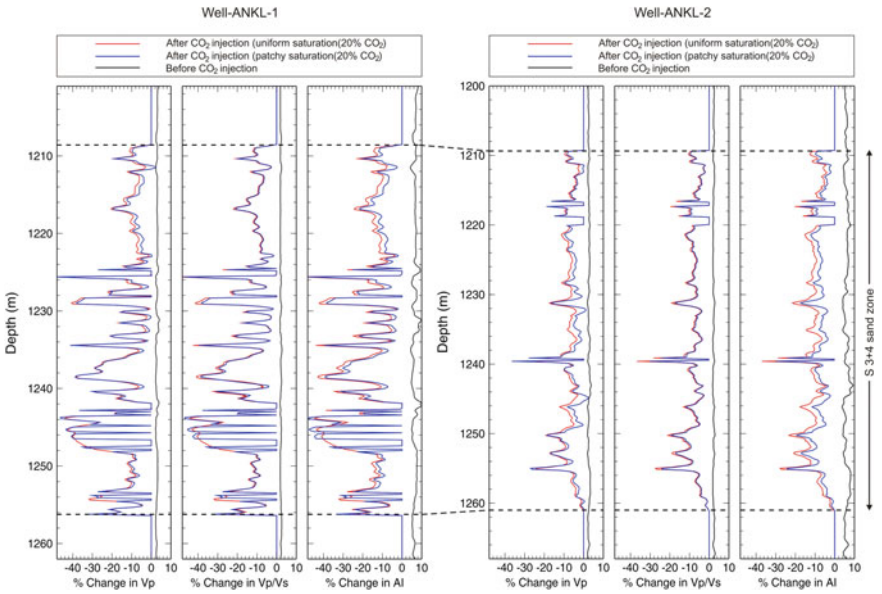

Fig. 5.21 Time-lapse (4D) variation of the elastic parameters such as P-wave velocity, Vp/Vs ratio, and acoustic impedance from Wells, ANKL-1 (*Left*) and ANKL-2 (*Right*), respectively, within the major pay zone of Ankleshwar reservoir due to CO_2 injection for EOR. Here, both the uniform- and patchy-saturation models at 20% CO_2 saturation are considered. Note that patchy-saturation model at 20% CO_2 saturation provides very efficient thin layer saturation information, which is not attempted by the uniform saturation model

$$E_{diff} = 100 * [E_{mon2} - E_{mon1}]/E_{mon1}, \tag{5.19}$$

where E_{diff} is any elastic property, and E_{mon2} and E_{mon1} are the elastic properties measured during monitor 2 and 1, respectively. Shear velocity and shear impedance are almost insensitive to fluid saturation change, hence, we didn't analysed the 4D changes in these elastic attributes. Figure 5.21 illustrates the time-lapse (4D) relative changes in elastic attributes such as P-wave velocity (Vp), Vp/Vs ratio, and P-impedance, respectively, when CO_2 replaces the residual oil in Ankleshwar reservoir.

One can note that small amount of CO_2 changes Vp and P-impedance drastically in comparison to Vp/Vs, and the change in case of uniform saturation is significantly larger than in the case of patchy saturation within the Ankleshwar formation. It is interesting to observe the saturation heterogeneity in patches which is identified clearly by patchy saturation (especially in well ANKL-1) since there is no pressure communication between small patches, unlike in uniform saturation where the fine scale heterogeneity is not observed (Figs. 5.21 and 5.22). Nevertheless, these changes may not be noticeable in seismic since well measurement and seismic has completely different spatial resolution.

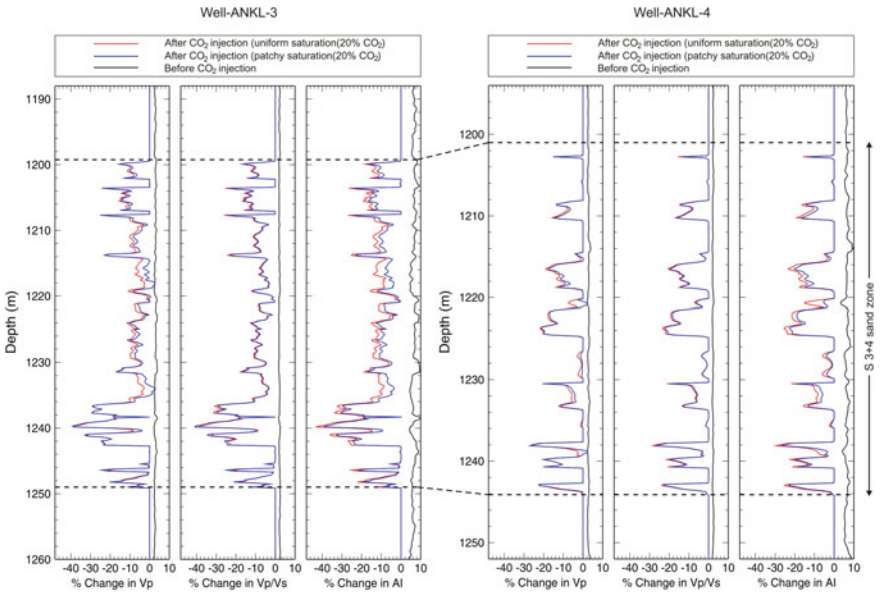

Fig. 5.22 Time-lapse (4D) variation of the elastic parameters such as P-wave velocity, Vp/Vs ratio, and acoustic impedance from Wells, ANKL-3 (*Left*) and ANKL-4 (*Right*), respectively, within the major pay zone of Ankleshwar reservoir due to CO_2 injection for EOR. Here, both the uniform- and patchy-saturation models at 20% CO_2 saturation are considered

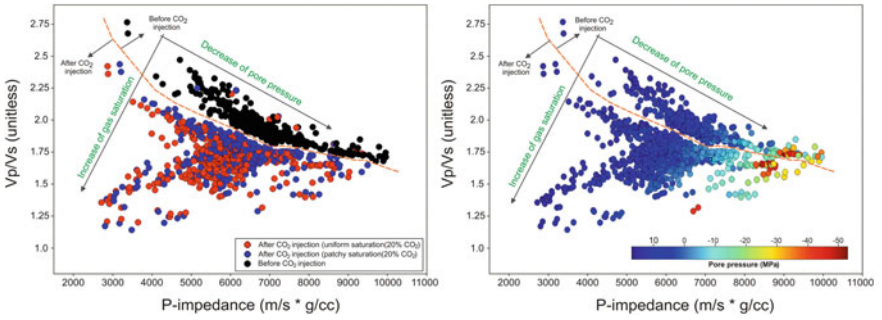

Fig. 5.23 Dynamic RPT analysis within the major pay zone (*sands* only) of Ankleshwar reservoir, both pre- and post- CO_2 injection scenario is visualized using all the well-logs. Here, both the uniform- and patchy-saturation models at 20% CO_2 saturation are considered. The *arrow* indicates the direction of increase in CO_2 saturation and decrease in pore pressure, respectively. A *dashed orange curve* is drawn to separate the sands before and after CO_2 injection, respectively. The colour bar in the right plot signifies pore pressure variation

To quantify the 4D changes in reservoir properties, a cross plot of Vp/Vs ratio and P-impedance was built wherein the decrease in Vp/Vs ratio with the increase in CO_2 saturation is clearly observed, both in case of uniform and patchy saturation (Fig. 5.23). The dynamic classification was validated from the observation of significant decrease in pore pressure after CO_2 injection.

5.7 Conclusions

We investigated the feasibility of rock physics modeling approach to understand CO_2-EOR and properly monitor the injected CO_2 at Ankleshwar oil field. Based on the observations, following specific conclusions were made:

- We conducted shear log (Vs) prediction study since Vs log was not provided, and we found that Greenberg-Castagna and G-method are most suitable Vs data prediction technique than the other available methods.
- We provided a rock physics modeling work flow to diagnose the reservoir sands of Ankleshwar oil field in Cambay Basin. Rock physics diagnostic approach confirms that the theoretical models are useful in diagnosing the reservoir sands for possible for CO_2-EOR from the available well data penetrating Ankleshwar formation. We propose that no single model can explain the data adequately; yet a combination of three RPMs could explain better the well data of this reservoir. It is also noteworthy that, the velocity-porosity trends from all the available wells under study indicates that the reservoir sands were undergone different cementation schemes, and the velocity differentiation in high porosity and unconsolidated sands is related to the grain sorting. It is also found that the oil producing sands fall into the well-known constant cement model.
- The cross plot analysis with superimposed RPMs was found to be effective to classify and interpret the lithology and pore fluid saturated sands. We identified the density versus P-impedance cross plot as a powerful tool for fluid discriminator than a lithologic identifier. From the Vp/Vs versus porosity cross plot, we observed that CO_2 sands correlated reasonable to the model with distinguishably lower Vp/Vs ratio values, suggesting a feasible CO_2-EOR at the field for bypassed oil recovery. Also, the effect of CO_2-EOR on Well ANKL-1 is comparatively larger than the others.
- P-wave velocity (Vp) and density changes before and after CO_2 injection are comparatively larger than S-wave velocity (Vs) changes, and the decrease in Vp in case of uniform saturation is significantly larger than in the case of patchy saturation, demonstrating an upper and lower bounds for Vp changes for the given saturation, respectively.
- RPT analysis was also implemented on the well data by cross plotting the elastic properties in conjunction with the RPTs, and we found that Ankleshwar formation contains clean sands with significant residual oil saturation after witnessing massive water flooding, and the major pay zone can be a potential target for CO_2-EOR.
- Quantitative time-lapse (4D) relative changes in elastic parameters were analysed, which is an important part of reservoir management during enhanced oil recovery operation at the field. We identified that the percentage changes in P-wave velocity and P-impedance are drastic in comparison to Vp/Vs, and the changes in case of uniform saturation are significantly larger than in case of patchy saturation, within the Ankleshwar formation. Additionally, 4D effects of saturation heterogeneity changes were observed clearly for patchy saturation, unlike in uniform saturation.

References

Andersen CF, Grosfeld V, Wijngaarden AJV, Haaland AN (2009) Interactive interpretation of 4D prestack inversion data using rock physics templates, dual classification, and real-time visualization. Lead Edge 28(8):898–906

Avseth P (2000) Combining rock physics and sedimentology for seismic reservoir characterization of North Sea turbidite systems. PhD thesis, Stanford University, p 181

Avseth P, Dvorkin J, Mavko G, Rykkje J (2000) Rock physics diagnostics of North Sea sands: link between microstructure and seismic properties. Geophys Res Lett 27(17):2761–2764

Avseth P, Mukerji T, Mavko G (2005) Quantitative seismic interpretation: applying rock physics to reduce interpretation risk. Cambridge University Press, Cambridge

Avseth P, Mukerji T, Mavko G, Dvorkin J (2010) Rock-physics diagnostics of depositional texture, diagenetic alterations, and reservoir heterogeneity in high-porosity siliciclastic sediments and rocks—a review of selected models and suggested workflows. Geophysics 75(5):75A31–75A47

Batzle M, Wang Z (1992) Seismic properties of pore fluids. Geophysics 57(11):1396–1408

Berryman JG (1980) Long-wavelength propagation in composite elastic media. J Acoust Soc Am 68:1809–1831

Biot MA (1956) Theory of propagation of elastic waves in a fluid saturated porous solid. I. Low frequency range and II. Higher-frequency range. J Acou Soc Am 28:168–191

Castagna JP, Batzle ML, Eastwood RL (1985) Relationships between compressional wave and shear-wave velocities in clastic silicate rocks. Geophysics 50:571–581

Chi X, Han D (2009) Lithology and fluid differentiation using rock physics templates. Lead Edge 28:60–65

Digby PJ (1981) The effective elastic moduli of porous granular rocks. J Appl Mech 48(4):803–808

Dvorkin J, Nur A (1996) Elasticity of high-porosity sandstones: theory for two North Sea data sets. Geophysics 61:1363–1370

Dvorkin J, Nur A, Yin H (1994) Effective properties of cemented granular materials. Mech Mater 18:351–366. doi:10.1016/0167-6636(94)90044-2

Gassmann F (1951) Über die elastizität poröser medien: Vierteljahrss-chrift der Naturforschenden Gesellschaft in Zurich 96, 1–23. The English translation of this paper is available at http://sepwww.stanford.edu/sep/berryman/PS/gassmann.pdf

Greenberg ML, Castagna JP (1992) Shear-wave velocity estimation in porous rocks: theoretical formulation, preliminary verification and applications. Geophys Prospect 40(2):195–209

Han D (1986) Effects of porosity and clay content on acoustic properties of sandstones and unconsolidated sediments. PhD thesis, Stanford University

Han DH, Batzle ML (2004) Gassmann's equation and fluid-saturation effects on seismic velocities. Geophysics 69(2):40–398

Hashin Z, Shtrikman S (1963) A variational approach to the elastic behavior of multiphase materials. J Mech Phys Solid 11:127–140

Hill R (1952) The elastic behavior of crystalline aggregate. Proc Phys Soc Lond A 65:349–354

Hossain J (2011) Rock physics modelling of the North Sea greensand. PhD thesis, Department of Environmental Engineering, Technical University of Denmark

Klimentos T (1991) The effects of porosity-permeability-clay content on the velocity of compressional waves. Geophysics 56:1930–1939

Krief M, Garat J, Stellingwerff J, Ventre J (1990) A petrophysical interpretation using the velocities of P and S waves (full-waveform sonic). Log Anal 31:355–369

Kuster GT, Toksöz MN (1974) Velocity and attenuation of seismic waves in two-phase media. Geophysics 39:587–618

Mavko G, Jizba D (1991) Estimating grain-scale fluid effects on velocity dispersion in rocks. Geophysics 56:1940–1949

Mavko G, Mukerji T (1998) Bounds on low frequency seismic velocities in partially saturated rocks. Geophysics 63(3):918–924
Mavko G, Mukerji T, Dvorkin J (2009) The Rock physics handbook: tools for seismic analysis of Porous media, 2nd edn. Cambridge University Press, Cambridge
Meneses CCC (2013) Dynamic reservoir characterization using 4D multicomponent seismic data and rock physics modeling at Delhi field, Louisiana. Master thesis, Colorado School of Mines
Mindlin RD (1949) Compliance of elastic bodies in contact. J Appl Mech 16:259–268
Mukerji T, Berryman JG, Mavko G, Berge PA (1995a) Differential effective medium modeling of rock elastic moduli with critical porosity constraints. Geophys Res Lett 22:555–558
Mukerji T, Mavko G, Mujica D, Lucet N (1995b) Scale-dependent seismic velocity in heterogeneous media. Geophysics 60:1222–1233
Ødegaard E, Avseth P (2004) Well log and seismic data analysis using rock physics templates. First Break 22:37–43
Reuss A (1929) Berechnung der Fliessgrenzen von Mischkristallen auf Grund der Plastizitätsbedingung für Einkristalle. Z Ang Math Mech 9:49–58
Smith TM, Sondergeld CH, Rai CS (2003) Gassmann fluid substitutions: a tutorial. Geophysics 68:430–440
Vernik L, Nur A (1992) Petrophysical classification of siliciclastics for lithology and porosity prediction from seismic velocities. AAPG Bull. 76:1295–1309
Voigt W (1910) Lehrbuch der Kristallphysik. Teubner, Berlin
Walton K (1987) The effective elastic moduli of a random packing of spheres. J Mech Phys Solid 35:213–226
Xu S, White RE (1995) A new velocity model for clay-sand mixtures. Geophys Prospect 43: 91–118
Zimmerman RW (1991) Elastic moduli of a solid containing spherical inclusions. Mech Mater 12:17–24

Chapter 6
Implication of CO_2-EOR and Storage at Ankleshwar Oil Field—A Reservoir Geomechanics Viewpoint

6.1 Introduction

CO_2-Enhanced oil recovery (EOR) is considered as an encouraging solution to recover by-passed/residual oil, and also an attractive option to mitigate the impact of rise of anthropogenic CO_2 on climate if sequestration is implemented (Schrag 2007). Hydrocarbon reservoirs are considered to be safe storage sites due to their historic record of trapping buoyant fluids for millions of years, implying the presence of effective trap and seal mechanisms (Holt et al. 1995; Chiaramonte 2008; Bickle 2009; Jenkins et al. 2012; Srivastava et al. 2015). Additionally, the advantage of CO_2 storage in mature hydrocarbon fields is the fact that much of the surface infrastructures for fluid injection (e.g. well-bores, compressors, pipelines) are already exists in the field. However, it has been reported that CO_2 injection into the reservoir causes change in the pore pressure and stress field that could potentially create or reactivate fracture networks in the sealing cap-rocks or triggering slip on pre-existing faults by reducing the effective normal stress on fault plane (Grasso 1992; Hawkes et al. 2005; Lucier et al. 2006; Chiaramonte et al. 2008; Verdon et al. 2013), providing a pathway for CO_2 leakage. In light of this, it is equally necessary to ascertain the safety associated with the CO_2-EOR and storage operation for a viable carbon management solution. If the potential for CO_2 leakage is significant, then the project will not be encouraged even though it possesses the needed capacity (Lucier et al. 2006). A key step in the risk assessment for geologic carbon sequestration project is the ability to predict whether the increased pressures associated with CO_2 injection are likely to affect the seal integrity and well-bore stability or not. Additionally, the study has great relevance to investigate the occurrence of any induced seismicity from CO_2 injection. A great many of studies (Shapiro et al. 2007; Cappa and Rutqvist 2011; Nicol et al. 2011; Zoback and Gorelick 2012; Davies et al. 2013; Kim 2013; Verdon et al. 2015) have been done to analyse the risk of inducing seismic activity by underground injection of large volumes of CO_2.

S.S. Ganguli, *Integrated Reservoir Studies for CO_2-Enhanced Oil Recovery and Sequestration*, Springer Theses,
DOI 10.1007/978-3-319-55843-1_6

As discussed in the previous Chaps. 2 to 5, Ankleshwar oil field in Cambay Basin (Western India) is a mature oil field that witnessed massive water flooding for ~50 years. Thus, injecting CO_2 for EOR and storage may cause unfavourable geomechanical changes such as changes in in situ effective stresses, consolidation, and depressurization in the reservoir, which could lead to potential instabilities. Moreover, sound understanding of in situ stresses can aid in designing maximum allowable injection pressure accurately that could improve the safety and cost-effectiveness of drilling and production during CO_2-EOR.

In this chapter, we investigated the geomechanical aspects of feasible CO_2-EOR and storage operation focusing on Ankleshwar reservoir in Cambay Basin, India. A preliminary geomechanical model has been developed to estimate the pore pressure, in situ stresses in the reservoir using available well log data from the four wells drilled through the Ankleshwar formation in Cambay Basin. A very effective methodology by Zoback et al. (2003) was adapted for evaluating in situ stress field as direct stress measurements are not available. Both, pre- and post-CO_2 injection situations were realized to evaluate the geomechanical response of the reservoir to CO_2 injection.

6.2 Building a Geomechanical Model: Ankleshwar Oil Field Example

From a geomechanical perspective, a suitable site for CO_2 storage followed by EOR should have sufficient injectivity while maintaining cap rock integrity. Otherwise, wellbore stability will be disturbed since wellbore stability is dominated by the in situ stress system. Figure 6.1 elucidates the potential geomechanical instabilities, and variety of methods that can be used to monitor geomechanical deformation in a field.

Although the implication of evaluating geomechanical deformation in hydrocarbon reservoirs is becoming increasingly appreciated, monitoring it in the field remains rather of a niche activity (Verdon et al. 2013). There are several advantages of storing CO_2 after successful EOR operation in the field, such as known capacity, provable seal and known injectivity (Fig. 6.2).

The main objectives of this study are (a) to estimate the mechanical properties of Ankleshwar formation, (b) to compute the pore pressure, (c) to detect overpressure zones, (d) to estimate the minimum horizontal stress and fracture pressure, and (e) to recommend safe CO_2 injection pressure. In order to investigate the in situ stresses in the reservoir for performance assessment, we used the sonic travel-time and bulk-density logs from the available wells (i.e. ANKL-1, ANKL-2, ANKL-3 and ANKL-4) that penetrates the Ankleshwar formation and adjacent rock layers.

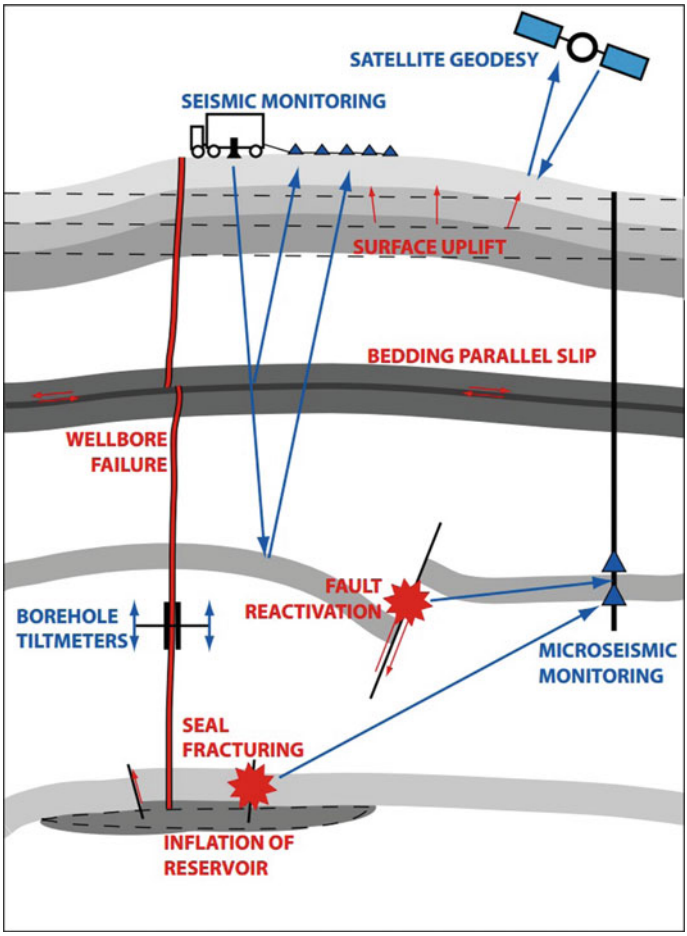

Fig. 6.1 Schematic diagram showing how subsurface deformation can influence the geomechanical response of a reservoir while considering CO_2 storage (*red text*), and potential monitoring options (*blue text*) that can be implemented (Verdon et al. 2013)

6.2.1 Estimation of Mechanical Properties

It is prudent to build a mechanical earth model (MEM) as a base case scenario of geomechanical performance assessment. A general mechanical earth model was developed that covers the dynamic elastic properties of most of the stratigraphic column including upper to middle Eocene Ankleshwar formation. In order to obtain mechanical properties associated with different lithologies, we used P- and S-wave velocity logs and the density log from the suite of geophysical logs available from various wells. Since the shear wave log was absent, we used the V_s log as predicted

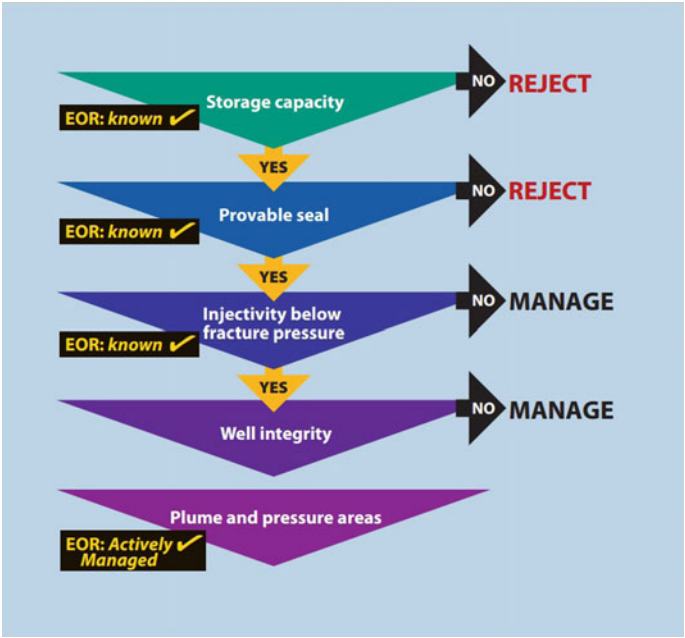

Fig. 6.2 Representation of the characterization and monitoring system for considering CO_2 storage in EOR. This also shows the criteria to accept or reject a storage proposal in EOR field (Hill et al. 2013)

in the previous chapter (i.e. Chap. 5). Poisson's ratio (ν) is calculated from the following relationship between P-wave velocity (V_p) and S-wave velocity (V_s):

$$\nu = 0.5\left[\frac{(V_p/V_s)^2 - 2}{(V_p/V_s)^2 - 1}\right], \tag{6.1}$$

Young's modulus (E) is then calculated using rock bulk density (ρ), V_s, and ν:

$$E = \rho V_s^2\left[\frac{3(V_p/V_s)^2 - 4}{(V_p/V_s)^2 - 1}\right], \tag{6.2}$$

Figure 6.3 illustrates the 1D MEM comprising of calculated elastic moduli (i.e. Shear modulus, Bulk modulus, Young's modulus, and Poisson's ratio) along with the general litho-stratigraphy of Ankleshwar reservoir. The zone of interest for CO_2 injection, S3+4 sand layers was marked by solid blue curve.

It is noteworthy to mention that overall Ankleshwar sands are strong enough to sustain CO_2, having high value of Young's modulus with reasonably smaller value in Poisson's ratio. Moreover, the presence of shale assemblage has severely reduced the strength of the Ankleshwar formation, indicating prone situation of sanding.

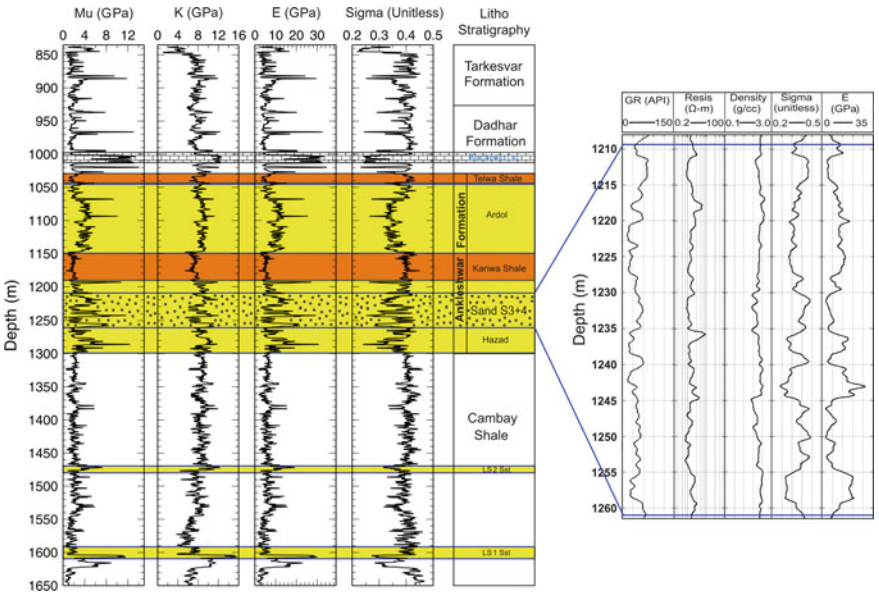

Fig. 6.3 Schematic representation of 1D mechanical earth model along a well trajectory for Ankleshwar reservoir. From *left* to *right*, the plot shows: Shear modulus (*Mu*), Bulk modulus (*K*), Young modulus (*E*), Poisson's ratio (*Sigma*), and a generalized litho-stratigraphy. The area of interest, S3+4 pay sands (*blue curve*), is zoomed for detailed analysis. A bio-clastic limestone formation has been identified at a depth interval of 998–1012 m in Dadhar formation

Further, a bio-clastic limestone is fairly identified in the litho-stratigraphy with an excellent log marker of increase in Shear, bulk and Young's modulus (Fig. 6.3).

6.2.2 *Estimation of Vertical Stress, Minimum Horizontal Stress, Fracture Pressure and Pore Pressure for Ankleshwar Oil Field*

In general, when sediment is buried to greater depth, the weight of the overlying sediment increases and compaction of sediment occurs (Negi et al. 1973). This leads to increase in vertical stress (or overburden stress), resulting in rearrangements of the grains that decreases the porosity and permeability (Sayers 2010). If the rate of loading exceeds the rate at which pore pressure can dissipate via expulsion of fluid, then a situation may arise that compels the pore fluids to carry a large of the overburden load. This process is referred as under compaction or compaction disequilibrium and considered as a part of overpressure mechanism. Nevertheless, in normal pressure zone, the fluid (mostly water) in the pore space is in pressure communication with the surface, and the load of the solid phase is

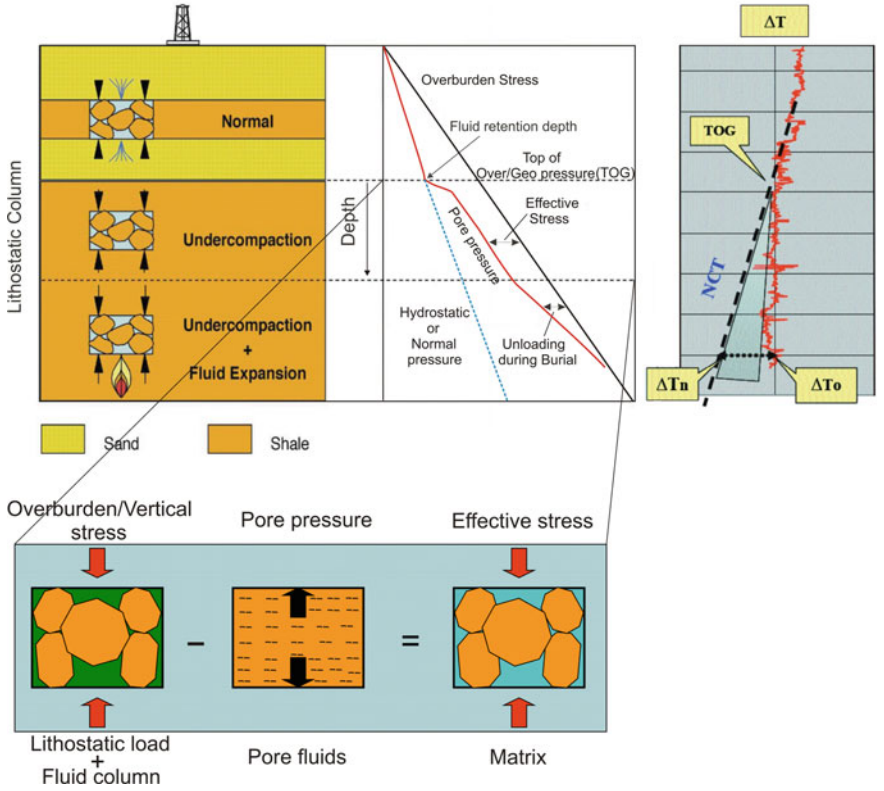

Fig. 6.4 Schematic diagram illustrating the in situ stress system including overburden stress, pore pressure, effective stress in a fictional well. The various mechanisms that lead to overpressures in a reservoir along with the responses recorded in sonic travel time log is also plotted for better understanding of the system. The pressures are plotted against depth (adapted from Bowers 2002)

supported at the grain contacts, and has no influence on the pressure in the fluid (Bourgoyne et al. 1986; Sayers 2010). A schematic illustration of various mechanisms that lead to increase in overburden stress and pore pressure has been provided in Fig. 6.4 for better understanding the overpressure condition in a reservoir. It is to be noted that the terminology "pressure" and "stress" has been used interchangeably throughout this chapter. They are not strictly the same, but can be so considered for the discussion (Bruce and Bowers 2002).

In order to characterize the stability of the well, in situ stress distribution need to be known correctly. The overburden stress/vertical stress (S_v) is due to the combined weight of rock matrix and fluids in the pore space overlying the formation of interest as a function of depth. This can be calculated by integrating the bulk density log over the depth of the well (Eaton 1975; Plumb et al. 1991):

$$S_v = \int_0^z \rho(z) g dz, \tag{6.3}$$

where, $\rho(z)$ is the bulk density of the rock, represented as function of depth (z), and g is the gravity acceleration. Gardner et al. (1974) suggested alternative techniques to estimate the sediment density, if density log is unavailable.

Further, the formation pore pressure (PP) is described as the pressure due to the pore fluids within the rock, which can be higher than the hydrostatic or normal pressure of the region. The point at which fluid pore pressure exceeds the hydrostatic pressure is known as the "top of overpressure/geopressure (TOG)" where part of load of the overlying sediments bear by the pore fluids (Fig. 6.4). The magnitude of formation pore pressure is traditionally calculated from well-log or seismic data in combination with Terzaghi's hypothesis (Terzaghi 1943). Hottmann and Johnson (1965) first attempted the study on pore pressure prediction using well-log data where overpressure was estimated by investigating any deviation in shale properties from its normal trend. Subsequently, several studies (e.g., Mathews and Kelly 1967; Pennebaker 1968; Eaton 1972, 1975; Bowers 1995, 2002; Sayers et al. 2002; Sarker and Batzle 2008; Zhang 2011; Azadpour et al. 2015) on pore pressure prediction were conducted successfully using well-log data and seismic data. The most common methods used to determine pore pressure from compressional seismic velocity include the Eaton's method (Eaton 1975), Bower's method (Bower 1995) and the Tau model (López et al. 2004; Zhang and Wieseneck 2011). We have used Eaton's method to estimate pore pressure of Ankleshwar oil reservoir in Cambay Basin.

Eaton (1975) in accordance with Terzaghi (1943) had given an empirical relation between the pressure and the sonic transit time to determine pore pressure (PP):

$$PP = S_v - (S_v - P_{hyd}) \times \left(\frac{DT_n}{DT}\right)^3, \tag{6.4}$$

where, P_{hyd} is the hydrostatic pressure; DT_n is sonic travel time in low permeable zone (i.e. shales) which is calculated from the normal compaction trend (NCT); DT is observed sonic travel time during well-logging. The hydrostatic pressure gradient was taken as 10.9 MPa/Km during the analysis.

We were also interested in evaluating the fracture pressure, i.e. the pressure in the wellbore at which a formation will crack. In general, a formation will be fractured when the pressure in the wellbore exceeds the least of the stresses within the rock, and the fractures will propagate in a direction perpendicular to the least principal stress. The fracture pressure (FP) can be determined in terms of minimum horizontal stress (S_h), vertical stress (S_v), and pore pressure (PP), using Matthews-Kelly's equation (Matthews and Kelly 1967), represented as:

$$FP = PP + \left(\frac{S_h}{S_v}\right) \times (S_v - PP). \tag{6.5}$$

Here, the least principal stress, minimum horizontal stress (S_h), can be estimated using the equation based on poroelastic theory (Mandl and Harkness 1987; Engelder and Fischer 1994):

$$S_h = PP + [\nu/(1-\nu)] \times (S_v - PP), \tag{6.6}$$

where, ν is Poison's ratio of the rock formation in Cambay Basin, which is reported to be 0.2–0.25 (Kumar et al. 2008).

Abnormal pressure zone and top of overpressure (TOP) has been realized by spotting deviations from NCT in sonic transit time and bulk density logs from four wells under investigation. NCT represents the optimum fitted linear trend in low permeable zone (i.e. shale layers) and represents the normal loading path, wherein abnormal pressures are associated with unloading path. Figure 6.5 portrays the sonic transit time and density trend of normal compacted and under compacted

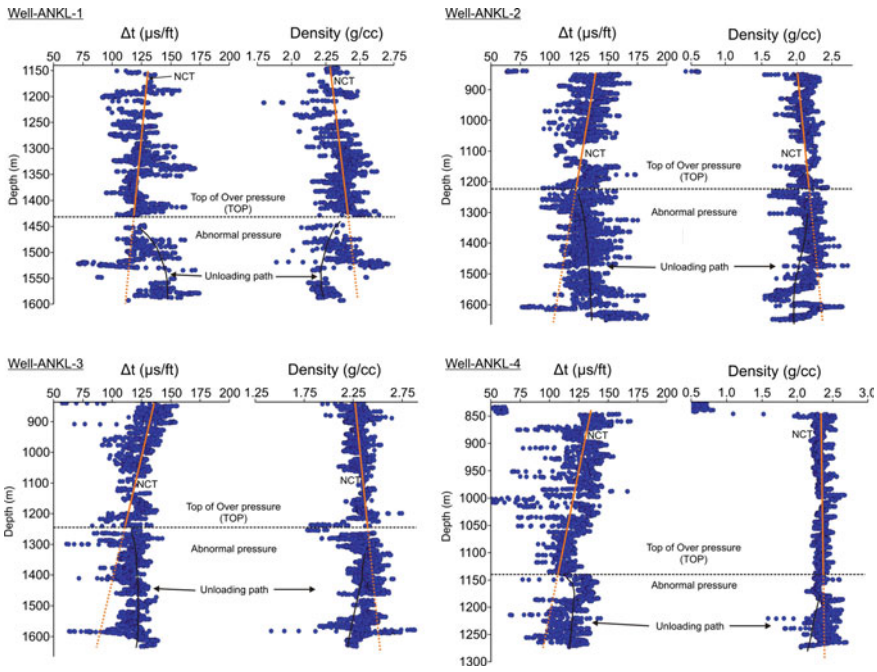

Fig. 6.5 Representation of normal compaction trend (*NCT*) and top of overpressure (i.e. TOP) from four well trajectories of Ankleshwar reservoir: wells, ANKL-1 and ANKL-2 (*Top*), and wells, ANKL-3 and ANKL-4 (*Bottom*). The plots show the sonic transit time (Δt) and bulk density trend within the reservoir. The loading (NCT) and unloading trend has been indicated for better understanding of the abnormal pressure system in the reservoir

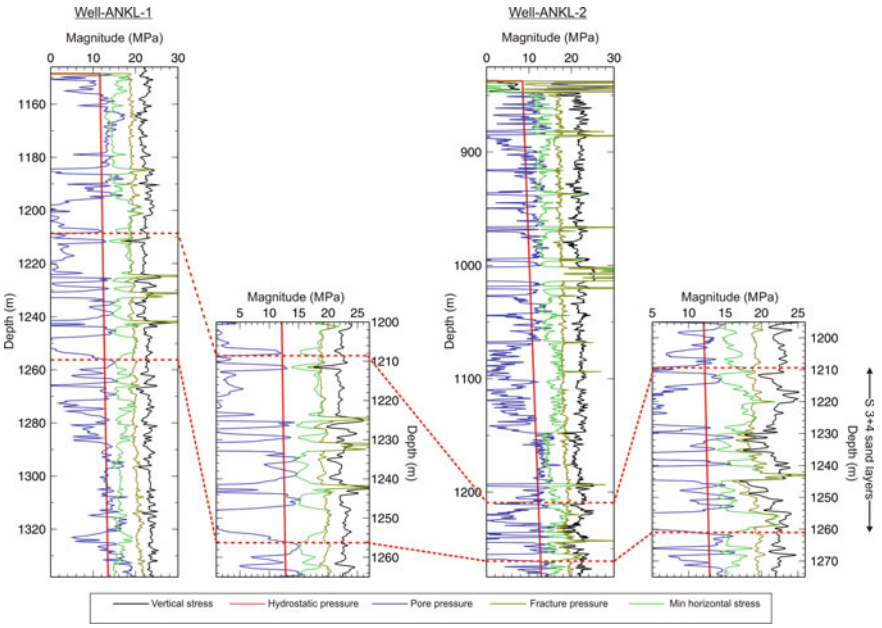

Fig. 6.6 In-situ stress profile along depth from two well trajectories of Ankleshwar reservoir: well-ANKL-1 (*Left*), and well-ANKL-2 (*Right*). The *black*, *blue*, *dark green*, *red*, and *green curve* represents overburden/vertical stress, pore pressure, fracture pressure, hydrostatic pressure and minimum horizontal pressure, respectively. The zone demarcated by *red dashed line* signifies the pay sands, S3+4, potential for CO_2-EOR, and storage

shale formation. Abnormal pressure is identified with excess sonic travel time and high porosity (low density) at the same depth interval while compared to NCT. This is most likely due to occurrence of cementation concurrently with pressure changes. It is also to be noted that comparatively sonic transit time trend is a better indicator of TOP than density log.

We investigated the in situ stress behaviour in S3+4 sand layers, the zone of interest for feasible CO_2 injection. We found that the pore pressure magnitudes for S3+4 sand layers from all wells (i.e. ANKL-1, ANKL-2, ANKL-3) are sub-hydrostatic, albeit well ANKL-4 shows value offset from the hydrostatic pressure magnitudes (Figs. 6.6 and 6.7). This is justified since the reservoir has witnessed peripheral water flooding for long time and the anomalous pore pressures could be mostly due to the under-compaction (or compaction disequilibrium) phenomena since these pressures correlates well to the decrease in vertical stress. Under-compaction is usual phenomenon in sedimentary basins, and occurs when there is a transition from sand-prone to a shale prone environment (Bowers 2002).

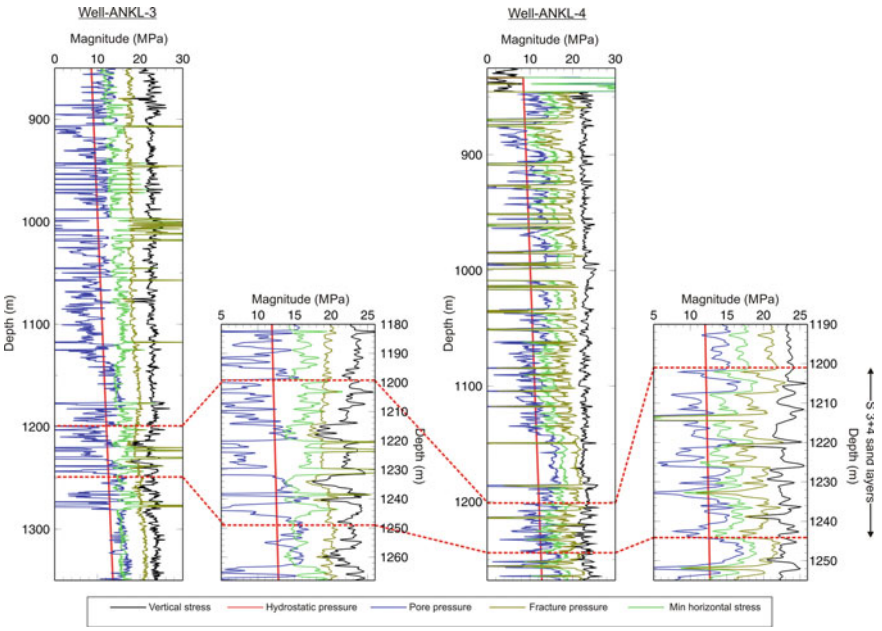

Fig. 6.7 In-situ stress profile along depth from two well trajectories of Ankleshwar reservoir: well-ANKL-3 (*Left*), and well-ANKL-4 (*Right*). The *black*, *blue*, *dark green*, *red*, and *green curve* represents overburden/vertical stress, pore pressure, fracture pressure, hydrostatic pressure and minimum horizontal pressure, respectively. The zone demarcated by *red dashed line* signifies the pay sands, S3+4, potential for CO_2-EOR, and storage

The average overburden stress and minimum horizontal stress in Ankleshwar reservoir is 23 and 16 MPa, respectively, suggesting upper and lower bound of the fracture pressure.

6.3 Feasibility of Dynamic In Situ Stress System: Ankleshwar Oil Field Example

The dynamic in situ stress analysis can be performed by evaluating the changes in in situ stress system due to CO_2 injection in a reservoir during its tertiary production life history. We have investigated by assessing the pore pressure, vertical stress, fracture pressure and the reservoir pressure at post CO_2 injection condition. Additionally, to demonstrate the effect of CO_2 saturation on various pressure distributions, we considered two different saturation scenarios, *uniform*-and *patchy*-saturation, since incase of mixed pore fluids, pore pressure induced in each phase by passing wave will be different, leading to saturation heterogeneity.

6.3.1 Estimation of Time-Lapse Vertical Stress, Minimum Horizontal Stress, Fracture Pressure and Pore Pressure for Ankleshwar Oil Field

Time-lapse/4D in situ stress distributions were realized for all the wells by considering 20% of uniform -and patchy- CO_2 saturation model. We identified that there is a significant change in pore pressure, overburden pressure and the fracture pressure after CO_2 flooding, and the average pore pressure is 28% higher than the pore pressure estimated before CO_2 injection (Figs. 6.8 and 6.9). However, the predicted pore pressure is not higher than the fracture pressure, which is the upper limit for the pressure in well should be kept below in order to maintain safe and economic drilling. Also, the uniform saturation model results in greater magnitude in pore pressure ($\sim$2–3%) while compared to patchy saturation model. It is to be noted that the reduction in effective pressure (i.e. the difference between the overburden and pore pressure) after CO_2 injection is not due to unloading/under-compaction, like the pre-injection scenario, rather due to fluid expansion since CO_2 behaves as supercritical fluid as it enters the pore space of the formation.

6.3.2 Reservoir Pressure Profile During Production at Ankleshwar Oil Field

Figure 6.10 traces the pressure profile for feasible CO_2-EOR and storage at Ankleshwar reservoir. As we can see the original formation pressure prior to commencing the oil production was about 119 bar, correlates well to the actual field reservoir pressure (i.e. 118 bar) as discussed in Chap. 3.

Moreover, reservoir pressure during the start of production is considerably below the average formation fracture pressure which is calculated as 190 bar (i.e. 19 MPa). Over 4–5 years of primary production, the reservoir pressure declines, however, started rising as soon as water flooding has been implemented (cyan curve in Fig. 6.10). Eventually, an economic limit was reached and now, the field is in mature stage. Therefore, we anticipated the field pressure performance as if we commenced CO_2 injection in the year 2015. The goal normally was to raise the reservoir pressure slightly above its original pressure, but not approaching to fracture pressure. As shown by Fig. 6.10, the reservoir responded well and the average field pressure increased $\sim$3 bar. It is important to note that even after 're-pressurization' of the reservoir, the operating pressure is 121 bar, mostly below the formation fracture pressure, i.e. 190 bar, over the life of operation ($\sim$50 years) and indeed ensure a safe CO_2-EOR and storage process if considered.

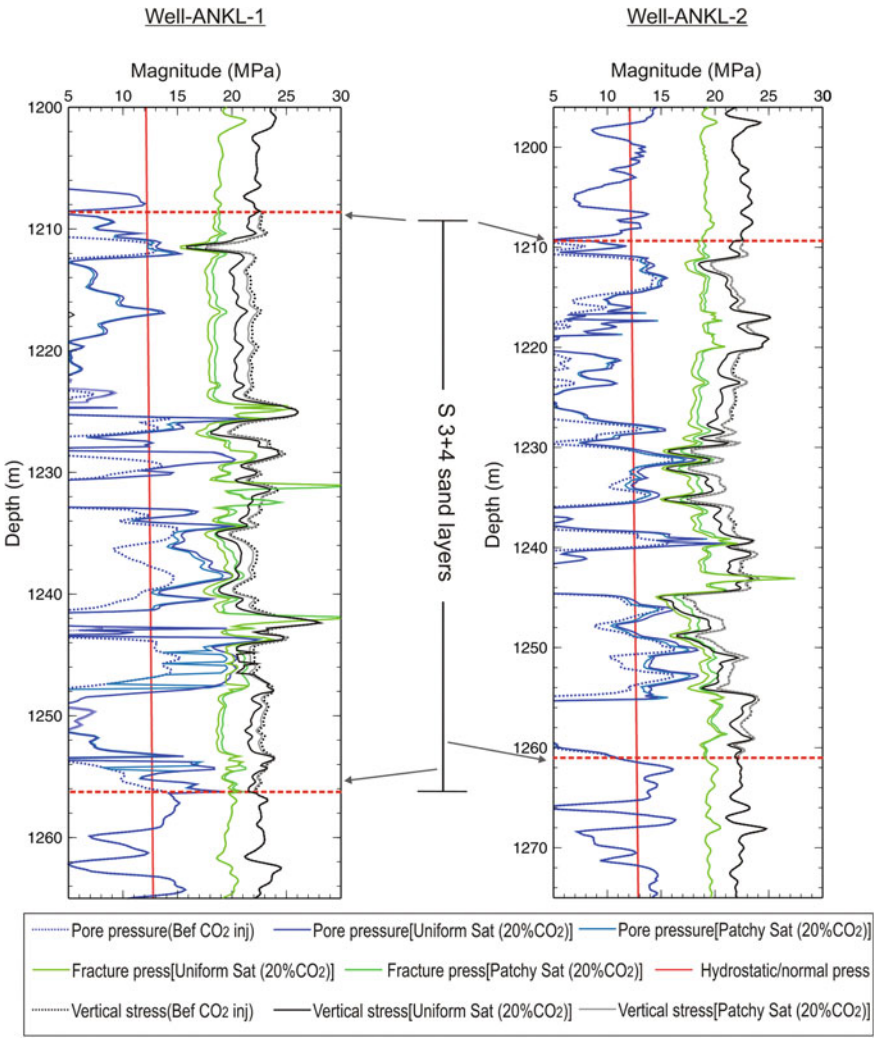

Fig. 6.8 In-situ stress profile obtained from two well trajectories of Ankleshwar reservoir: well-ANKL-1 (*Left*) and well-ANKL-2 (*Right*). The plots show the overburden/vertical stress, pore pressure, fracture pressure, and hydrostatic pressure before and after CO_2 injection. The *dotted* and *solid curves* illustrate the pressure prior and after CO_2 injection, respectively. The *dark colours* and *light colours* represent the uniform- and patchy saturation models at 20% CO_2 saturation. The zone demarcated by *red dashed line* signifies the pay sands, S3+4, potential for CO_2-EOR, and storage

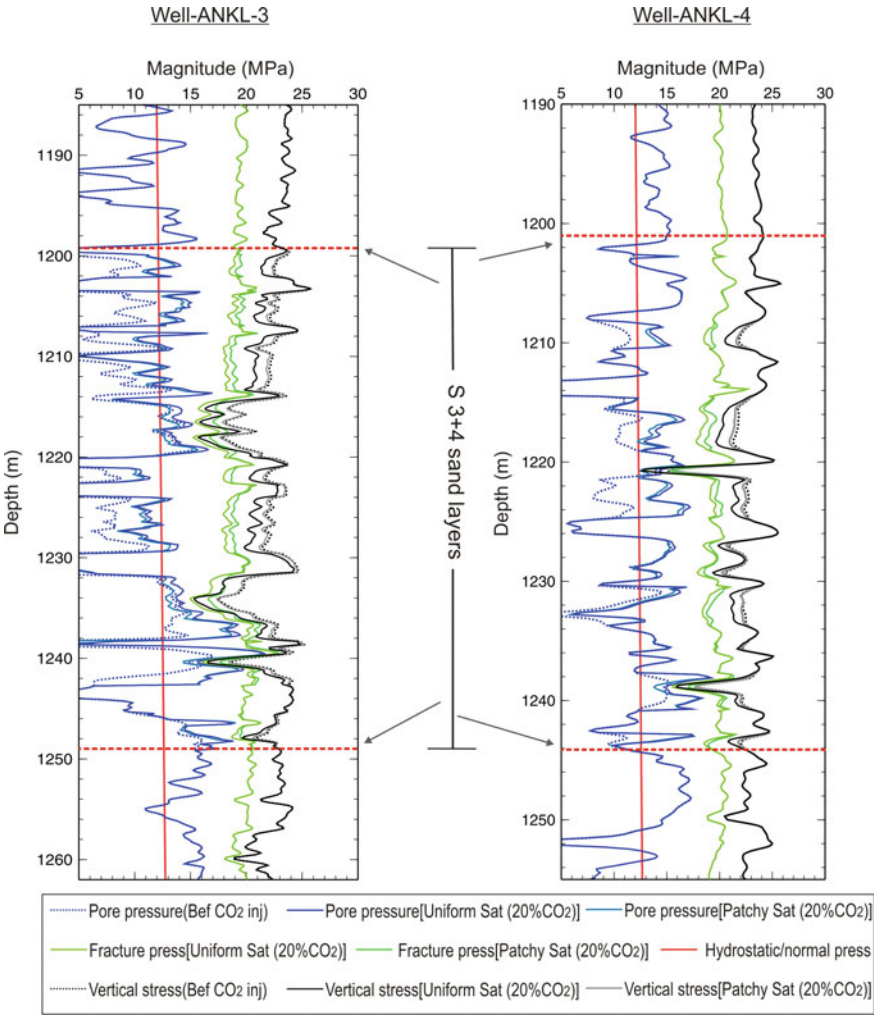

Fig. 6.9 In-situ stress profile obtained from two well trajectories of Ankleshwar reservoir: well-ANKL-3 (*Left*), and well-ANKL-4 (*Right*). The plots show the overburden/vertical stress, pore pressure, fracture pressure, and hydrostatic pressure before and after the CO_2 injection. The *dotted* and *solid curves* illustrate the pressure prior and after CO_2 injection, respectively. The *dark colours* and *light colours* represent the uniform- and patchy saturation models at 20% CO_2 saturation. The zone demarcated by *red dashed line* signifies the pay sands, S3+4, potential for CO_2-EOR, and storage

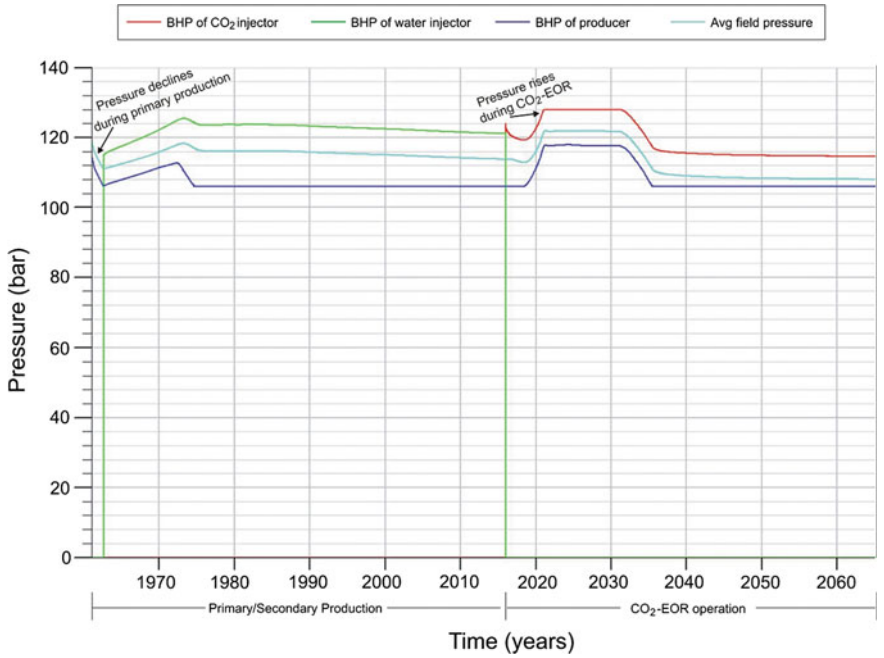

Fig. 6.10 Illustrative pressure profile of Ankleshwar reservoir during primary/secondary and CO_2-EOR operation. The *red*, *green*, *blue*, and *cyan curve* represents the bottom hole pressure (*BHP*) of CO_2 injector, water injector, producer, and average reservoir pressure, respectively. The pressure profile of 50 years has been envisaged for feasible CO_2-EOR and storage at Ankleshwar oil field in Cambay Basin

6.4 Conclusions

A feasibility study of geomechanical aspects of CO_2-EOR and storage at Ankleshwar oil field was performed and based on the present study following conclusions were reached:

- We developed a suitable 1D mechanical earth model to analyse the strength of the reservoir formation with respect to CO_2 injection. We identified that overall Ankleshwar sands are strong enough to support CO_2 injection with reasonably high value of Young's modulus. Nevertheless, we found that the strength of the Ankleshwar formation was significantly reduced due to the presence of shale assemblage, indicating a prone situation of sanding, which will not affect much to the formation if CO_2 is injected. Of course, field sanding data could explain it properly which is not available.
- Quantitative analysis of the in situ stress distribution in the wells from Ankleshwar oil field reveal that the pore pressure magnitudes for the major pay sands (S3+4) are sub-hydrostatic. These findings have significant implications

for CO_2-EOR and storage in S3+4 sand layers. Of course, a comprehensive geomechanical model including fracture characterization, stress orientation, static rock strength analysis, fault stability analysis, etc. is highly encouraged prior to decide any field scale storage process.

- Post CO_2 injection scenarios were also envisaged by investigating the time-lapse/4D changes in in situ stress distribution. We identified a significant change in pore pressure, overburden pressure and fracture pressure after CO_2 injection, and the average pore pressure is 28% higher than the pore pressure estimated prior to CO_2 injection. Nevertheless, the predicted pore pressure is not higher than the fracture pressure (i.e. the upper limit of the allowed pressure in well), suggesting a safe and economic drilling during CO_2-EOR and storage. This has been validated from the monitoring of pressure profile which suggests even after re-pressurization of the reservoir, the operating pressure is 121 bar, which is much below the average formation fracture pressure (i.e. 190 bar) over the life of operation.

References

Azadpour M, Manaman NS, Ilkhchi KA, Sedghipour MR (2015) Pore pressure prediction and modeling using well-logging data in one of the gas fields in south of Iran. J Pet Sci Eng 128:15–23

Bickle MJ (2009) Geological carbon storage. Nature Geosci 2:815–818

Bourgoyne ATJ, Millhelm KK, Chenevert ME, Young FS (1986) Applied drilling engineering. Society of Petroleum Engineers

Bowers GL (1995) Pore pressure estimation from velocity data: accounting for overpressure mechanisms besides undercompaction. SPE Drill Completion 10:89–95

Bowers GL (2002) Detecting high overpressure. Lead Edge 21:174–177

Bruce B, Bowers G (2002) Pore pressure terminology. Lead Edge 21:170–173

Cappa F, Rutqvist J (2011) Impact of CO_2 geological sequestration on the nucleation of earthquakes. Geophys Res Lett 38:2–7

Chiaramonte L (2008) Geomechanical characterization and reservoir simulation of a CO_2 sequestration project in a Mature Oil Field, Teapot Dome, Wy. Ph.D. Thesis, Stanford University

Chiaramonte L, Zoback MD, Friedmann J, Stamp V (2008) Seal integrity and feasibility of CO_2 sequestration in the Teapot Dome EOR pilot: Geomechanical site characterization. Environ Geol 54:1667–1675

Davies R, Foulger G, Bindley A, Styles P (2013) Induced seismicity and hydraulic fracturing for the recovery of hydrocarbons. Mar Pet Geol 45:171–185

Eaton BA (1972) Graphical method predicts geopressures worldwide. World Oil 182:100–104

Eaton BA, (1975) The equation for geopressure prediction from well logs. In: Fall Meet, Soc Pet Eng, AIME, Texas, U.S.A. doi:10.2118/5544-MS

Engelder T, Fischer MP (1994) Influence of poroelastic behaviour on the magnitude of minimum horizontal stress, Sh, in overpressured parts of sedimentary basins. Geology 22:949–952

Gardner GHF, Gardner LW, Gregory AR (1974) Formation velocity and density—the diagnostic basics for stratigraphic traps. Geophysics 39:770–780

Grasso JR (1992) Mechanics of seismic instabilities induced by the recovery of hydrocarbons. Pure appl Geophys 139:507–534

Hawkes C, Mclellan P, Bachu S (2005) Geomechanical factors affecting geological storage of CO_2 in depleted oil and gas reservoirs. J Can Pet Technol 44:52–61

Hill B, Hovorka S, Melzer S (2013) Geologic carbon storage through enhanced oil recovery. Energy Procedia 37:6808–6830

Holt T, Jensen JI, Lindeberg E (1995) Underground storage of CO_2 in acquifers and oil reservoirs. Energy Convers Manag 36:535–538

Hottmann CE, Johnson RK (1965) Estimation of formation pressures from log-derived shale properties. J Pet Technol 17:717–722

Jenkins CR, Cook PJ, Ennis-King J, Undershultz J, Boreham C, Dance T, Caritat PD, Etheridge DM, Freifeld BM, Hortle A, Kirste D, Paterson L, Pevzner R, Schacht U, Sharma S, Stalker L, Urosevic M (2012) Safe storage and effective monitoring of CO_2 in depleted gas fields. Proc Natl Acad Sci 109:E35–E41

Kim WY (2013) Induced seismicity associated with fluid injection into a deep well in Youngstown, Ohio. J Geophys Res 118:3506–3518

Kumar A, Rana S, Nair S, Chowdhury S, Chakraborty D, Nath G (2008) Relevance of formation strength estimations from wireline logs in oil exploitation from fields of mehsana asset. In: 7th Int Conf and Exp, North Cambay Basin, India p 411

López JL, Rappold PM, Ugueto GA, Wieseneck JB, Vu CK (2004) Integrated shared earth model: 3D pore-pressure prediction and uncertainty analysis. Lead Edge 23:52–59

Lucier A, Zoback M, Gupta N, Ramakrishnan TS (2006) Geomechanical aspects of CO_2 sequestration in a deep saline reservoir in the Ohio River Valley region. Environ Geosci 13:85–103

Mandl G, Harkness RM (1987) Hydrocarbon migration by hydraulic fracturing. In: Jones ME, Preston RM (eds) Deformation of sediments and sedimentary rocks. Geological Society Special Publication, London, pp 39–53

Mathews WR, Kelly J (1967) How to predict formation pressures and fracture gradient from electric and sonic logs. Oil Gas J 65:92–106

Negi JG, Dimri VP, Garde SC (1973) Ambiguity assessment of gravity interpretation for an inhomogeneous multilayer sedimentary basin. J Geophys Res 78:3281–3286

Nicol A, Carne R, Gerstenberger M, Christophersen A (2011) Induced seismicity and its implications for CO_2 storage risk. Energy Procedia 4:3699–3706

Pennebaker ES (1968) Seismic data indicate the depth, magnitude of abnormal pressure. World oil 166:73–82

Plumb RA, Evans KF, Engelder T (1991) Geophysical log responses and their correlation with bed-to-bed stress contrasts in Paleozoic rocks, Appalachian Plateau, New York. J Geophys Res 96:14509–14528

Sarker R, Batzle M (2008) Effective stress coefficient in shales and its applicability to Eaton's equation. Lead Edge 27:798–804

Sayers CM (2010) Geophysics under stress : geomechanical applications of seismic and borehole acoustic waves. Distinguished instructor series, Society of Exploration Geophysicists, USA, pp 5–44

Sayers CM, Johnson GM, Denyer G (2002) Predrill pore-pressure prediction using seismic data. Geophysics 67:1286–1292

Schrag DP (2007) Preparing to capture carbon. Science 315:812–813

Shapiro SA, Dinske C, Kummerow J (2007) Probability of a given-magnitude earthquake induced by a fluid injection. Geophys Res Lett 34:L22314

Srivastava RP, Vedanti N, Akervoll I, Bergmo P, Yerramilli RC, Yerramilli SS, Dimri VP (2015). Study of CO_2 EOR in a sector model from Mature Oil Field, Cambay Basin, India. In: Mukherjee S (ed) Petroleum geosciences: Indian Contexts. Springer International Publishing, pp 87–98

Terzaghi K (1943) Theoretical soil mechanics. John Wiley, New York, London

Verdon JP, Kendall JM, Stork AL, Chadwick RA, White DJ, Bissell RC (2013) Comparison of geomechanical deformation induced by megatonne-scale CO_2 storage at Sleipner, Weyburn, and In Salah. Proc Natl Acad Sci 110:E2762–E2771

Verdon JP, Stork AL, Bissell RC, Bond CE, Werner MJ (2015) Simulation of seismic events induced by CO_2 injection at In Salah, Algeria. Earth Planet Sci Lett 426:118–129

Zhang J (2011) Pore pressure prediction from well logs: methods, modifications, and new approaches. Earth-Science Rev 108:50–63

Zhang J, Wieseneck J (2011) Challenges and surprises of abnormal pore pressure in the shale gas formations. Annual In: Technical conference and exhibitions, SPE, Colorado, U.S.A., SPE-145964-MS

Zoback MD, Gorelick SM (2012) Earthquake triggering and large-scale geologic storage of carbon dioxide. Proc Natl Acad Sci 109:10164–10168

Zoback MD, Barton CA, Brudy M, Castillo DA, Finkbeiner T, Grollimund BR, Moos DB, Peska P, Ward CD, Wiprut DJ (2003) Determination of stress orientation and magnitude in deep wells. Int J Rock Mech Min Sci 40:1049–1076

Chapter 7
Time-Lapse Monitoring of CO_2 Response at Ankleshwar Oil Field: A Seismic Modeling Approach for Feasible CO_2-EOR and Storage

7.1 Introduction

The CO_2-Enhanced oil recovery (EOR) project at Ankleshwar oil field in Cambay Basin is the first Indian onshore pilot study aimed at investigating nearly all components of CO_2-EOR/Sequestration. One of the most important aspects of this project is the monitoring of CO_2 with time-lapse seismic during and after injection. The time-lapse seismic images can identify bypassed oil to be targeted for infill drilling by monitoring the small-scale physical property changes due to CO_2 injection in a reservoir (Lumley 2001, 2004; Rickett and Lumley 2001; Vedanti et al. 2009; Amini et al. 2014). Time-lapse seismic technique has been used successfully for decades in many contexts of enhanced oil recovery operations in the field through thermal EOR such as steam or fire-flood (Pullin et al. 1987; Greaves and Fulp 1987; Eastwood et al. 1994; Lumley 1995; Jenkins et al. 1997; Waite and Sigit 1997; Ecker et al. 1999; Bianco 2008; Vedanti and Sen 2009; Zadeh et al. 2010; Cotton et al. 2013). Additionally, there are several studies in the literature that document the utilization of time-lapse monitoring to map CO_2 flood front during EOR and storage projects (Harris et al. 1996a, b; Herawati 2002; Davis et al. 2003; Arts et al. 2004; Meadows 2008; Urosevic et al. 2010; Lumley 2010; Bergmann et al. 2011; Meadows and Cole 2013; Zhang et al. 2013).

Several factors such as subsurface heterogeneities, CO_2 properties at subsurface conditions, and data quality influence the CO_2 response on surface seismic data, results in poor monitoring of the injected CO_2 (Kazemeini et al. 2010). In the scope of this, it is essential to conduct a feasibility of time-lapse seismic prior to CO_2 injection to ensure that (i) the injected CO_2 will significantly alter the elastic properties of the reservoir that would be detectable in the seismic response, and (ii) acquired seismic data will be able to resolve these changes under the given geological and reservoir conditions.

In this chapter, we conducted numerical seismic forward modeling on an approximate model of the reservoir to simulate the response of seismic wave

S.S. Ganguli, *Integrated Reservoir Studies for CO_2-Enhanced Oil Recovery and Sequestration*, Springer Theses,
DOI 10.1007/978-3-319-55843-1_7

propagation for feasible CO_2-EOR and storage. We developed the geological 2D model based on the available well logs from four well drilled through the Ankleshwar formation. In addition to this, we incorporated the rock physics model that developed in Chap. 5 to understand the response of the reservoir elastic properties in the presence of CO_2. Both, pre- and post-CO_2 injection scenarios at 20% CO_2 saturation were realized to map the time-lapse seismic changes within the reservoir due to CO_2 injection. Finally, we draw conclusions concerning the competency of seismic method to map CO_2 flood front at Ankleshwar oil field.

7.2 Seismic Modeling of CO_2 Response: Ankleshwar Oil Field Example

In order to assist in the survey design and interpretation of real seismic data, numerical simulations have become increasingly important in the past decades (Bianco 2008). To validate the predictions about the changes in reservoir seismic properties manifested when subjected to CO_2 injection, simulated seismic study can be carried out on an approximate reservoir model. In the focus of this, we developed a 2D Earth model using a commercial seismic modeling package by RokDoc (ikon Science) based on the stratigraphic information available from the interpretation of wells. It is assumed that the medium is isotropic and elastic, and the elastic parameters of this model were estimated by incorporating the rock physics model as developed in Chap. 5, and directly interpolating data between the well logs. Moreover, it is assumed that the model is suitable and represents the simplification of real case. Figure 7.1 illustrates the input geological model used for seismic forward modeling. Our goal is to resolve the seismic changes being occurred in the target zone (S3+4 sand zone) within Ankleshwar reservoir where CO_2 injection is proposed.

The seismic pulse used is a zero-phase Ricker wavelet with 30 Hz peak frequency. Choosing a 30 Hz center frequency of Ricker wavelet sounds realistic to resolve the S3+4 pay sands, which has 45 m of thickness. This can be explained by the evaluating the resolution requirements in the area of interest:

$$\lambda = V_p/f, \tag{7.1}$$

where λ, V_P, f are the wavelength, P-wave velocity and frequency in the layer of interest. The average V_P of S3+4 pay sands is taken as 3013 m/s. Calculating with corresponding values:

$$\lambda = \frac{3013\ \frac{m}{s}}{30\ \frac{1}{s}} = 100.43\ m$$

Therefore, the resolution $\sim$¼ of wavelength = 25.10 m, which is smaller than the thickness of S3+4 sand layer, i.e. 45 m.

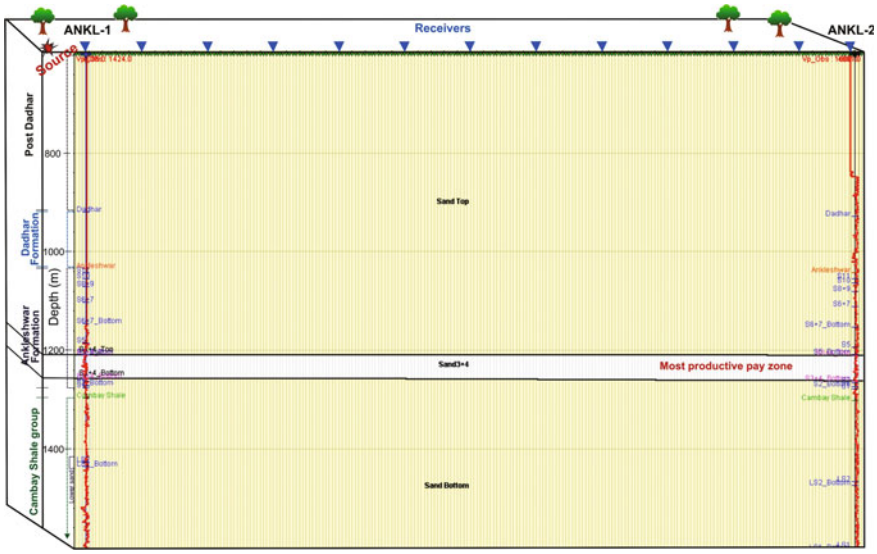

Fig. 7.1 Schematic 2D earth model of the proposed CO_2 injection site at Ankleshwar oil field in Cambay Basin with two wells: ANKL-1 (*Left*) and ANKL-2 (*Right*). The seismic line is 3000 m in length and the trace spacing is 12.5 m. The major stratigraphic units have been demarcated in the model including the target zone (*solid black curve*) for CO_2 injection

Table 7.1 Summary of surface seismic modeling parameters and their values used for seismic modeling study for feasible CO_2-EOR and storage at Ankleshwar

Parameters	Values (Units)
Length of the model	3000 m
Thickness of model	1590 m
Thickness of S3+4 sand zone	45 m
Wavelet type and peak frequency	Ricker Wavelet, 30 Hz
Receiver spacing	12.5 m
No. of traces	240

The surface seismic modeling parameters used to simulate the response of seismic wave propagation for feasible CO_2-EOR and storage were summarized in Table 7.1.

The reflection and transmission coefficients for plane elastic waves as a function of reflection angle at each interface/horizon were calculated using Zoeppritz equations (Zoeppritz 1919). The solution of Zoeppritz equations is as follows:

$$\begin{bmatrix} R_p \\ R_s \\ T_p \\ T_s \end{bmatrix} = \begin{bmatrix} -\sin\theta_1 & -\cos\varphi_1 & \sin\theta_2 & \cos\varphi_2 \\ \cos\theta_1 & -\sin\varphi_1 & \cos\theta_2 & -\sin\varphi_2 \\ \sin 2\theta_1 & \frac{V_{P1}}{V_{s1}}\cos 2\varphi_1 & \frac{\rho_2 V_{s2}^2 V_{P1}}{\rho_1 V_{s1}^2 V_{P2}}\cos 2\theta_1 & \frac{\rho_2 V_{s2} V_{P1}}{\rho_1 V_{s1}^2}\cos 2\theta_2 \\ -\cos 2\varphi_1 & \frac{V_{s1}}{V_{P1}}\sin 2\varphi_1 & \frac{\rho_2 V_{P2}}{\rho_1 V_{P1}}\cos 2\varphi_2 & -\frac{\rho_2 V_{S2}}{\rho_1 V_{P1}}\sin 2\varphi_2 \end{bmatrix}^{-1} \begin{bmatrix} \sin\theta_1 \\ \cos\theta_1 \\ \sin 2\theta_1 \\ \cos 2\varphi_1 \end{bmatrix}, \tag{7.2}$$

where $R_p, T_p, V_P, R_S, T_S, V_S$ are the P-wave reflectivity, transmissivity, velocity and S-wave reflectivity, transmissivity and velocity, respectively. $\theta_1, \varphi_1, \theta_2, \varphi_2$ signifies the angle of reflected P and S-wave, transmitted P and S-wave, and the subscript 1 and 2 signifies medium 1 and 2, respectively. Thus, the seismic trace $(T(t))$ is obtained by the convolution of the reflection coefficient series $(R(t))$ with source wavelet $(W(t))$ (Dimri 1992).

$$T(t) = R(t) * W(t), \tag{7.3}$$

Figures 7.2 and 7.3 depict the synthetic seismograms as an outcome from the seismic forward modeling using ray theory. The horizons in the synthetic model correspond to the lithostratigraphic boundaries of the oil field. Two saturation scenarios: (i) uniform and (ii) patchy saturation model at 20% CO_2 saturation were considered which have been discussed in details in Chap. 5. SEG reverse polarity convention was used to describe the reflectivity, which states that a hard reflection will be represented by a red trough whilst a soft reflection will be represented by a blue peak. In the synthetic seismogram, the top of the Ankleshwar reservoir was easily identified by bright reflection, and we observed a drastic decrease in seismic amplitude as a result of CO_2 injection in the S3+4 sands of Ankleshwar formation (Fig. 7.2). The decrease in amplitude in case of uniform saturation is significantly greater than in the case of patchy saturation, which has been validated from the results of Chap. 5. Nevertheless, we may expect more CO_2 saturation in this oil field, and the changes will be visible in surface seismic albeit in the case of patchy saturation model.

Additionally, we found that the amplitude changes is not very prominent between the wells ANKL-3 and 4 (Fig. 7.3) when compared to that between the wells ANKL-1 and 2 (Fig. 7.2). Thus, seismic change due to CO_2 injection differs from well to well in the same studied area which was also noticed in Chap. 5. Furthermore, we investigated the time-lapse seismic differences within S3+4 sand zone of Ankleshwar formation for each saturation model so that changes related to CO_2 injection can be highlighted. This has been done by subtracting the monitor data from the baseline data (pre-CO_2 injection case). The top of sand S3+4 was demarcated by positive amplitude (black arrow), and we identified a strong negative amplitude layer which suggests the CO_2 saturated layer (Fig. 7.4). Additionally, the saturation heterogeneity is quite visible in the patchy saturation model.

Nonetheless, we couldn't identify strong amplitude changes between the wells ANKL-3 and 4 (Fig. 7.5) when compared to ANKL-1 and 2 (Fig. 7.4), yields weak reflection response in the synthetic seismogram.

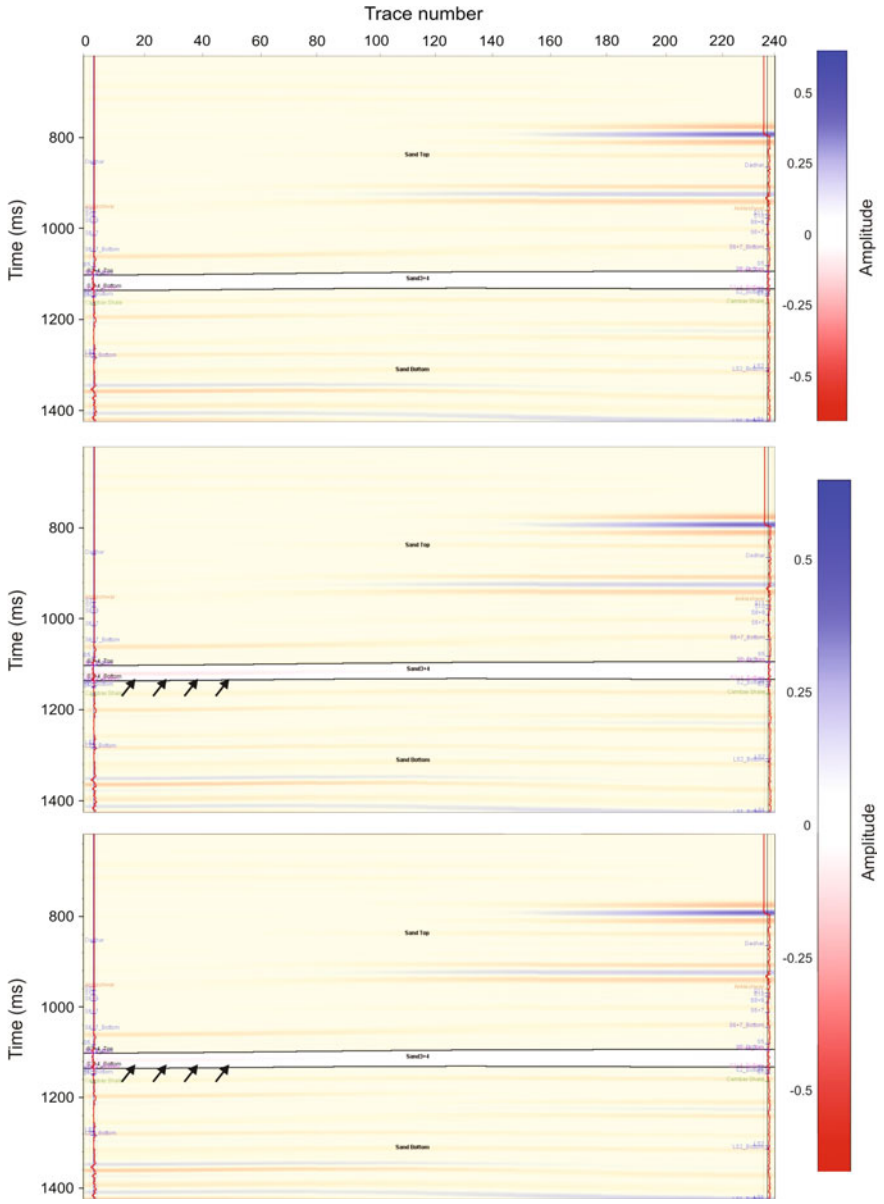

Fig. 7.2 Synthetic seismograms: pre-injection (*Top*), uniform- (*Middle*) and patchy-saturation (*Bottom*) models at 20% CO_2 saturation between two well trajectories (ANKL-1 and ANKL-2) penetrating Ankleshwar reservoir. The area of interest, S3+4 sand zone is highlighted by *solid black lines*. The *black arrows* indicate changes in seismic amplitude due to CO_2 injection

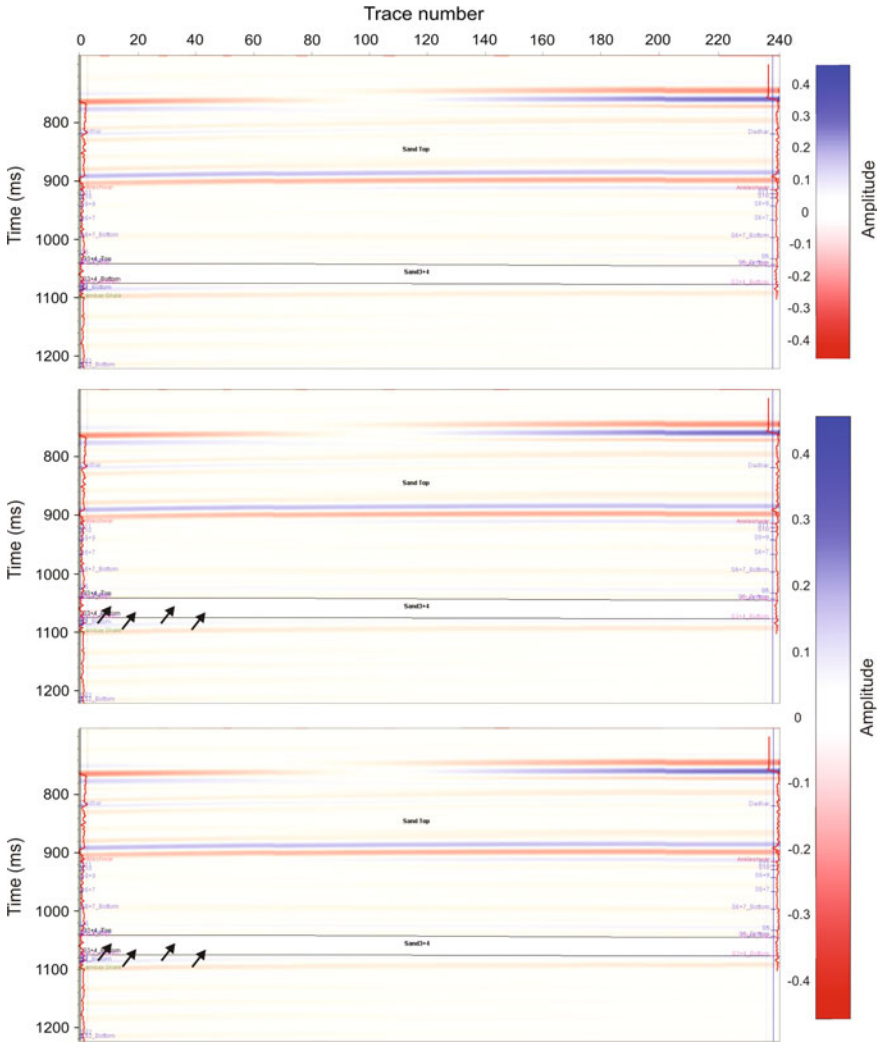

Fig. 7.3 Synthetic seismograms: pre-injection (*Top*), uniform- (*Middle*) and patchy-saturation (*Bottom*) models at 20% CO_2 saturation between two well trajectories (ANKL-3 and ANKL-4) penetrating Ankleshwar reservoir. The area of interest, S3+4 sand layer is highlighted by *solid black lines*. The *black arrows* indicate changes in seismic amplitude due to CO_2 injection

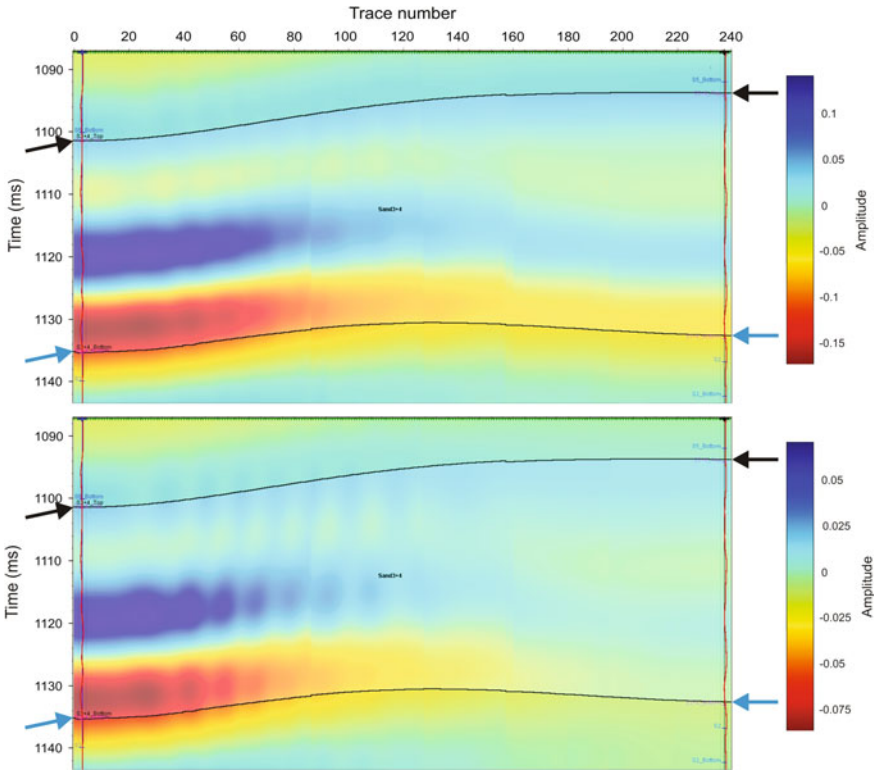

Fig. 7.4 Time-lapse amplitude difference for both: uniform- (*Top*) and patchy-saturation (*Bottom*) models at 20% CO_2 saturation between two well trajectories, ANKL-1 and ANKL-2. *Black* and *cyan arrows* on the sides indicate the top and bottom S3+4 horizons, respectively. Saturation heterogeneity is clearly observed in seismic amplitude for patchy saturation model

The time-lapse AI difference between the wells was calculated by subtracting the post-from pre-injection impedance and shown in Figs. 7.6 and 7.7. We observed significant drop in impedance, suggesting CO_2 accumulation. The horizons, top and bottom of S3+4 pay sand was represented by black and cyan arrow, respectively.

7.3 Feasibility of 4D Seismic Analysis at Ankleshwar Oil Field

In general, two approaches are considered during the observations on seismic time-lapse study: (a) amplitude analysis, where amplitude variation from one survey to another is studied, and (b) time-shift analysis in which changes in seismic travel time is studied from one survey to another (Landrø 2001; Dimri et al. 2012;

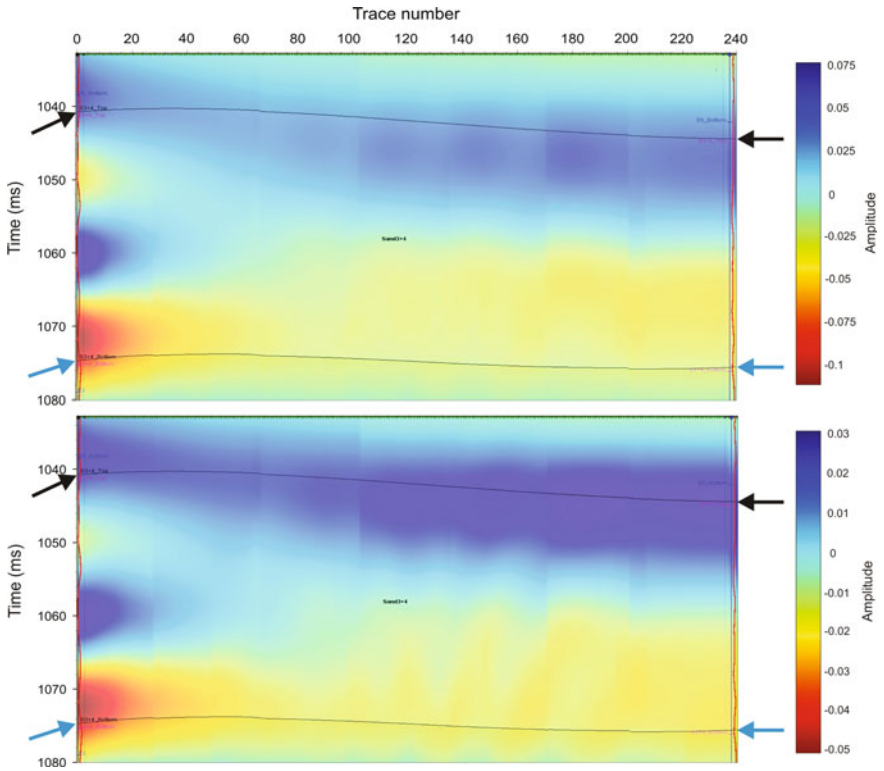

Fig. 7.5 Time-lapse amplitude difference for both: uniform- (*Top*) and patchy-saturation (*Bottom*) models at 20% CO_2 saturation between two well trajectories (ANKL-3 and ANKL-4) passing through the target zone, S3+4 sand of Ankleshwar reservoir. *Black* and *cyan arrows* on the sides indicate the top and bottom S3+4 horizons, respectively

Sodagar and Lawton 2014). Basically, combined effect of pressure and saturation will result in amplitude anomalies. It is also reasonable to observe pull-up or push-down effect in seismic travel time during time-shift analysis (Fig. 7.8).

The amplitude anomaly is more sensitive to repeatability study than the seismic travel time as travel time is less affected by variations in positioning, acquisition, or processing. Thus, time-shift analysis will be a more robust one if changes in reservoir parameters affect the seismic travel time (Brown 2003; Landrø and Stammeijer 2004).

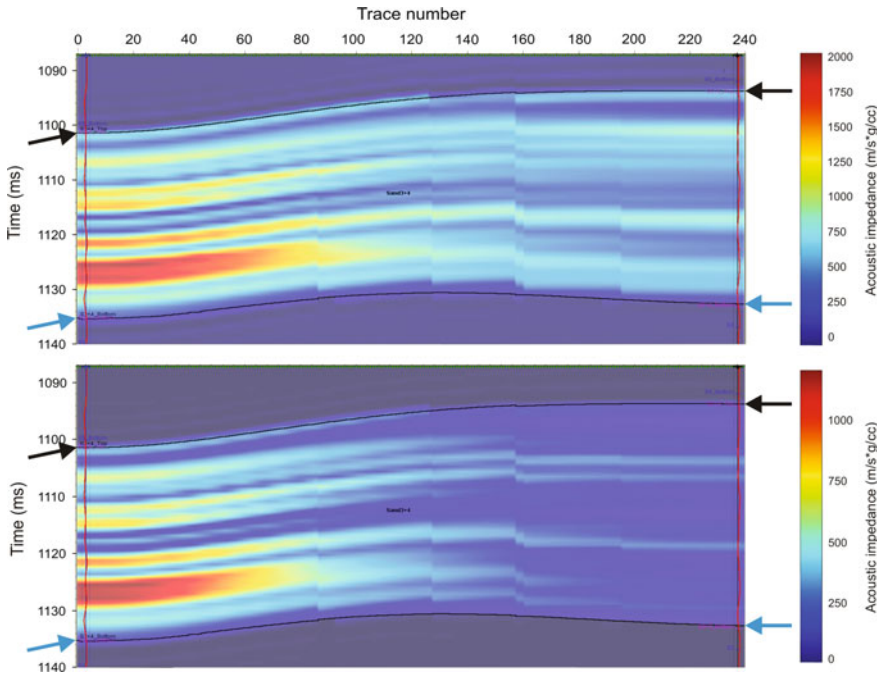

Fig. 7.6 Time-lapse change in acoustic impedance (AI) for both: uniform- (*Top*) and patchy-saturation (*Bottom*) models at 20% CO_2 saturation between two well trajectories (ANKL-1 and ANKL-2) invading the target zone of Ankleshwar reservoir. *Black* and *cyan arrows* on the sides indicate the top and bottom S3+4 horizons, respectively. The *colour bar* represents the change in AI, the more the value; more is the change due to injected CO_2 and vice versa

The time delay at the reflector can be calculated using the equation:

$$\Delta T = T_2 - T_1 = 2h\left(\frac{1}{V_{P2}} - \frac{1}{V_{P1}}\right). \tag{7.4}$$

In this case, h is the thickness of S3+4 pay sands (45 m), V_{P2}, V_{P1} are the P-wave velocity after and before CO_2 injection in the target zone, respectively. We assessed the average two-way delay time as 7.53 ms.

Figure 7.9 illustrates the seismic gather during pre-and post-CO_2 injection. We could observe a nice example of push-down effect (time-shift) caused by the lower velocity of CO_2. This has been marked by white arrow, while the amplitude change is marked by yellow ellipse (Fig. 7.9).

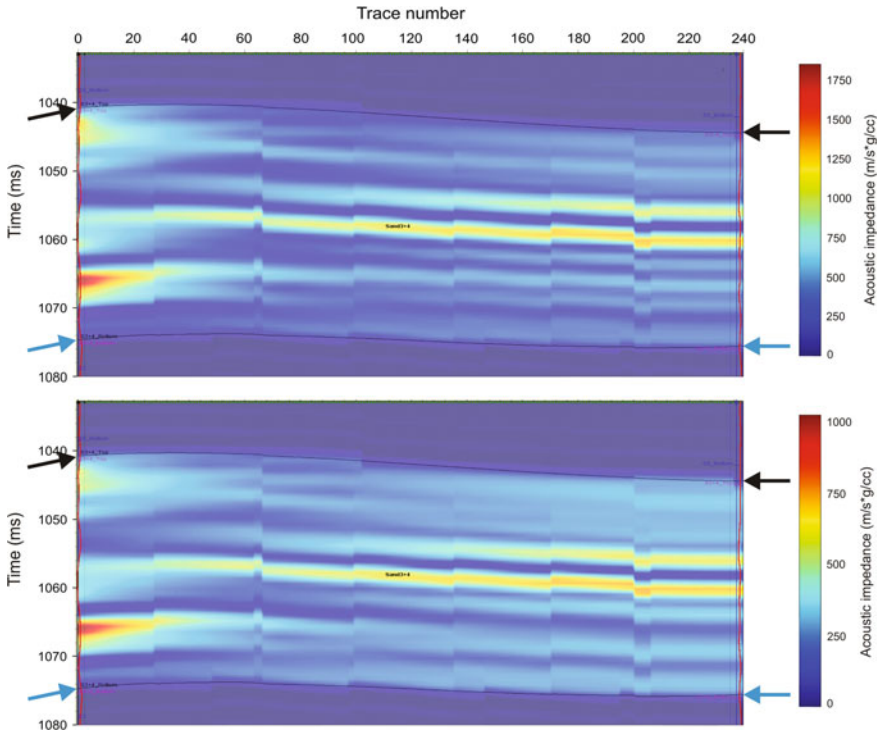

Fig. 7.7 Time-lapse change in acoustic impedance (AI) for both: uniform- (*Top*) and patchy-saturation (*Bottom*) models at 20% CO_2 saturation between two well trajectories (ANKL-3 and ANKL-4) running through the target zone, S3+4 sand of Ankleshwar reservoir. *Black* and *cyan arrows* on the sides indicate the top and bottom S3+4 horizons, respectively. The *colour bar* represents the change in AI, the more the value, more is the change and vice versa

7.4 Conclusions

We have studied how CO_2 will be effectively monitored using 4D seismic at Ankleshwar, and based on the present study following conclusions were made:

- We developed a suitable 2D synthetic seismic model based on ray tracing method which allows us to reproduce the reservoir conditions in the area of interest, and analyse the seismic changes on surface seismic data including two saturation models: uniform –and –patchy saturation model at 20% CO_2 saturation. It suggests that even in the case of patchy saturation, the seismic response of CO_2 should be observable in surface seismic. Nevertheless, like in all the case of time-lapse seismic, whether the seismic changes related to injected CO_2 can actually be detected on real data for Ankleshwar reservoir will depend upon the S/N ratio, repeatability survey, relocalization accuracy, etc.

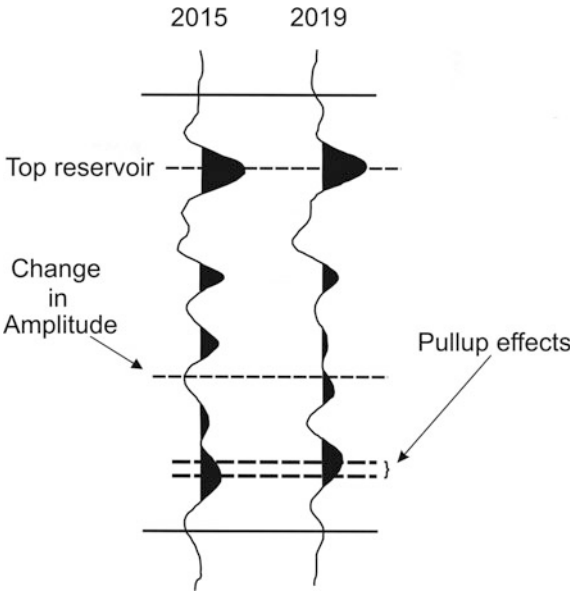

Fig. 7.8 Representation of two ways to analyse time-lapse seismic data (modified after Landrø et al. 2001). Pullup effect and the change in amplitude have been shown for better understanding while analysing 4D seismic data

- Time-lapse analysis shows a dramatic decrease in seismic amplitude due to CO_2 injection in the S3+4 sand of Ankleshwar formation. As discussed earlier in Chap. 5, the decrease in amplitude in case of uniform saturation is significantly larger than in the case of patchy saturation, is still valid. However, we couldn't identify strong amplitude changes between the wells ANKL-3 and 4 (Fig. 7.5) compared to ANKL-1 and 2 (Fig. 7.4). The seismic response with respect to the injected CO_2 differs in different wells.
- We estimated the average two-way delay time is 7.53 ms, and observed push-down effect (time-shift) caused by the lower velocity of CO_2 (Fig. 7.9). These findings have significant implications that time-lapse seismic surveys should be carried out prior to embark on real project for monitoring the injected CO_2 within S3+4 sand of Ankleshwar for feasible EOR and storage.

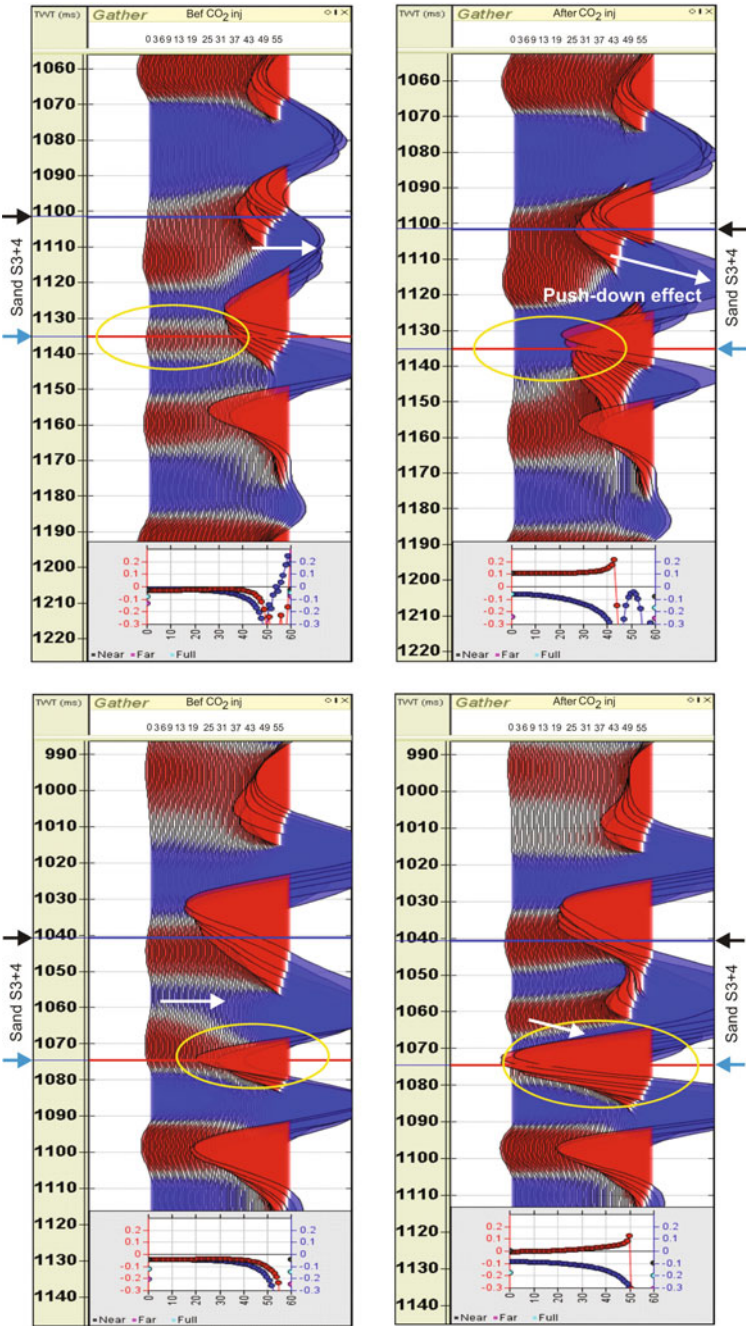
TWT (ms)
Gather
Bef CO2 inj
After CO2 inj
0 3 6 9 13 19 25 31 37 43 49 55
Sand S3+4
Push-down effect
Near
Far
Full

◄**Fig. 7.9** Representation of gather, both pre (*Left*)-and post (*Right*)-CO_2 injection scenario for analysing the feasible time-lapse seismic data using four wells (ANKL-1 and ANKL-2 *Top panel* and ANKL-3 and ANKL-4 *Bottom panel*) from Ankleshwar oil field. *White arrow* and the *ellipse* (*yellow*) indicate the push-down effect due to CO_2 injection in the target zone. *Black* and *cyan arrows* on the *sides* indicate the top and bottom S3+4 horizons, respectively

References

Amini H, Alvarez E, Wilkinson D, Lorsong J, Slater J, Holman G, Timofeeva O (2014) 4D seismic feasibility study for enhanced oil recovery (EOR) with CO_2 injection in a mature North Sea Field. 4th EAGE CO_2 Geological Storage Workshop, Stavanger, Norway, p P33

Arts R, Eiken O, Chadwick A, Zweigel P, van der Meer L, Zinszner B (2004) Monitoring of CO_2 injected at Sleipner using time-lapse seismic data. Energy 29:1383–1392

Bergmann P, Yang C, Lüth S, Juhlin C, Cosma C (2011) Time-lapse processing of 2D seismic profiles with testing of static correction methods at the CO_2 injection site Ketzin (Germany). J Appl Geophys 75:124–139

Bianco E (2008) Seismic rock physics of steam injection. Master thesis, University of Alberta, p 200

Brown AR (2003) Interpretation of three-dimensional seismic data, 6th edn, AAPG Memoir 42. SEG Investigations in Geophysics, Tulsa, USA

Cotton J, Michou L, Forgues E (2013) Continuous land seismic reservoir monitoring of thermal EOR in the Netherlands. 75th EAGE Conference & Exhibition incorporating SPE EUROPEC, Canada, pp 1–9

Davis TL, Terrell MJ, Benson RD (2003) Multi-component seismic characterization and monitoring of the CO_2 flood at Weyburn Field, Saskatchewan. Lead Edge 22:696–697

Dimri VP (1992) Deconvolution and inverse theory: application to geophysical problems. Elsevier Science Publishers, Amsterdam, p 230

Dimri VP, Srivastava RP, Vedanti N (2012) Fractal models in exploration geophysics, vol 41, Elsevier Science Publishers, Amsterdam, p 165

Eastwood J, Lebel P, Dilay A, Blakeslee S (1994) Seismic monitoring of steam-based recovery of bitumen. Lead Edge 13:242–251

Ecker C, Lumley DE, Tura A, Kempner W, Klonsky L (1999) Estimating separate steam thickness and temperature maps from 4-D seismic data: an example from San Joaquin Valley, California. 69th Annual International Meeting, SEG, Expanded Abstracts, pp 2032–2034

Greaves RJ, Fulp TJ (1987) Three-dimensional seismic monitoring of an enhanced oil recovery process. Geophysics 52:1175–1187

Harris JM, Langan RT, Fasnacht T, Melton D, Smith B, Sinton J, Tan H (1996a) Experimental verification of seismic monitoring of CO_2 injection in carbonate reservoirs. 66th Annual Meeting, SEG, Expanded Abstracts, pp 1870–1872

Harris JM, Yin F, Quan Y (1996b) Enhanced oil recovery monitoring using P-wave attenuation. SEG Tech Prog Expand Abstr 66:1882–1885

Herawati I (2002) The use of time-lapse P-wave impedance inversion to monitor CO_2 flood at Weyburn Field, Saskatchewan, Canada. Thesis of the Reservoir Characterization Project, Colorado School of Mines

Jenkins SD, Waite MW, Bee MF (1997) Time-lapse monitoring of the Duri steamflood: a pilot and case study. Lead Edge 16:1267–1274

Kazemeini SH, Juhlin C, Fomel S (2010) Monitoring CO_2 response on surface seismic data; a rock physics and seismic modeling feasibility study at the CO_2 sequestration site, Ketzin, Germany. J Appl Geophys 71:109–124

Landrø M (2001) Discrimination between pressure and fluid saturation changes from time-lapse seismic data. Geophysics 66:836–844

Landrø M, Stammeijer J (2004) Quantitative estimation of compaction and velocity changes using 4D impedance and traveltime changes. Geophysics 69:949–957

Landrø M, Strønen LK, Digranes P, Solheim OA, Hilde E (2001) Time lapse seismic as a complementary tool for in-fill drilling. J Petrol Sci Eng 31, 81–92

Lumley DE (1995) Seismic time-lapse monitoring of subsurface fluid flow. Ph.D. Thesis, Stanford University

Lumley DE (2001) Time-lapse seismic reservoir monitoring. Geophysics 66:50–53

Lumley DE (2004) Business and technology challenges for 4D seismic reservoir monitoring. Lead Edge 23:1166–1168

Lumley D (2010) 4D seismic monitoring of sequestration. Lead Edge 29:150–155

Meadows M (2008) Time-lapse seismic modeling and inversion of CO_2 saturation for storage and enhanced oil recovery. Lead Edge 27:506–516

Meadows MA, Cole SP (2013) 4D seismic modeling and CO_2 pressure-saturation inversion at the Weyburn Field, Saskatchewan. Int J Greenhouse Gas Control 16:S103–S117

Pullin N, Matthews L, Hirsche K (1987) Techniques applied to obtain very high resolution 3-D seismic imaging at an Athabasca tar sands thermal pilot. Lead Edge 6:10–15

Rickett JE, Lumley DE (2001) Cross-equalization data processing for time-lapse seismic reservoir monitoring: a case study from the Gulf of Mexico. Geophysics 66:1015–1025

Sodagar TM, Lawton DC (2014) Time-lapse seismic modelling of CO_2 fluid substitution in the Devonian Redwater Reef, Alberta, Canada. Geophys Prospect 62:518–529

Urosevic M, Pevzner R, Kepic A, Wisman P, Shulakova V, Sharma S (2010) Time-lapse seismic monitoring of CO_2 injection into a depleted gas reservoir—Naylor Field, Australia. Lead Edge 29:164–169

Vedanti N, Sen MK (2009) Seismic inversion tracks in situ combustion: A case study from Balol oil field, India. Geophysics 74:B103–B112

Vedanti N, Pathak A, Srivastava RP, Dimri VP (2009) Time lapse (4D) seismic: some case studies. e-J Earth Sci India 2:230–248

Waite MW, Sigit R (1997) Seismic monitoring of the Duri steamflood: Application to reservoir management. Lead Edge 16:1275–1278

Zadeh HM, Srivastava RP, Vedanti N, Landro M (2010) Seismic monitoring of in situ combustion process in a heavy oil field. J Geophys Eng 7:16–29

Zhang R, Ghosh R, Sen MK, Srinivasan S (2013) Time-lapse surface seismic inversion with thin bed resolution for monitoring CO_2 sequestration: a case study from Cranfield, Mississippi. Int J Greenhouse Gas Control 18:430–438

Zoeppritz K (1919) Erdbebenwellen VIIIB, On the reflection and propagation of seismic waves. Gottinger Nachr I, 66–84

Chapter 8
Conclusions

The principle objective of the present study has been fulfilled to the extent that some generalized conclusions can be drawn, as detailed below, about CO_2-EOR and sequestration potential in Ankleshwar oil field at the Cambay Basin (Western India) based on the input from integrated reservoir studies. We first present the overall conclusions of the thesis with limitations of the study, and then we provide a set of recommendations or future scopes of research regarding CO_2-EOR and sequestration in Ankleshwar oil field. This thesis mainly investigated four approaches for the study of CO_2-EOR and sequestration at Ankleshwar: reservoir modeling and simulation to optimize the production scenario, rock physics for reservoir characterization, geomechanical study for safe storage, time lapse seismic for effective monitoring of injected CO_2.

The following specific conclusions can be drawn from the present work:

1. From the reservoir modeling and flow simulation study, we assessed that compared to CO_2-WAG, continuous CO_2 injection is better option for both, EOR as well as storage at Ankleshwar, providing additional oil recovery of $\sim$10.4% of original oil in place and sequestrate about 15.04 million metric ton of CO_2. This will lead to sequestration of $\sim$150.4 million metric tons, if the full field reservoir is considered, as the full-field model is about 10 times larger than this conceptual model. In this way, if we can identify 10–15 more potential reservoirs for CO_2 storage, then we could restrict the CO_2 emission by sequestrating almost 2256 million metric tons of CO_2.
2. We developed a 50 m grid size (horizontal x-and y-directions) black oil simulation model with optimized parameters for industrial scale simulations, obtained from sensitivity analysis of various operational parameters (grid size, Corey exponent for oil and water, and T & L mixing parameters) for miscible flood displacement. This model is in good agreement with the fine scale (25 m grid) compositional simulation model of high accuracy. Additionally, this study is first to synthesize a new injection fluid, which reduces the MMP for miscible and more efficient displacement of CO_2.

S.S. Ganguli, *Integrated Reservoir Studies for CO_2-Enhanced Oil Recovery and Sequestration*, Springer Theses,
DOI 10.1007/978-3-319-55843-1_8

3. We report the development of an isotropic rock physics model to diagnose the Ankleshwar productive sands for successful implementation of CO_2-EOR at the field. We identified that the reservoir sands were undergone different cementation schemes and the velocity differentiation in high porosity and unconsolidated sands, is related to sorting. Also, the oil producing sands fall into constant cement model and no single theoretical model is sufficient to elucidate the reservoir properties adequately; yet a combination of three RPMs could explain reservoir properties better.
4. We identified density versus P-impedance cross plot as a powerful tool for fluid discriminator than a lithologic identifier. RPT analysis of well log data suggests that Ankleshwar formation consists of clean sands with significant residual oil saturation, which could be potential targets during CO_2-EOR in field. In addition to this, quantitative time-lapse rock physics study shows a decrease in amplitudes of elastic properties (e.g. Vp, P-impedance, Vp/Vs) after CO_2 injection, and the relative change in case of uniform saturation model (20% CO_2 saturation) is comparatively larger than the case of patchy saturation model, suggesting upper and lower bounds of these parameters.
5. After geomechanical characterization of the Ankleshwar oil field, we found that the Ankleshwar sands represent high value of Young's modulus, and pore pressure magnitudes for S3+4 sand layer (most productive pay sand of Ankleshwar formation) are sub-hydrostatic. A significant change in pore pressure, overburden pressure and fracture pressure is observed after CO_2 injection and the average pore pressure is 28% higher than the pore pressure estimated prior to CO_2 injection. Nevertheless, the predicted pore pressure is not higher than the fracture pressure (i.e. the upper limit of the allowed pressure in well), suggesting a safe and economic drilling during CO_2-EOR and storage. This has been validated from the monitoring of pressure profile which suggests even after re-pressurization of the reservoir, the operating pressure is 121 bar, which is much below the average formation fracture pressure computed (i.e. 190 bar) over the life of operation.
6. Feasibility study of time-lapse seismic response due to the changes in fluid pressure, composition and saturation during CO_2-EOR and sequestration at Ankleshwar suggests that even in the case of patchy saturation, the seismic response of CO_2 should be observable in surface seismic. Also, we observed a dramatic decrease in seismic amplitude soon after CO_2 injection in the most productive sand group (S3+4 pay sand) of Ankleshwar formation. The seismic response with respect to the injected CO_2 differs in different wells since we couldn't identify strong amplitude changes between the wells ANKL-3 and 4 when compared to ANKL-1 and 2. We assessed an average two-way delay time of 7.53 ms at S3+4 pay sand, and observed push-down effect (time-shift) caused by the lower velocity of CO_2. Thus, time-lapse seismic survey is highly recommended in this field for effective monitoring.

8.1 Limitations of the Study

Like every study, this research work is also dependent largely on the reservoir data and as a consequence, the present study suffers due to limited data provided by the operator, ONGC. Nevertheless, for detailed study, to implement CO_2-EOR and sequestration on field scale, we have to depend on more data like, seismic with well data at the precise locations, in situ stress data, etc. Limited data was unable to support suitable history matching, estimation of accurate field scale recovery factor, quantitative analysis for CO_2 sequestration in large scale for the Ankleshwar oil field. Likewise, this study encompasses several assumptions which have been discussed in the respective chapters. However, this study was successful in the attempt to assess the potential of CO_2-EOR and sequestration in Ankleshwar oil field at Cambay Basin, India and thus provides abundant possibilities for future studies in detail.

8.2 Future Research

For future research purposes pertaining to the proposed injection site, the following recommendations may be taken into account:

- More experiments could be conducted to study the impact of viscous and capillary forces on CO_2-EOR under actual reservoir conditions. This will also help to understand the amount of CO_2 that can be entrapped permanently within the reservoir.
- Anisotropic rock physics modeling can be considered to study the feasibility of CO_2 leakage through fault and other small scale channels in the field for safe CO_2 sequestration.
- Till date, there have been a very few studies reported on the role of attenuation on enhanced oil recovery and sequestration from mature oil field. Laboratory investigations and rigorous study conducted by Toksöz et al. (1979); Johnston et al. (1979) suggests that both, pore fluids and effective pressure affect attenuation of P- and S-waves in rocks. Also, Harris et al. (1996) shows how P-wave attenuation can be used to monitor the injected CO_2 in carbonate. This indicates that attenuation could play a significant role in time-lapse seismic monitoring, and hence needed to be done.
- Future work should includes 3D elastic seismic wave propagation modeling, which could help to characterize more details of the changes in reservoir elastic properties on seismic response due to CO_2 injection, and identifying proper location pathways of CO_2 plumes at Ankleshwar site.

8.3 Concluding Remarks

India desperately needs CO_2-EOR and-geological sequestration as an immediate option to recover the ultimate oil from mature field and mitigate the climate change issue due to excess CO_2 release into the atmosphere. This study highlights the importance of CO_2-EOR and storage in India and report an assessment of CO_2-EOR and storage potential of Ankleshwar in Cambay Basin, an Indian mature oil field based on integrated reservoir studies. Nevertheless, keeping in mind the age of the field, the operator should evaluate the proposal very carefully before embarking on a large (field) scale CO_2-EOR and sequestration.

References

Harris JM, Yin F, Quan Y (1996) Enhanced oil recovery monitoring using P-wave attenuation. SEG Tech Prog Expand Abstr 66:1882–1885

Johnston DH, Toksöz MN, Timur A (1979) Attenuation of seismic waves in dry and saturated rocks: II. Mechanisms. Geophysics 44:691–711

Toksöz MN, Johnston DH, Timur A (1979) Attenuation of seismic waves in dry and saturated rocks: I. Laboratory measurements. Geophysics 44:681–690